**EVALUATION OF CONTACT AND NON-CONTACT LAP SPLICES IN**

**CONCRETE BLOCK MASONRY SPECIMENS**

A Thesis Submitted to the College of

Graduate Studies and Research

In Partial Fulfillment of the Requirements

For the Degree of Master of Science

In the Department of Civil & Geological Engineering

University of Saskatchewan

Saskatoon

By

KAWSAR AHMED

# PERMISSION TO USE

In presenting this thesis in partial fulfilment of the requirements for a Postgraduate degree from the University of Saskatchewan, I agree that the Libraries of this University may make it freely available for inspection.  I further agree that permission for copying of this thesis in any manner, in whole or in part, for scholarly purposes may be granted by the professor or professors who supervised my thesis work or, in their absence, by the Head of the Department or the Dean of the College in which my thesis work was done.  It is understood that any copying or publication or use of this thesis or parts thereof for financial gain shall not be allowed without my written permission.  It is also understood that due recognition shall be given to me and to the University of Saskatchewan in any scholarly use which may be made of any material in my thesis.

Requests for permission to copy or to make other use of material in this thesis in whole or part should be addressed to:

Head of the Department of Civil and Geological Engineering

University of Saskatchewan

Engineering Building

57 Campus Drive

Saskatoon, Saskatchewan, S7N 5A9

Canada

# ABSTRACT

An experimental program was performed for qualitative and quantitative comparison of the maximum tensile resistance of contact and non-contact lap spliced bars in reinforced concrete block masonry using double pullout and wall splice specimens. A total of 32 specimens were tested, consisting of an equal number of double pullout specimens and full-scale wall splice specimens. Both specimen types had the identical cross-section. Eight replicate specimens for each specimen type were constructed with both contact and non-contact lap splice arrangements. Grade 400 deformed reinforcing bars with a 300 mm lap splice length were provided in all specimens.

The double pullout specimens were tested applying direct tension to the lapped reinforcing bars. The splice resistance and displacement were recorded during testing. All double pullout specimens with contact lap splices developed, as a minimum, the yield strength of the reinforcing bars and generally displayed evidence of a yield plateau. In contrast, the double pullout specimens with non-contact lap splices failed when only 46.1% of the theoretical yield strength of the reinforcing bars was recorded as the maximum splice resistance. The difference between the average value of the tensile resistance in the contact and non-contact spliced bars was identified as being statistically significant at the 95% confidence level.

Wall splice specimens were tested under a four-point loading arrangement with the lapped bars located in the constant moment region. The applied load and specimen

deflection were recorded until failure occurred. A numerical analysis was then performed to calculate the maximum resistance of the spliced bars. The specimens with contact lap splices developed the theoretical yield capacity of the reinforcing bars. In contrast, the wall splice specimens with non-contact lap splices developed an average tensile resistance of 78% of the theoretical yield capacity. The difference between the average tensile resistances of the lapped bars in the two splice arrangements was identified as being statistically significant at the 95% confidence level.

On average, the contact and non-contact lap spliced bars in the double pullout specimens developed 8.47% and 41.2% less tensile resistance, respectively, as compared to the wall splice specimens with the identical splice arrangement. Both differences were identified as being statistically significant at the 95% confidence level.

Bond loss between the reinforcing bars and the surrounding grout was identified as the failure mode for both the double pullout and wall splice specimens with contact lap splices. In contrast, bond loss at the masonry block/grout interface was observed along the non-contact lapped bars in both specimen types, as identified by visual observations upon removal of the face shell and the surrounding grout. Based on the test results of the wall splice specimens with non-contact lap splices, a correction factor of 1.5 is suggested when calculating the effective splice length for the non-contact splice arrangement as tested.

## CO-AUTHORSHIP

All the experimental and analytical work presented in this thesis was performed by Kawsar Ahmed and reviewed by Dr. Lisa R. Feldman. Test results from the first phase of the experimental program was published in the $8^{th}$ International Masonry Conference, Dresden, 2010. Test results from all double pullout specimens was accepted for publication in the proceedings of the $11^{th}$ North American Masonry Conference, Minneapolis, 2011. A working draft summarizing the entire work has been prepared for submission to the Canadian Journal of Civil Engineering.

## ACKNOWLEDGEMENTS

# TABLE OF CONTENTS

CHAPTER 1
INTRODUCTION

CHAPTER 2
LITERATURE REVIEW

CHAPTER 3
EXPERIMENTAL DESIGN, SPECIMEN CONSTRUCTION, AND TEST SETUP

CHAPTER 4
RESULTS AND ANALYSIS

CHAPTER 5
CONCLUSIONS

# LIST OF FIGURES

# LIST OF SYMBOLS

$A_s$        Cross-sectional area of a reinforcing bar

b        Width of the wall splice specimen

C        Total compressive force in the masonry

c        Neutral axis depth from the compression (i.e. top) face

$C_1$        Non linearity constant

C.O.V        Coefficient of variation

$d_b$        Reinforcing bar diameter

$d_{eff}$        Effective depth of the reinforcing bars

$d_i$        Mid-segment depth of the $i^{th}$ segment with respect to the neutral axis

d.o.f        Degrees of freedom

$E_m$        Modulus of elasticity for masonry

$E_s$        Modulus of elasticity of the reinforcing steel

$E_{sh}$        Slope at the beginning of the strain hardening region

$f_{gt}$        Grout tensile strength

$f_m$        Compressive strength of the masonry

$f_{mi}$        Compressive stress in the $i^{th}$ segment

$f_s$        Tensile stress in reinforcing steel

$f_y$        Yield stress of the reinforcement

$f_{ult}$        Ultimate reinforcing steel stress

$I_g$        Gross moment of inertia of the wall splice specimens

$I_{cr}$        Cracked moment of inertia of the wall splice specimens

$I_{eff}$        Effective moment of inertia of the wall splice specimens

| K | Strength enhancement factor |
|---|---|
| $K_1$ | Minimum clear cover to the reinforcement in inches |
| L | Span length of the wall splice specimens |
| $L_i$ | Distance of the $i^{th}$ segment from the nearest support. |
| $l_d$ | Development length |
| $M_{cr}$ | Cracking moment |
| $M_a$ | Applied moment |
| $M_i$ | Average moment in the $i^{th}$ layer |
| $M_\phi$ | Moment corresponding to curvature $\phi = 0.025/m$ |
| $N_1, N_2$ | Number of specimens in a population |
| n | Number of segments |
| $P_{cr}$ | Experimentally measured cracking load for the wall splice specimens |
| $P_y$ | Theoretically calculated load at yielding of the reinforcement |
| $P_{Ey}$ | Experimentally determined load at bar yield |
| R | Reaction at support |
| $S_1, S_2$ | Standard deviation of a sample population |
| T | Applied tension |
| T | Thickness of the masonry specimen |
| u | Average bond stress |
| $X_1, X_2$ | Assumed average splice resistance of a sample population |
| Z | Empirical constant for the falling stress-strain curve segment for the masonry prisms. |
| $\varepsilon_c$ | Compressive strain in masonry |
| $\varepsilon_s$ | Tensile strain in the reinforcing steel |
| $\varepsilon_{sh}$ | Reinforcing steel strain at the beginning of strain hardening |

| | |
|---|---|
| $\varepsilon_x$ | Compressive strain in the extreme fibre |
| $\varepsilon_{ult}$ | Reinforcing steel strain at the ultimate stress |
| $\varepsilon_y$ | Yield strain in the reinforcing steel |
| $\phi$ | Curvature |
| $\phi_{cr}$ | Curvature in the fully cracked section |
| $\phi_i$ | Curvature in the $i^{th}$ segment |
| $\phi_g$ | Curvature in the uncracked gross section |
| $\phi_{uc}$ | Curvature just before cracking |
| $\Delta_{30P}$ | Midspan deflection corresponding to an applied load, P= 30 kN |
| $\Delta_{mid}$ | Midspan deflection |
| $\sum_o$ | Perimeter of all longitudinal reinforcement |

CHAPTER 1
INTRODUCTION

## 1.1 Background

Masonry has been successfully used as a building material since the time that early civilizations were established. It is only recently that it has been reinforced with steel to improve its structural response (Hamid, 2004). The overlapping of bars, more commonly referred to as lap splices, is frequently provided at the base of reinforced masonry walls where dowels from footings extend into the walls. Lap splices also occur at locations of discontinuities of the reinforcement along the height of tall walls as bars are supplied in specific lengths of 6 or 12 m to ease handling and delivery. These spliced reinforcing bars are typically subjected to tensile forces when the masonry wall experiences flexure. The resulting tensile force must be transferred between the lapped bars through bond development between the grout and reinforcing bars along the lap splice length. Insufficiently short lap lengths therefore cannot effectively transfer tensile forces between the bars, and so cause a failure at the splice location at a flexural resistance that is lower than that calculated assuming that the reinforcement is continuous. In most cases, splice failures are brittle in nature and result in a sudden and potentially catastrophic failure for a structure.

Development length and lap splice provisions for reinforced masonry in CSA S304.1-04 - "Design of Masonry Structures" (CSA, 2004a) are identical to those reported for reinforced concrete (Drysdale & Hamid, 2004) in CSA A23.3-04 – "Design of Concrete Structures" (CSA, 2004b). Unlike reinforced concrete, reinforced masonry has weak bed joints, complex grout block friction, and generally reduced lever arms between the centroid of the compression zone in the masonry units and the steel reinforcement. Moreover, flexural cracks in masonry are arrested at bed joints and results in a few, wide cracks in these members. This response in flexure differs from that exhibited by reinforced concrete members and will likely affect splice performance. A better understanding of splice behaviour in reinforced masonry is therefore necessary.

In practise, masonry block walls are constructed with concrete hollow blocks placed first; the reinforcement is then placed, and finally the cells are grouted. The process is often completed in two lifts. Reinforcing bars for the second stage of the wall construction are spliced with those from the first lift, requiring a mason to lift successive blocks over the previously placed bars. This either slows down the construction process or requires the purchase of more expensive open-ended blocks. If spliced bars are placed after erecting the masonry blocks in second lift, the reinforcement may be unintentionally positioned in the adjacent cells. Non-contact splices with the reinforcing bars located in adjacent cells are also provided intentionally when lintel beams spanning across door and window openings and utility boxes within a wall interrupts the otherwise continuous vertical reinforcement. Non-contact lap splices are commonly used by masons and are permitted in accordance with the current Canadian masonry

design code (CSA, 2004a) without any correction factor applied. A review of the existing literature did not identify any research that compared the performance of non-contact lap splices with typical contact lap splices in reinforced masonry construction.

In fact, few reports of lap splices in reinforced masonry of any type have been identified in the literature. Those that exist are based on tests of different specimen types which may or may not accurately capture the performance of reinforced masonry structure. Pullout specimens, though popular among researchers, have many limitations including the fact that they tend to induce an unrealistic compressive stress state in the grout surrounding the reinforcing bars. Full-scale wall splice specimens are able to represent actual structural performance but are more costly and difficult to construct and test. Though the geometry and testing arrangement used for pullout specimens has improved over time, including the development of more suitable specimens such as double pullout specimens (NCMA, 1999) which provide a better representation of the actual stress state surrounding the reinforcement, comparisons have not been found in the literature that relate test data for splice capacities from double pullout specimens to those of full-scale wall specimens.

## 1.2 Objectives

The primary objective of the current study is the quantitative and qualitative comparison of the maximum tensile resistance of lap spliced bars including both contact and non-contact lap splices in small scale double pullout specimens and wall splice specimens. In this study, all spliced bars are located in the middle of the common cell grouting width

of vertically adjacent blocks. The non-contact lap spliced bars are located in the adjacent cells.

The specific primary objectives are as follows:

1. To establish whether non-contact lap splices in either double pullout or wall splice specimens can develop an average tensile resistance of the spliced bars that is significantly different compared to that developed by identical specimens with contact lap splices;

2. To establish whether the average tensile resistances of lap spliced bars in double pullout and wall splice specimens with identical lap splice arrangements are significantly different; and

3. To compare splice behaviour such as: load versus displacement, failure mode, and bond deterioration for contact and non-contact lap splices in both specimen types.

## 1.3 Methodology and Scope

A total of 32 specimens, including an equal number of double pullout and wall splice specimens, were tested to investigate the maximum tensile resistance of the lap splices provided. The double pullout specimens were tested in direct tension, while lateral loads were applied to the wall splice specimens using a four-point loading arrangement such that the spliced bars were within the specimens' constant moment region. The maximum tension resisted by the splices in the double pullout specimens was obtained directly from the data logged during testing, whereas a numerical analysis was performed

incorporating material properties obtained from tests of companion specimens for the grout, mortar, masonry blocks, and reinforcing steel to establish the available maximum tensile resistance of the spliced bars based upon the maximum moment resisted by each wall splice specimen. Eight replicate specimens were tested for each specimen type with both contact and non-contact lap splices to investigate if a statistically significant difference existed between the mean maximum splice resistance of the two specimen populations. The splice length, reinforcing bar size, and clear cover to the lapped bars was held constant for all the specimens. The material properties used in the masonry assemblage, including: block strength, grout strength, mortar strength, and the yield stress of the reinforcement were kept as constant as practically possible for all specimens.

**1.4 Thesis Outline**

Chapter 1 – Presents the background for the current study followed by the specific objectives and scope of the research program.

Chapter 2 – Relevant experimental programs and findings identified in the literature are briefly presented in chronological order to demonstrate the development of the specimen type typically used to evaluate bond in reinforced masonry and to provide a understanding of splice behaviour as developed over time. These findings formed the basis for the current experimental program.

Chapter 3 – Specimen geometry, material properties, construction and testing methods are explained in this chapter.

Chapter 4 – Results from the companion specimens are first presented in this chapter to establish the material properties of the primary test specimens. The splice resistance versus splice displacement, maximum tensile resistance of the spliced bars and failure modes are then compared for double pullout specimens with both contact and non-contact lap splice arrangements. Load versus midspan deflection, external crack propagation, and observed failure modes are compared for wall splice specimens with contact and non-contact lap splices. The experimental observations are followed by a theoretical analysis to obtain the maximum tensile resistance of the spliced bars based on the recorded maximum loads resisted by the wall splice specimens. The calculated resistances are then compared with those obtained for the double pullout specimens with identical splice arrangements.

Chapter 5 – The summarized results and conclusions are presented to address the objectives as stated. Recommendations for future relevant research are also described.

CHAPTER 2
LITERATURE REVIEW

## 2.1 Introduction

In reinforced masonry, the tension force carried by the reinforcing steel under flexural loads must be transferred to the surrounding grout to develop effective flexural resistance in a member. This force transfer occurs by mechanical interaction between the reinforcing steel and the surrounding grout, which is commonly known as bond. Lap splices in a flexural members, as described in Section 1.1, need to be sufficiently long to allow the tensile force to be effectively transferred between the spliced bars by developing sufficient bond. Though bond research in reinforced concrete has a long history (e.g. Abrams, 1913), research on bond and splice capacity in reinforced masonry was not explored until the latter half of the twentieth century.

A limited number of publications describing bond development and splice performance in reinforced masonry has been identified. As influenced by bond research in reinforced concrete, experimental investigations using pullout tests have been conducted for reinforced masonry. In such tests, reinforcing bars are pulled out from a small-scale masonry assemblages in direct tension. Few reported investigations include reviews of anchorage and splice performance in full-scale flexural specimens that are capable of

more accurately capturing the stress state in the grout and block surrounding the reinforcement seen in typically constructed members such as walls.

This chapter describes the basic bond mechanics in reinforced masonry, followed by reviews of both small-scale pullout tests and full scale flexural specimen test investigations.

## 2.2 Mechanics of Bond

An adequate reinforcing bar length must be provided to transfer a tensile force, T, from the reinforcement to the surrounding grout by bond. Figure 2.1 shows a generalization of the bond stress that develops in a plain reinforcing bar being pulled out from its surrounding grout. From equilibrium, the average bond stress, $u$, assumed to be uniformly distributed over the development length, $l_d$, leads to the relationship:

$$T = A_s f_s = u \sum_o l_d \quad\dots\dots\dots\dots\dots\dots\dots\dots\dots\dots\dots\dots\dots\dots\dots\dots\dots\dots \text{ (2.1)}$$

where, $A_s$ is the cross-sectional area of the reinforcing bar, $f_s$ is the stress in the bar under tension, and $\sum_o$ is the perimeter of the reinforcing bar. Rearranging Equation 2.1 and recognizing that $A_s = \dfrac{\pi}{4} d_b^2$, and $\sum_o = \pi d_b$ , leads to the following relationship for the required development length:

$$l_d = \frac{d_b}{4u} f_s \quad\dots\dots\dots\dots\dots\dots\dots\dots\dots\dots\dots\dots\dots\dots\dots\dots\dots\dots\dots\dots\dots \text{ (2.2)}$$

Though Equation 2.2 provides a simplified equation to calculate development length, it is not representative of the actual bond mechanics in deformed reinforcing bars. Figure

2.2(a) shows that the ribs of deformed reinforcing bars bear against the surrounding grout upon bar slip, thus forming inclined compressive forces. The radial component of this force creates a circumferential tensile force while the horizontal component creates shear in the surrounding grout. Bar pullout occurs by shearing of the grout keys formed between the bar ribs when the horizontal component of the applied force overcomes the shear strength of the grout. Bar pullout then occurs and is accompanied by splitting of the surrounding grout and masonry block, when the radial component overcomes the tensile strength of the surrounding grout considering the confining resistance of a full masonry cell. Figure 2.2(b) shows that an additional lateral tensile force is produced when relative movement between adjacent lapped reinforcing bars in contact cause the ribs of the bars to ride over one another (Schuller at al., 1993).
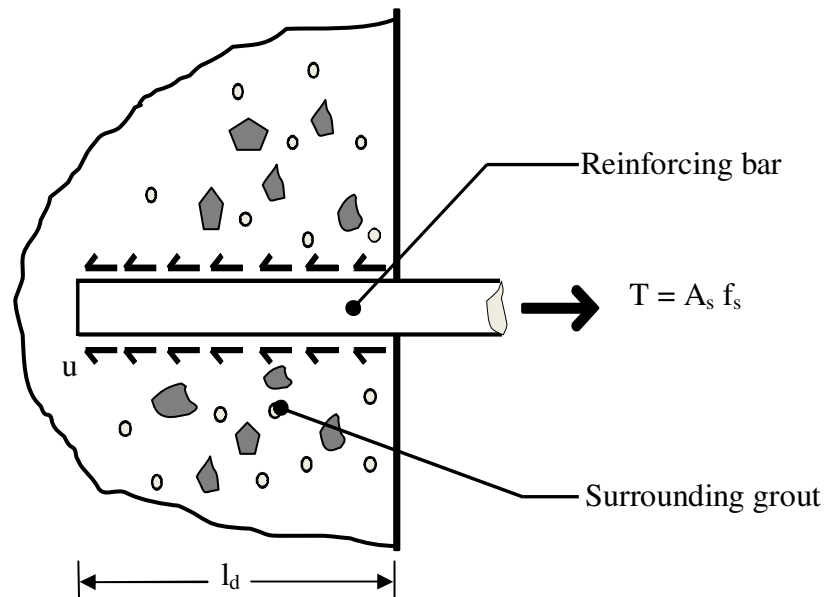


Figure 2.1: The concept of average bond stress.
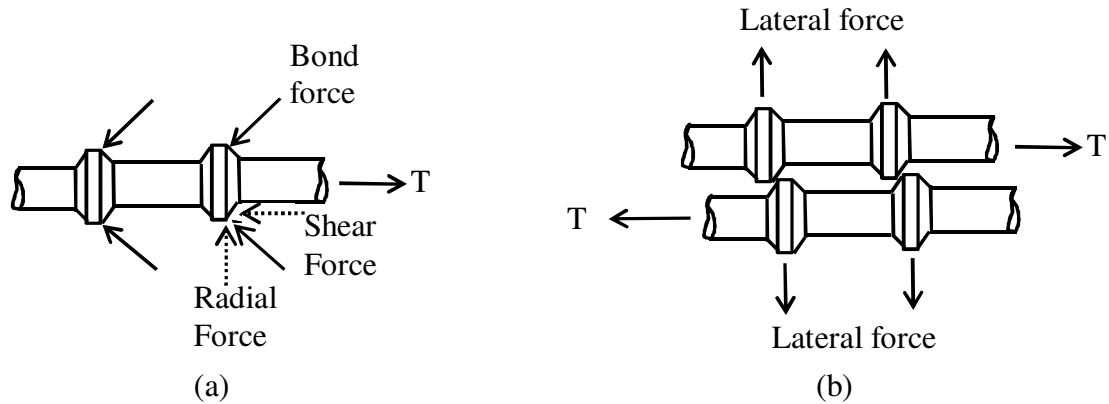
Figure 2.2: Bond mechanisms in deformed reinforcing bars: (a) components of bond force, and (b) additional lateral force caused by relative bar movement.

The concept of average bond stress oversimplifies the actual bond distribution of reinforcing bars; however, some previous editions of masonry design codes (i.e. CSA S304, 1977) specified allowable values for u, as it is an easily calculated quantity. In fact, researchers such as Soric and Tulin (1989), and Cheema and Klingner (1985a) have proven that the bond stress distribution along the length of a reinforcing bar is non-linear with the existence of high peak values of localized bond stress that shifted along the length of the development length. Present day masonry design codes (i.e. CSA S304.1-04, 2004a; ACI 530, 1999) therefore provide empirical equations in terms of the required development length as developed from results of reported research.

The following sections discuss a review of reported studies of bond in reinforced masonry. The research programs are grouped based on specimen type (i.e. small scale pullout tests and full scale wall and beam tests). Reports of each type of specimens are presented chronologically to show the evolution of typical specimen geometry and test setups. Research related to the bond of non-contact lap splices is reviewed based on

research of reinforced concrete specimens due to the lack of reported studies in reinforced masonry. American studies and some older Canadian studies are reported in U.S customary units (Imperial bar sizes) including those sizes no longer manufactured in Canadian markets. These studies are presented with the original bar sizes used with the designation No. X (I), where X represents the size of the bar in imperial units, and the "(I)" designation signifying that Imperial units have been reported.

## 2.3 Pullout Tests

Pullout tests are conducted with small-scale specimens in which a tension force is applied to the reinforcing bars to cause them to pull out from the specimen. Pullout tests are inexpensive, easy to fabricate, and requires a simple test setup. They have, therefore, been popular among researchers [Baynit,1980; Cheema & Klingner,1985a; Soric & Tulin, 1989); and Schuller et al., 1993] for investigating bond and anchorage in reinforced masonry. Even though these specimens are unable to capture realistic stress conditions in the surrounding grout, significant improvements in test specimens as well as in test methods were developed over time to better represent actual bond development under flexural stresses.

### 2.3.1 Baynit's (1980) pullout test program

Pullout specimens constructed with concrete blocks with knocked-out webs were tested by Baynit (1980). Knocked-out webs are generally used in the construction of lintel beams used to frame doors and window openings. Figure 2.3 shows the test arrangement
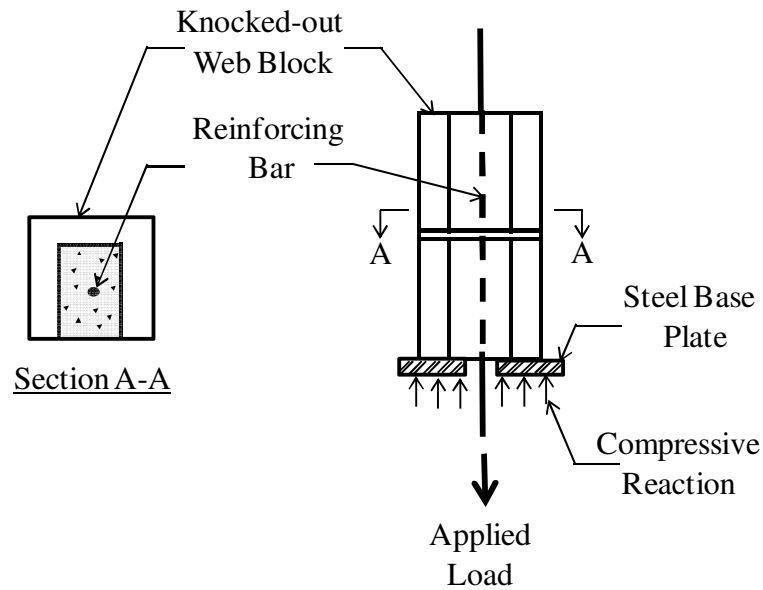
Figure 2.3: Baynit's pullout specimens (modified from Baynit, 1980).

used in this experimental program. Direct tension was applied at one end of the reinforcing bar with the specimens supported on a square steel plate fixed within the testing apparatus. The steel plate had a hole in its centre to allow the reinforcing bar to pass through it. Slip of the bar with respect to the grout surface at the free (i.e. top) end of the specimen was measured using a dial gauge mounted on the reinforcing bar.

Two parameters were investigated in this experimental program: bar size and embedment length. Twenty seven pullout specimens were constructed, and were reinforced with either No. 4 (I), No. 6 (I) or No. 8 (I) bars. Three embedment lengths were provided for each bar size with three replicate specimens for each embedment length. Embedment lengths of 7 in. (178 mm), 9 in. (229 mm) and 11 in. (279 mm) were

provided for the No. 4 (I) bars, while 7 in. (178 mm), 9 in. (229 mm) and 15 in. (381 mm) embedment lengths were provided for the No. 6 (I) and No. 8 (I) bars.

An interface failure between the grout and the concrete block was observed for the specimens reinforced with No. 4 (I) reinforcing bars and a 7 in. (178 mm) embedded length when the grout sheared off from the adjacent concrete block. All 18 specimens with embedment lengths greater than 7 in. (178 mm) reinforced with No.4 (I) bars developed their yield capacity. Specimens reinforced with No. 6 (I) bars with embedment lengths of 7 in. (178 mm) displayed reinforcing bar pullout after splitting of the masonry block. Pullout of the reinforcement after shear failure of the surrounding grout was observed exclusively for specimens with 9 in. (229 mm) embedment lengths. All three specimens with a 15 in. (381 mm) embedded length with either No. 6 (I) or No. 8 (I) bars developed the full yield capacity of the reinforcement.

A review of the data for specimens with a single bar size showed that the ultimate failure load increased in proportion to the embedment length. No specific trend was established for the average bond stress. Specimens with shorter embedment lengths reinforced with No. 4 (I) bars showed higher ultimate bond stress as compared to those with longer development lengths. This behaviour was not exhibited by specimens reinforced with larger bar sizes.

One of the limitations of Baynit's specimens is the presence of a confining pressure in the grout and block surface at the supported bottom end due to the compressive reaction

that occurs when the section is subjected to load and bears against the test apparatus. This confining pressure is likely to increase the resistance of the surrounding grout and thus can result in an artificially high ultimate failure load (Cheema & Klingner, 1985a). The knockout web masonry blocks also lack the confining effect offered by full block masonry walls. Moreover, the specimens were constructed in a stack bond assemblage in which the grout filled cells are aligned in vertically adjacent cells. These vertically aligned cells offered a shear failure surface between the adjacent concrete blocks which may permit an interface failure between the blocks and the grout in some specimens. Running bond masonry assemblages, which are more typically used in Canadian construction, do not have vertically aligned cells, and this create additional resistance due to interlock between the adjacent grouted cells.

**2.3.2 Cheema and Klingner's (1985) single bar pullout tests**

Figure 2.4 shows a typical single bar pullout specimen tested by Cheema & Klingner (1985a). The reinforcing bar projected above the running bond masonry wall and was pulled out by a center-hole ram supported on a steel reaction beam. The reactions induced in the wall were applied far from the bar so that the resulting confining compressive force in the vicinity of the reinforcing bar was negligible. Classic elastic theory for a concentrated load applied along the depth of a simply supported beam was used to calculate the minimum distance between the reinforcing bar location and the reaction point so as to limit the resulting confining pressure to 100 psi (0.7 MPa) when the applied load caused yielding of the reinforcing bar. The average bond stress distribution and anchorage capacity were investigated for No. 4 (I), 8 (I), and 11 (I) bars.
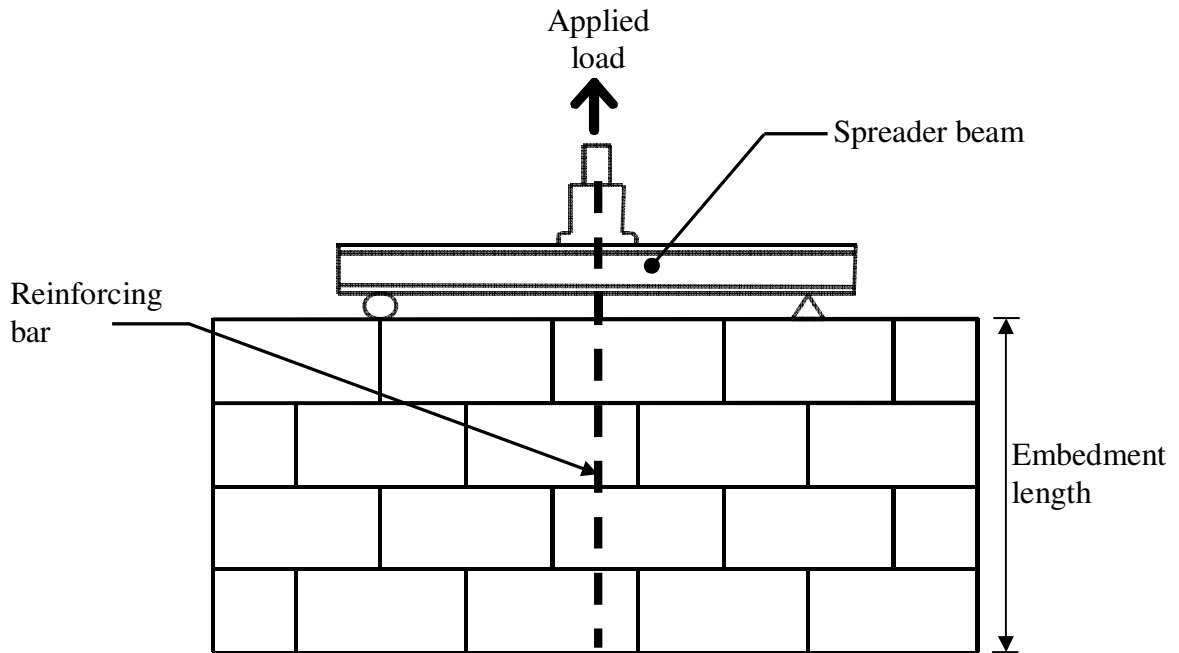
Figure 2.4: Single bar pullout specimen tested by Cheema & Klingner (modified from Cheema and Klingner, 1985a).

Specimens reinforced with No. 4 (I) bars with 5 in. (125 mm) embedment lengths showed either bar pullout or excessive slip, defined as being a slip of more than 0.0005 in. at the tail (i.e. bottom) end of the reinforcing bars. All specimens in this group that were provided with an embedment length of 10 in. ( 250 mm) or more achieved yielding of the reinforcing bar regardless of the size of bar used. Radial horizontal cracks propagated through the grout towards the face of surrounding concrete block at the loaded end. Specimens reinforced with No. 8 (I) reinforcing bars with a minimum of 20 in. (508 mm) embedment length showed splitting cracks along both faces of the concrete block near the loaded end, and subsequently failed by pullout. Some of these specimens showed a noticeable uplift of an entire concrete block in addition to splitting when the total bond force transferred exceeded the resistance available to maintain the

block position. The yield capacity of No. 8 (I) bars was achieved prior to failure for specimens with an embedment length 43 in. (1090 mm) without any slip of the loaded end of the bar or a block uplift.

Cheema & Klingner (1985a) described the bond failure as a progressive process. Once the maximum bond capacity of the reinforcing bar reached roughly one third to half of the embedment length from the loaded end, a sudden failure occurred for the remaining bonded length adjacent to the unloaded end.

### 2.3.3 Soric and Tulin's (1989) stack bond pullout specimens

Figure 2.5 shows the stack bond single cell grouted concrete block specimens tested by Soric and Tulin (1989). Half-block cells cut from full blocks were used for specimen construction. These half blocks provided the confinement that was absent in Baynit's (1980) test specimens. The reinforcing bar extended below the specimen, and was pulled out in direct tension with the specimen supported on the face shells only. A total of six pullout specimens with a single geometry and two reinforcing bar sizes (No. 4 (I) and 7 (I)) were tested. Embedment lengths of 16 in. (406 mm) and 32 in. (812 mm) were used for the specimens reinforced with the No. 4 (I) and 7 (I) bars, respectively. Three replicate specimens were tested with for each bar size. Thirty pullout specimens with short embedment lengths of 1 to 6 in. (25 to 152 mm) were also investigated for both bar sizes.

All six specimens with long embedment lengths developed the yield capacity of the reinforcing bar. Bond deterioration in the form of visible cracks were observed at the loaded end of the specimens. One of the specimens reinforced with a No.12 (I) bar was split open after testing, revealing that approximately one third of the bar adjacent to the specimen's loaded end showed shear failure of the grout keys that formed at the bar rib locations, accompanied by conical surface cracking within the grout. The middle third of the anchorage length showed crushing of the grout keys, while the remaining portion of the anchorage length adjacent to the unloaded end of the specimen showed no visible signs of damage.
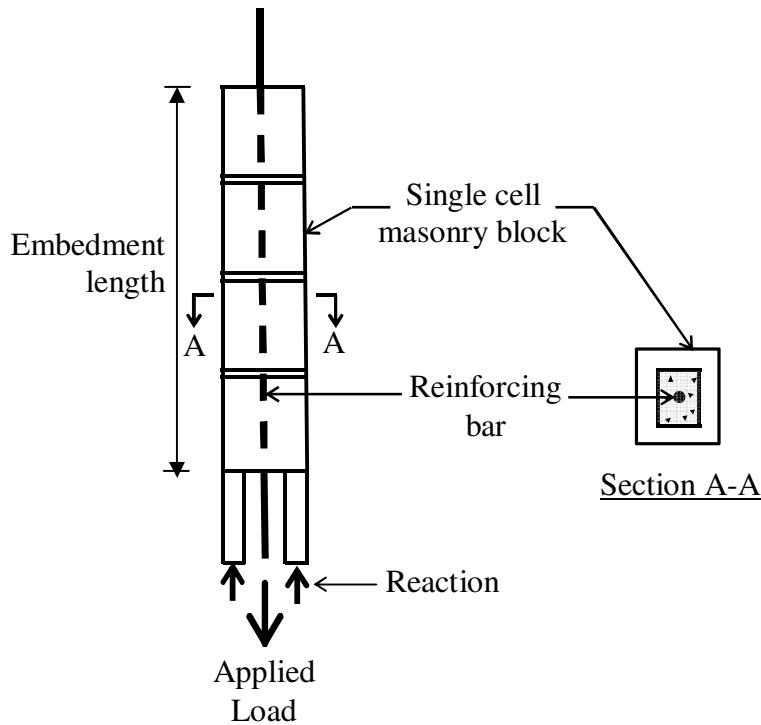


Figure 2.5: Stack bonded single-cell pullout specimen: (a) cross section, and (b) loading arrangement (modified from Soric & Tulin, 1989).

One of the three replicate specimens from each group (No. 4 (I) bar and No. 7 (I) bar) with a long embedment length was internally instrumented with four equally spaced strain gauges. Strain gauge data initially showed that all of the applied direct tension was resisted by approximately one third of the embedment length adjacent to the loaded end of the bar. Once the bond capacity of this bar region was exhausted, the remaining two thirds of the embedded length of the bar engaged and the peak bond stress shifted to within the middle third of the bar length. The assumption of uniform bond stress along the length was therefore shown to have contradicted reality. This behaviour was also observed by Cheema & Klingner (1985a) and is termed by these researchers as progressive bond failure. Though the strain gauge data gave some valuable insight related to the bond stress distribution at different load levels, the authors suspected that the actual bond development along the bar length was possibly affected at and near the instrumented locations as the protective coating surrounding the strain gauges affected the bond between the reinforcing bar and the surrounding grout.

The specimens with short embedment lengths of 1 in. (25 mm) developed an average bond stress of 3000 to 4000 psi (20 to 28 MPa) for both the No. 4 (I) and No. 7 (I) bars, which was notably higher than the 700 to 1500 psi (5 to 10 MPa) average stress developed when a 6 in. (150 mm) embedment length was provided. Soric and Tulin (1989) stated that the compressive reaction at the support might have increased the total bond force for the reinforcing bars, and, in particularly, those with short embedment lengths, by creating a confining pressure around the bar. This additional force created by

the confining pressure became less effective when a larger total bond force developed with longer development length.

### 2.3.4 Schuller et al.'s (1993) stack bond pullout specimens with lapped bars

Figure 2.6 shows a single cell stack bond specimen with the reinforcing bar lapped in the center of the cell, as tested by Schuller et al. (1993). Opposing tensile forces were applied to the extended portions of the reinforcing bars at the two ends of the specimens to eliminate the confining compression forces on the specimens that occurs in other types of pullout specimens (Baynit, 1980; Soric and Tulin, 1989). However, an eccentricity between the two applied loads resulted due to the configuration of the lap splice. These specimens were therefore subjected to combined axial loading and in-plane bending which complicated the analysis of the resulting test data.

The lap splice capacity was investigated for varying bar sizes [No. 4 (I), No. 6 (I), No. 8 (I), and No. 11 (I)] and block sizes [4 in. to 12 in. (100 mm to 300 mm)]. All specimens were constructed with typical 8 in. (200 mm) concrete blocks and reinforced with No. 4 (I) and No. 6 (I) bars developed the yield capacity of the bar. Lap lengths of 12 in. to 20 in. (305 mm  to 500 mm), and 20 in. to 36 in. (500 mm to 914 mm) were provided for specimens reinforced with No. 4 (I) and No. 6 (I) bars, respectively. These specimens failed by pulling out of one of the lapped reinforcing bars after either shear failure of the surrounding grout or the development of tensile splitting cracks along the lap splice length.
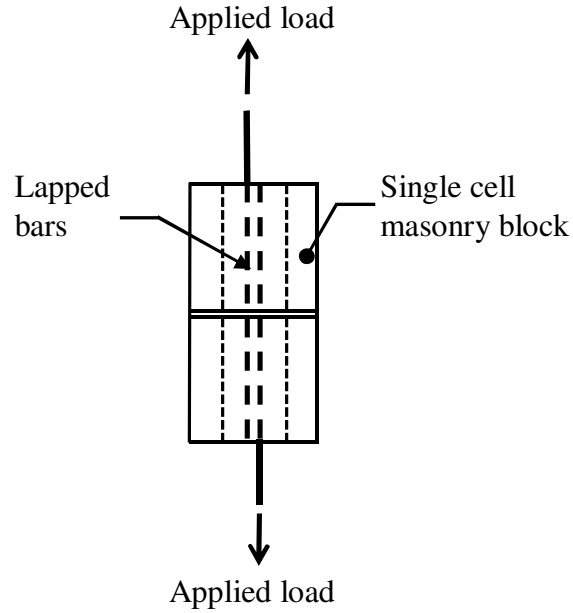
Figure 2.6: Single cell lap splice specimens tested by Schuller et al. (modified from Schuller et al, 1993).

### 2.3.5  NCMA's (1999) double pullout specimens

In 1999, the National Concrete Masonry Association (NCMA) carried out a research program to establish the minimum bar splice length required for concrete block masonry (NCMA, 1999). Figure 2.7 shows a typical one meter wide running bond masonry specimen with two symmetrically placed lap splices that were tested in direct tension. Two symmetrically placed reinforcing bars effectively developed two opposite in-plane flexure so that the net flexure in the specimen was eliminated and therefore gave advantage over the specimen types previously tested by other researchers (e.g. Schuller et al, 1993). Moreover, reinforced masonry walls are typically constructed in a  running bond pattern which makes the test results reported for these double pullout specimens more representative of typical construction.
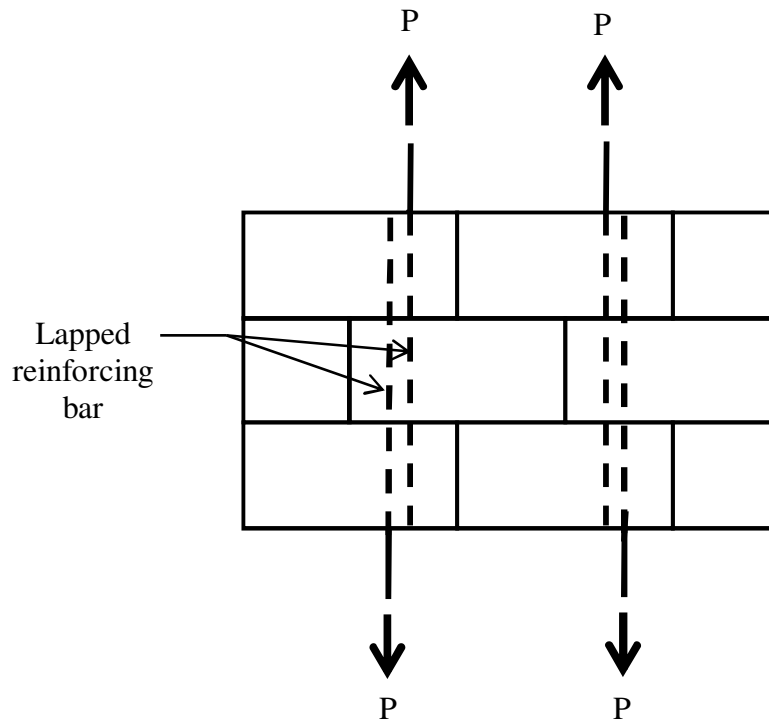
Figure 2.7: Double pullout test specimen tested by NCMA (NCMA, 1999)

A total of 108 reinforced and fully grouted concrete block masonry double pullout specimens were constructed and tested with varying geometric arrangements and material properties. Three replicate specimens were tested for each variation. The parameters investigated were: bar size, lap length, grout strength, and clear cover to the reinforcement. Minimum lap lengths provided for No. 4 (I) bars and No. 5 (I) bars were 18 in. (457 mm) and 25 in. (635mm) respectively.

The splice specimens were designed such that the splice length required to develop 1.25 times the yield capacity of the reinforcement could be achieved and all specimens did, in fact, attain yielding of the reinforcement. The dominant failure mode was longitudinal splitting of the masonry specimens along the lap splice length. Schuller et al. (1993)

observed a similar failure mode for their stack bond pullout specimens with lapped reinforcing bars.

A 20% increase in splice capacity was achieved when the lap splice length of the specimens reinforced with No. 6 (I) bars was increased from 42 to 74 in. (1067 mm to 1880 mm) with all other parameters held constant. Increasing the compressive strength of the masonry assemblage from 1700 to 4070 psi (11.7 to 28 MPa), a 140% increase, resulted in a 27% average increase in splice capacity for specimens reinforced with No. 4 (I) to No. 7 (I) bars. A ¼ in. (7 mm) increase in cover depth from 1 to 1 ¼ in. (25 mm to 32 mm) increased the splice capacity by 8%, whereas a 1 in. (25 mm) increase in clear cover depth increased the splice capacity by 8.5% and 18% for specimens reinforced with No. 6 (I) and 7 (I) reinforcing bars, respectively.

The testing of replicate specimens showed good repeatability of the reported splice capacity with a maximum coefficient of variation of 13%. The limited population size did not, however, allow for an accurate calculation of the mean splice capacity or the identification of outliers.

## 2.4  Full-scale Beam Tests

Flexure in beams and walls induces tension in both the reinforcement and the surrounding grout. This is in contrast to the pullout specimens discussed in the previous section where the reinforcement is subjected to tension while a compression stress is induced in the surrounding grout. Thus, pullout tests generally fail to actually capture

bond behaviour under flexural action. Though wall and beam splice tests more accurately represent the stress state in the reinforcement and masonry assemblage, the testing of full-scale specimens in the laboratory requires more space and a longer construction period and are, therefore, more costly. High capacity overhead cranes are also required to move these specimens around the laboratory. The instrumentation and analyses of the full-scale walls are also more complex. Very few reported results are available related to the investigation of splice strength or development lengths in full-scale flexural masonry specimens.

### 2.4.1 Baynit's (1980) beam tests

Figure 2.8 shows the full-scale lintel beams tested by Baynit (1980) to investigate the effects of: anchorage length, bar arrangement, and fill materials (i.e. grout and mortar) on bond capacity. Fifteen lintel beams reinforced with No. 4 (I), No. 6 (I), and No. 8 (I) (12, 20 and 25 mm, respectively) reinforcing bars were tested with anchorage lengths identical to the pullout specimens described in Section 2.3.1. The lintel beams were built from knockout web blocks and were tested for end anchorage.

All specimens reinforced with No. 4 (I) bars developed the yield capacity of the reinforcement with 7 to 11 in. anchorage lengths. A similar failure mode was observed in the companion pullout specimens. Specimens reinforced with No. 6 (I) and larger bar sizes failed in bond with evidence of pullout of the reinforcement from the surrounding grout. A pullout failure after splitting of the grout and masonry block was
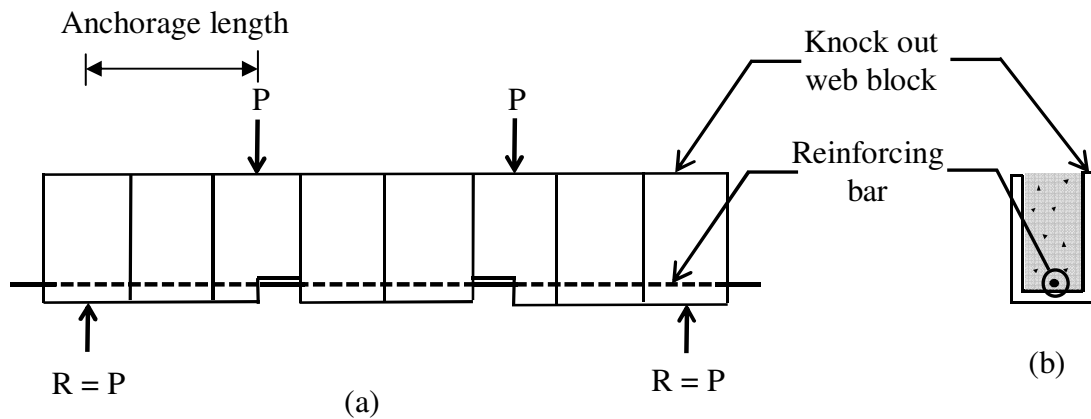
Figure 2.8: Lintel beam tests by Baynit : (a) beam elevation, and (b) cross-section
        (Baynit,1980).

also observed in the companion pullout tests with identical bar sizes and anchorage

lengths (Baynit, 1980).

Strain gauges were installed on the reinforcing bar surface at the points of applied load

on all specimens to allow for the calculation of the bar force at failure. The average

bond strength was then obtained by dividing the failure load by the embedded surface

area of the reinforcing bar. Similar to the companion pullout specimens, the average

bond stress decreased with increasing anchorage length for beams reinforced with No. 4

(I) bars. Similarly, beams reinforced with No. 8 (I) reinforcing bars also showed a

decrease in average bond stress with increasing anchorage length. Though both the

pullout tests and beam tests showed similar trends, the average bond stress was 1.2 to

1.7 times lower in the beam tests as compared to the pullout tests. Baynit stated that the

high compressive reaction developed adjacent to the support in the pullout specimens

resulted in higher average bond stresses in these specimens. The pullout test results may

provide an indication of general behaviour but should not be used as the basis of design requirements when an accurate quantitative assessment of splice capacity is required.

### 2.4.2 Matsumara et. al.'s (1997) beam tests with spliced reinforcing bars

Matsumara et al. (1997) tested two-cell wide by eleven block high concrete masonry specimens with reinforcing splices provided at mid-height. Figure 2.9 shows the test set-up where the vertically constructed specimens were rotated to the horizontal position for testing as a simply supported beam under four-point loading. Pull- pull test specimens similar to those reported by Schuller et al. (1993) (Figure 2.6) were also tested under direct tension to compare their capacity with the beam test specimens. The pull-pull specimens had identical splice lengths and material properties as the beam specimens.

The specimens were reinforced with No. 4 (I), No. 6 (I), and No. 8 (I) (12, 20 and 25 mm, respectively) bars with lap splice lengths ranging from 5 to 30 times the diameter of the spliced bars used.  All beams reinforced with No. 6 (I) bars failed by splitting of the masonry assemblage along the splice for splice lengths up to 20 times the diameter of the longitudinal bars. These specimens developed 1.3 to 1.6 times lower failure loads as compared to the pull-pull specimens with the same lap length and bar size. A clear explanation for this difference was not provided, though it was suspected that the cracks in the grout caused by the flexure in the beam might have reduced the failure load in these specimens.
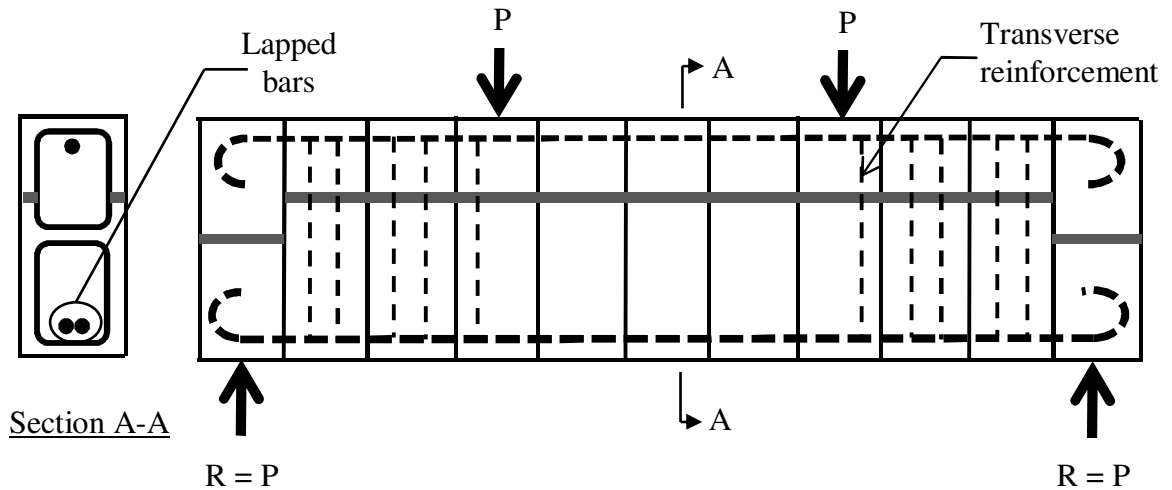
Figure 2.9: Beam lap splice tests by Matsumara (Matsumara et al., 1997).

## 2.5 Full-Scale Wall Tests

The flexural behaviour of lintel beam specimens is expected to be different than that of reinforced concrete block walls. Walls under flexure typically have a smaller moment arm as compared to the lintel beams due to their reduced effective depth. Moreover, shear reinforcement that improves splice capacity cannot be provided as effectively in flexural walls. These factors are likely to affect the tension splice capacity. The confining effect of the regular full blocks in running bond walls is also absent in lintel beams as they are usually constructed with open ended blocks. Observing the distinct anchorage failure behaviour in concrete block walls, Cheema and Klingner (1985a) stated that lintel beam specimens are not suitable for testing the bond capacity of deformed reinforcing bars in walls.

26

### 2.5.1 Uniat's (1983) full-scale wall tests

Uniat (1983) tested one and one half block wide by eighteen block high masonry walls under lateral loading to investigate splice capacity in walls. Figure 2.10 shows the elevation, side-view, and cross-section of the test specimens. The walls were constructed in running bond using standard 200 mm concrete blocks with deformed reinforcing bars spliced at mid-height. Only the middle cells containing the lapped reinforcing bars were grouted. The protruding reinforcing bars at top and bottom of the specimens were welded to ¼ in. x 3 in. (25 mm x 75 mm) square steel plates to provide end anchorage and prevent any end slip of the reinforcement. Four-point lateral loading was applied to create a constant moment region along the splice length.

Minimum splice lengths of 200, 350, and 500 mm were provided for specimens reinforced with No. 10, No. 15 and No. 20 reinforcing bars, respectively. The splice lengths were selected as per recommendations from Baynit's (1980) investigation to ensure that the specimens would fail in bond rather than flexure. Walls with continuous longitudinal reinforcing bars were also tested to compare to the performance of the walls with spliced bars.

The walls were tested in their vertical position with the applied load and deflection data logged as testing progressed. Surface mounted strain gauges attached to the reinforcing bar surface beyond the splice region were used to measure bar force. This internal instrumentation locally impairs the bond between the grout and the reinforcement and is likely to affect the splice capacity. The axial stress resulting from the self-weight of the
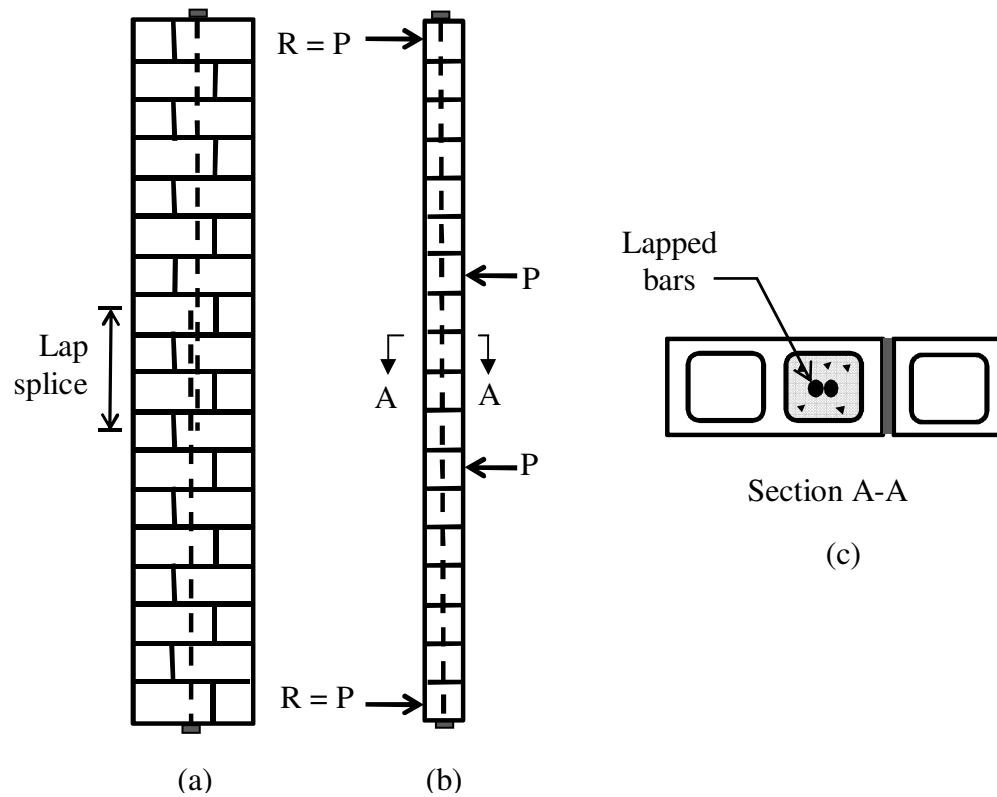
Figure 2.10: Full-scale wall tests by Uniat: (a) elevation, (b) side-view, and (c) cross-section (Uniat, 1983).

wall therefore reduced the tension within the lap splice length. Though rollers were used to allow the rotation at the bottom of the specimens, there is the possibility that some level of axial restraint occurred due to the specimen self-weight. The axial restraint under lateral load can exert a compression force, thus increasing the lateral-load carrying capacity. The presence of axial restraint causes the wall to be statically indeterminate and complicates the analysis. A disturbance in the ideal stress distribution surrounding the splice adjacent to the wall's tension face is very likely to occur due to this phenomenon.

An analysis of the strain gauge data showed that all specimens developed the yield capacity of the reinforcement prior to failure. Walls spliced with No. 10 bars failed by pullout of the reinforcement. Removal of the face shell and grout surrounding the splice reinforcing bars showed a large reduction in the bar's cross-sectional area (necking) without any indication of bond failure. The specimen reinforced with No. 15 bars and a 350 mm splice length showed a sudden failure with vertical splitting cracks at the tension face of the specimen accompanied by flexural horizontal cracks. The wall reinforced with continuous No. 15 deformed longitudinal reinforcing bars with no lap splice resulted in a flexural failure without developing any splitting cracks on the tension face.

The comparison of the mid-height moment versus mid-height deflection curves showed excellent agreement between the specimens with and without splices (i.e. continuous reinforcement) for all bar sizes. The mid-height deflection increased linearly with increasing moment from cracking up to the actual yield load. The slope of the curve then reduced and the specimen continued to deflect with a small increase in moment until failure occurred. The measured mid-height deflection after yielding of the longitudinal reinforcement varied between specimens. As all specimens failed by yielding of the reinforcement, the author concluded that Baynit's (1980) recommendations for splice lengths are overly conservative.

### 2.5.2 Ahmadi's (2001) full-scale wall tests

Ahmadi (2001) tested vertically constructed walls in the horizontal position as shown in Figure 2.11(a). The walls were 1½ blocks wide by seven blocks tall in running bond

assemblage with all cells fully grouted. Two symmetrically placed lap splices were provided at the mid-height of the specimens. Figure 2.11(b) shows that the specimens were simply supported and tested under four-point loading. This test setup allows rotation of the end blocks reducing the possibility of the development of an axial compression force. The report lacks information regarding the end anchorage detail used for the longitudinal reinforcing bars.

Two sets of walls with 5 walls in each set were tested. The walls were longitudinally reinforced with either No. 4 (I) or No. 5 (I) (12 and 16 mm) deformed steel bars. Control splice lengths of 600 mm and 770 mm were selected for No. 4 (I) and 5 (I) reinforcing bars respectively, as per the recommendation of Building Code Requirements for Masonry Structures (ACI 530/ASCE 5/ TMS 402, 1999). One wall in each set was constructed with the control splice length. Spliced reinforcing bars in the other four walls were debonded from the surrounding grout using tape at the splice locations. The debonded length was increased by 25% in each successive wall leaving the last wall with a completely debonded splice length (i.e. tape along the entire splice length).

The wall splice specimens with the control lap length and the specimens with 25% debonded splice lengths failed in shear as identified by diagonal cracks that started at the supports. Specimens with 50% and higher debonded splice lengths failed in bond with reinforcing bar pullout for both bar sizes. The walls reinforced with No. 5 (I) and No. 4 (I) bars with 50% debonded length showed a decreased splice capacity of 16%
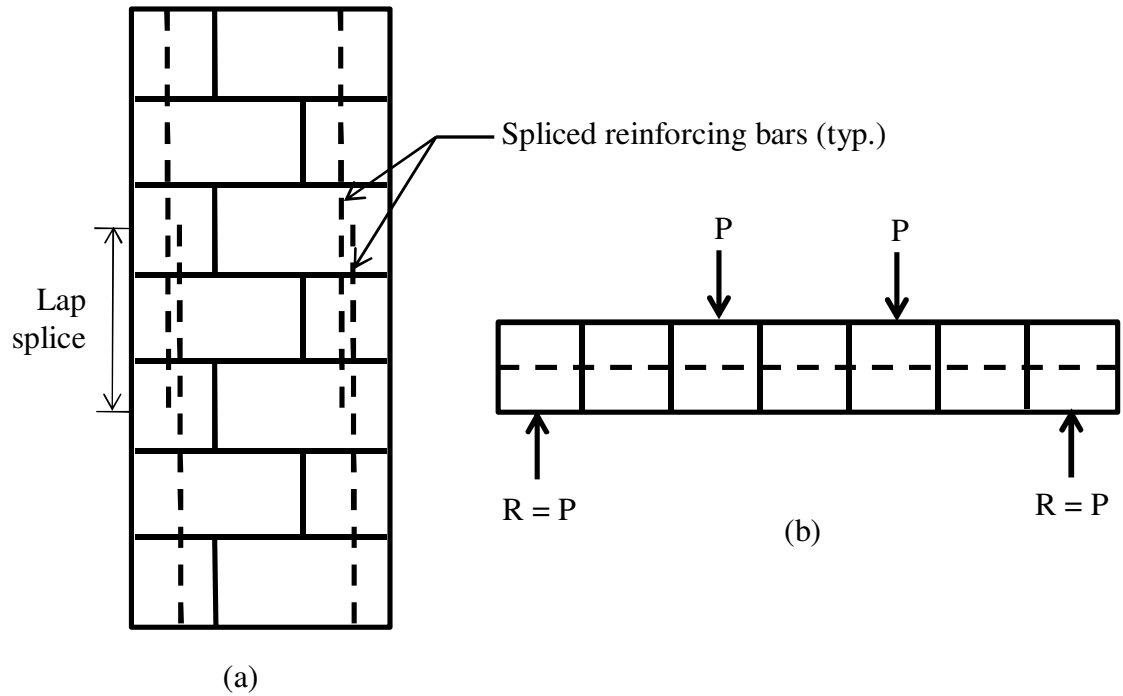
Figure 2.11: Flexural wall test specimens by Ahmadi: (a) plan, and (b) loading
arrangements (Reproduced from Ahmadi, 2001).

and 32%, respectively, as compared to the splice capacity of the control specimens. The

splice capacities of the specimens reinforced with smaller diameter reinforcing bars

reduced more rapidly as compared to reinforced with the larger reinforcing bar sizes.

## 2.6  Non-Contact Lap Splices

Non-contact lap splices are used in masonry construction and are permitted by the

current edition of the Canadian masonry code (CSA S-304.1, 2004). However, research

supporting this recommendation could not be identified though some works related to

the use of non-contact lap splices in reinforced concrete members were reviewed.

### 2.6.1  Sagan et. al.'s  (1991) flat plate concrete specimens

Sagan et al. (1991) tested 47 full-scale flat plate concrete specimens reinforced with two symmetrically spaced non-contact lap splices under direct tension. The length of the specimens varied from 34.5 to 42 in., while the width varied from 10 to 42 in. Figure 2.12(a) shows the reinforcing bar arrangement, and Figure 2.12(b) shows the cross-section of the flat plate specimens with thickness varying from 4.125 in. to 5.5 in. Two longitudinal reinforcing bar sizes and lap splice lengths were investigated: No. 20 bars with 22.5 in. lap splice lengths, and No. 25 bars with 30 in. lap splice lengths. The spacing between the lapped bars ranged from 0 (i.e. the lapped bars were in contact) to 8 in. The effect on the inclusion and spacing of the transverse reinforcement was also investigated in this research program.

The results showed that the transverse reinforcement plays a vital role for proper functioning of non-contact lap splices: without transverse reinforcement specimens showed a 30 to 40% reduction in splice capacity compared to similar specimens with transverse reinforcement. Diagonal surface cracking formed between the non-contact spliced bars in the specimens; failure then occurred with evidence of in-plane splitting of the concrete. The researchers concluded that, with the proper transverse reinforcement, it is conservative to neglect the effect of the spacing between the lapped bars provided that the spacing is less than 12 bar diameter or 12 in.

### 2.6.2   Hamad and Monsour's (1996) reinforced concrete slab tests

Non-contact lap splice performance when subjected to flexural effects was evaluated by Hamad and Monsour (1996). Seventeen slabs were tested with lap splices within the

constant moment region. Figure 2.13(a) shows the longitudinal dimensions of the specimens along with the loading condition, and Figure 2.13(b) shows the splice arrangements for the slabs. Three 300 mm lap splice lengths were provided within each specimen reinforced with either 14 or 16 mm diameter bars, and a 350 mm lap splice length was used for specimens reinforced with 20 mm diameter bars. Transverse reinforcement was only provided within the shear spans. The clear spacing between the spliced bars varied from 0 to 50% of the lap splice length. Information regarding anchorage at the ends of the longitudinal reinforcing bars was not presented in the report.
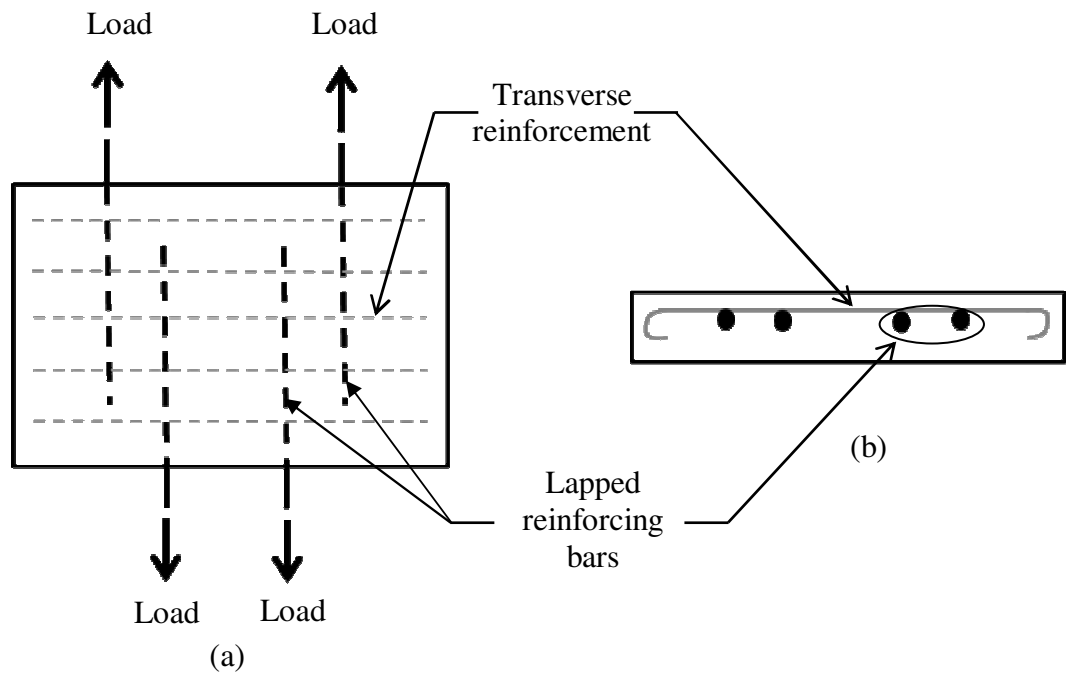


Figure 2.12: Full-scale wall plate tests by Sagan et al. (1991): (a) elevation, and (b) cross-section. (Sagan et al., 1991).
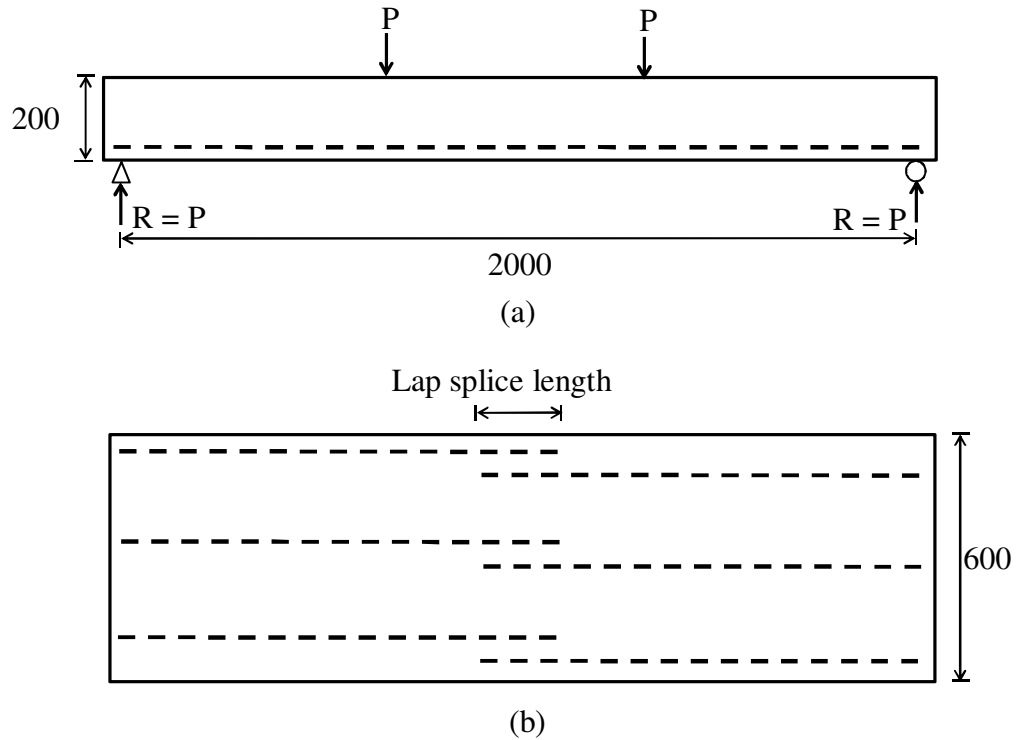
Figure 2.13: Full-scale reinforced concrete slab tests by Hamad & Monsour (1996): (a) elevation, and (b) plan (Hamad and Monsour, 1996).

Bond failure was observed in all specimens, with longitudinal splitting cracks evident along the splice length on the member's tension face. Diagonal surface cracks between the spliced bars were also observed when the spacing between the spliced bars exceeded 30% of the splice length. The specimen with a 300 mm long contact lap splice developed 70% of the yield load at failure. The splice capacity of the non-contact spliced bars improved by up to 10% compared to the contact lap splice when the clear spacing between the bars was less than 30% of the splice length. The effect diminished for further increases in clear spacing between the lapped bars. All reinforcing bar sizes showed similar trends.

## 2.7 Summary

A review of the existing literature showed that single bar pullout tests provide unrealistic results due to the confining pressure induced by the support reaction. Pullout specimens with lapped bars were therefore tested in direct tension by later researchers. Double pullout specimens such as those tested by the NCMA (1999) appear to be the most realistic pullout specimens to date, though their validity for evaluating splice capacity within flexural members has never been established.

A review of the literature showed that the lap splice capacity in full-scale beam specimens is lower than that obtained from single bar pullout specimens with identical geometry and material properties. Lap splices in full-scale walls with recommended lengths from beam test programs performed better than predicted theoretically. A lack of sufficient replicate specimens did not allow for the establishment of statistically confident results for the reported results in these test programs. It does not appear that the performance of non-contact lap splices has been evaluated in reinforced masonry.

An experimental program was therefore designed to evaluate lap splice capacity in both double pullout specimens and full-scale wall splice specimens to evaluate the performance of both contact and non-contact lap splices. Replicate specimens were tested to establish whether the splice performance differs significantly for each type of specimen tested. The following chapter describes the selection of splice length and the number of replicate specimens for the current test program followed by a description of the construction of the specimens and their test setups.

## CHAPTER 3
## EXPERIMENTAL DESIGN, SPECIMEN CONSTRUCTION, AND TEST SETUP

### 3.1 Introduction

Both double pullout and wall splice specimens with identical cross-sectional geometry
and splice lengths were constructed with two different splice arrangements: contact and
non-contact lap splices. The material properties and all other parameters were kept
constant. An equal number of replicate specimens were constructed for each splice
arrangement and specimen type. Direct tension was applied to the reinforcement in the
double pullout specimens while the wall splice specimens were tested under four-point
loading such that the specimens experienced out-of-plane bending. This chapter presents
the description of the specimens, including the companion specimens used to establish
material properties, followed by their construction process and test setup.

### 3.2 Splice Length Selection

A review of the available literature revealed several recommended equations for
development and splice length by different authors to achieve full development of the
reinforcement (Cheema and Klingner, 1985b; Schuller at al., 1993; MSJC, 1995).
Oragun et al. (1977) reported from statistical analysis that no definite trend exists that
could differentiate the development length requirement from that of the splice length

requirement and, thus, equations derived from experiments of specimens with development lengths can be used to calculate required splice length. In the current study, therefore, both development length and splice length recommendations from the reviewed literatures were used to calculate necessary splice length for No. 15 deformed bar, as that is the most common bar size used in masonry construction in Canada. A lap splice length was selected assuming typically used masonry, grout, and reinforcing steel properties, so that the specimens would fail in bond.

Suter and Keller (1982) recommended an average bond stress of 4.26 MPa, based upon the results of Baynit's (1980) beam anchorage tests, to calculate the necessary splice length. Their calculation yielded a 375 mm required splice length for Grade 400 No.15 bars using Equation 2.1. This is reasonably close to the 350 mm splice length for the same bar size and grade suggested by Suter and Fenton (1985) based on Uniat's (1983) test results, and to Cheema and Klingner's (1985c) resulting development length of 355 mm based on substituting their suggested average bond stress of 4.5 MPa for No.15 bars in Equation 2.1.

Schuller et. al. (1993) presented an equation from their test data to calculate the required splice length, which was assumed to be equivalent to the development length:

$$l_d = \frac{C_1 d_b{}^2 f_y}{(t - d_b) f_{gt}} \dots\dots\dots\dots\dots\dots\dots\dots\dots\dots\dots\dots\dots\dots\dots\dots\dots\dots\dots\dots\dots\dots\dots\dots\dots\dots(3.1)$$

where, $C_1$ is the nonlinearity coefficient determined from laboratory testing and set equal to 3.20, as recommended for typical grout, $d_b$ is the bar diameter in mm, $f_y$ is the yield stress of the reinforcing bars in MPa, t is the thickness of masonry specimen in

mm, and $f_{gt}$ is the tensile strength of grout in MPa. The basic development length calculated from Equation 3.1 is expected to result in a stress in the reinforcing bars at failure that is, at a minimum, 1.25 times the yield stress at failure. A 474 mm splice length therefore resulted for No.15 bars using a tensile grout strength of 3 MPa as recommended for typical grout with a minimum 25 MPa compressive strength.

The National Concrete Masonry Association (1999) found an excellent agreement of the lap splice capacity in double pullout specimens when the splice length was set equal to the development length recommended by the Masonry Standard Joint Committee (MSJC, 1995). The development length, $l_d$, is given as:

$$l_d = \frac{0.13 d_b^2 f_y}{K_1 \sqrt{f_m}} \dots\dots\dots\dots\dots\dots\dots\dots\dots\dots\dots\dots\dots\dots\dots\dots\dots\dots\dots\dots\dots(3.2)$$

where $d_b$ is the bar diameter in inches, $f_y$ is the reinforcement yield strength in psi, $K_1$ is the minimum clear cover to the reinforcement in inches, and $f_m$ is the compressive strength of the masonry in psi. Based on this equation, a 400 mm development length is therefore required for Grade 400 No.15 bars assuming a masonry compressive strength of 12 MPa, which is equivalent to the typical compressive strength for masonry assemblages used in Canadian construction.

The overall minimum reported development length for Grade 400 No.15 reinforcing bars in order to ensure yielding is 350 mm, based on results from Suter and Keller's work (1982). This value is somewhat greater than the minimum specified splice length of 300 mm required for all bar sizes required by the current edition of the Canadian Masonry Design Code CSA S304.1-04 (CSA, 2004a). A 300 mm splice length was

therefore provided for all the specimens in the current study in an attempt to ensure bond failure.

## 3.3 Determination of the Number of Replicate Specimens

A minimum of six replicate specimens are usually needed to produce statistical parameters that can successfully identify outliers and for reasonably calculating the mean splice capacity (Bartlett, 1999). The minimum number of specimens needed for investigating the existence of a statistically significant difference between the mean values of two populations (i.e. two specimen types or specimens with two different splice arrangements) was established from an assumed coefficient of variation and the difference between the means of the two specimen groups.

Previous reports with sufficient results from replicate specimens for either pullout specimens or wall specimens were not identified to provide the basis for the required assumptions of expected statistical parameters to calculate the number of required replicate specimens in each group. The statistical parameters for the current study were therefore assumed based on a previous experimental study by Paturova (2006) where masonry prisms were tested to investigate the effect of confinement on compressive strength. A coefficient of variation of 12.7% for the compressive strengths within each group was used to estimate the number of required replicate specimens when a minimum of 10% difference between the mean compressive strengths in the two groups could be identified as being statistically significant at a 90% confidence level. However, a review of existing literature (NCMA, 1999; Schuller et. al., 1993) using

only three replicate specimens suggested that the results of pullout specimens are less variable (COV = 3 to 6%). Considering the possibility of greater variability in wall and double pullout specimens, a value of 8% was selected as the coefficient of variation for calculating the necessary number of replicate specimens in the current investigation. A minimum of 8 replicate specimens was therefore required to establish the existence of a statistically significant difference between the means of two populations at the 95% confidence level. Appendix 3A presents the calculations supporting these findings.

Sixteen double pullout specimens were therefore constructed, with eight replicate specimens having either contact or non-contact lap splices. The same numbers of wall splice specimens were constructed with the same two lap splice arrangements.

## 3.4 Specimen Description

Double pullout specimens that were two and a half blocks wide and three courses tall were constructed in a running bond pattern with all cores fully grouted. The wall splice specimens were thirteen blocks high with the identical cross sectional geometry to those of the double pullout specimens. The splice lengths were kept constant for both specimens types with either contact or non-contact splices provided. The following sections provide the detailed geometry of the specimens tested.

### 3.4.1 Double pullout specimens

Figures 3.1(a) and (b) show the plan view and the elevation of the double pullout specimens with contact and non-contact lap splices, respectively. All of the double

pullout specimens were two and a half blocks wide and three courses tall to accommodate the 300 mm splice located at the specimen mid-height. The reinforcing bars were centered within the common 84 mm grouting width between vertically adjacent blocks. The excess 150 mm of bar length at the top and bottom of the specimens, outside of the lap splice length, yet within the specimen height, was debonded using lubricated plastic sheaths of diameter slightly greater than that of the reinforcing bars. The reinforcing bars extended beyond both the top and the bottom of the specimens to allow them to be mechanically spliced with the high strength bars used in the testing frame.
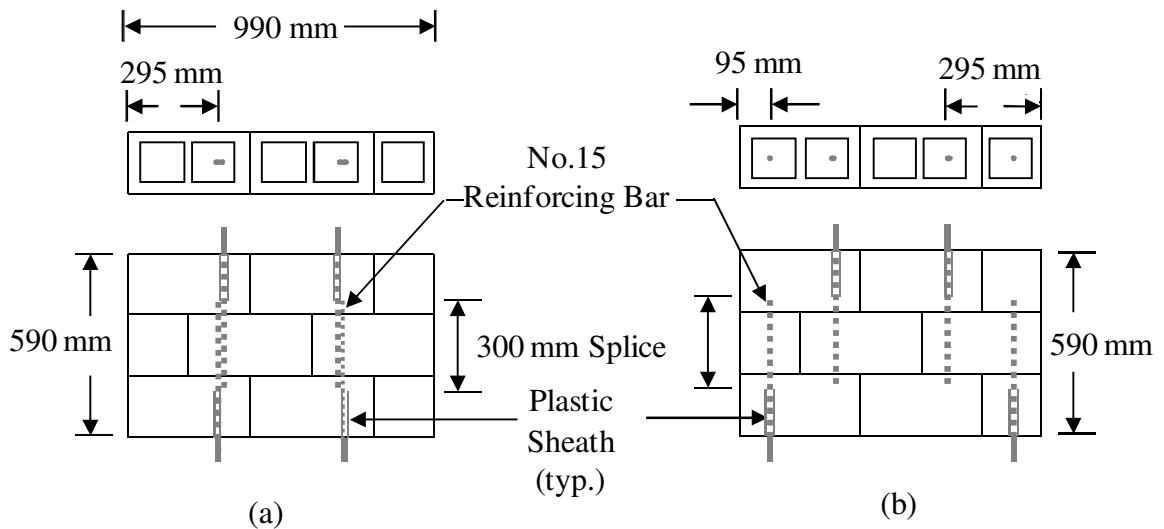


Figure 3.1: Elevation and plan of double pullout specimens with: (a) contact lap splices, and (b) non-contact lap splices.

### 3.4.2 Wall splice specimens

Wall splice specimens were built with the identical cross-sectional geometry as that used for the double pullout specimens. Figures 3.2(a) and (b) show the elevation of the
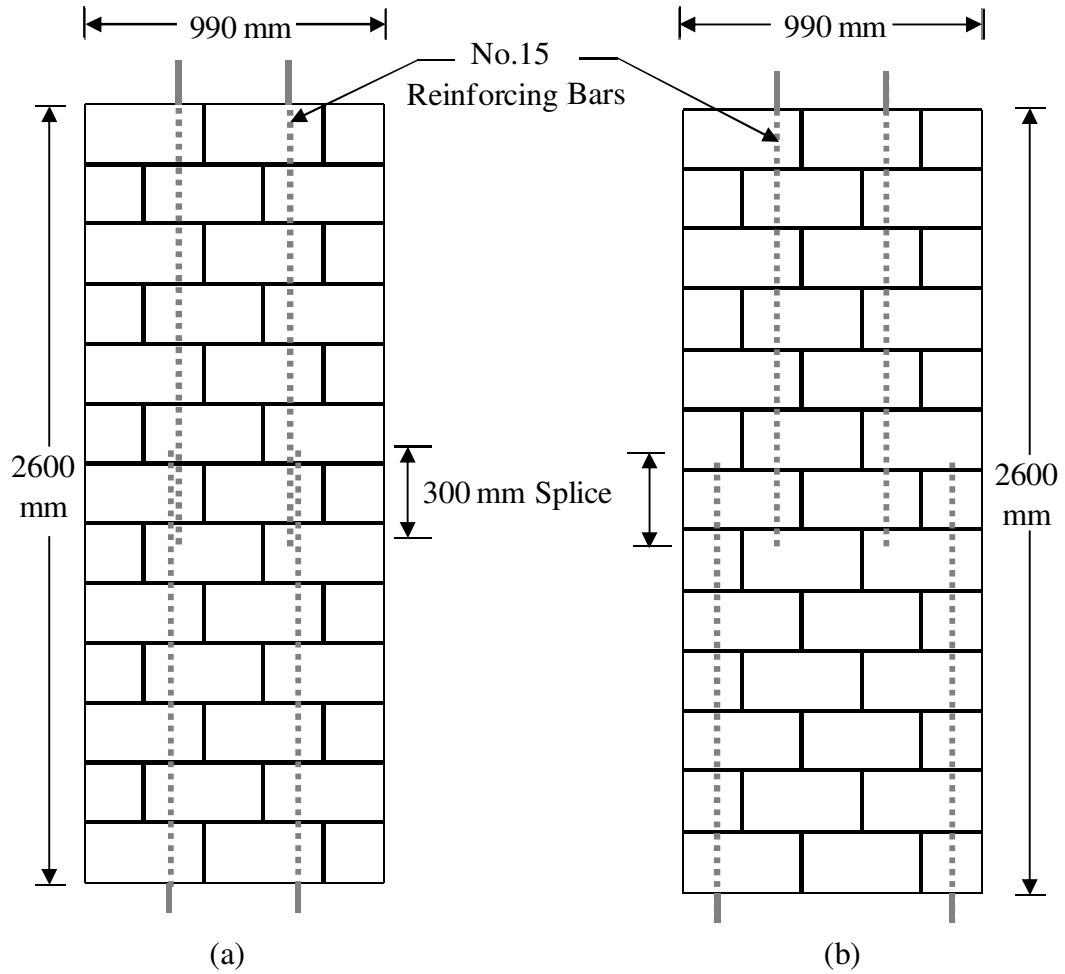
Figure 3.2: Elevation of wall splice specimens with: (a) contact lap splices, and (b) non-contact lap splices.

wall splice specimens with contact and non-contact lap splices, respectively. The specimens were thirteen courses tall and were constructed in a running bond pattern with the splices provided at mid-height. The location of the reinforcing bars was identical to that provided for the double pullout specimens.

The shear capacity of the walls without bed-joint shear reinforcement was sufficient to resist the shear resulting from the applied load predicted to cause yielding of the

reinforcement, and therefore, the specimens were constructed without shear reinforcement. The length of the reinforcing bars that extended beyond both top and bottom of the walls were connected to steel plates using mechanical bar couplers to prevent their end slip during testing and therefore ensure a bond failure within the lap splice length. The details of this end anchorage are provided in Section 3.7.2.

## 3.5 Materials

All specimens were constructed with locally available materials so that they represented typically constructed masonry walls. The materials were ordered in two phases due to limited storage facilities in the laboratory. Slight variations in the material properties therefore resulted between the two construction phases.

### 3.5.1 Concrete masonry block units

Standard full concrete blocks with overall dimensions of 390 mm x 190 mm x 190 mm and half concrete blocks with overall dimensions of 190 mm x 190 mm x 190 mm were supplied by Cindercrete Products Ltd. of Saskatoon.  Figure 3.3 shows the detailed dimensions of these blocks. The plastic wrapped concrete block pallets were stored in the laboratory for at least two weeks prior to specimen construction to equilibrate with the laboratory humidity and temperature. The blocks were supplied in three stages, though all came from the same production batch. Three block samples from each stage were tested for compressive strength.
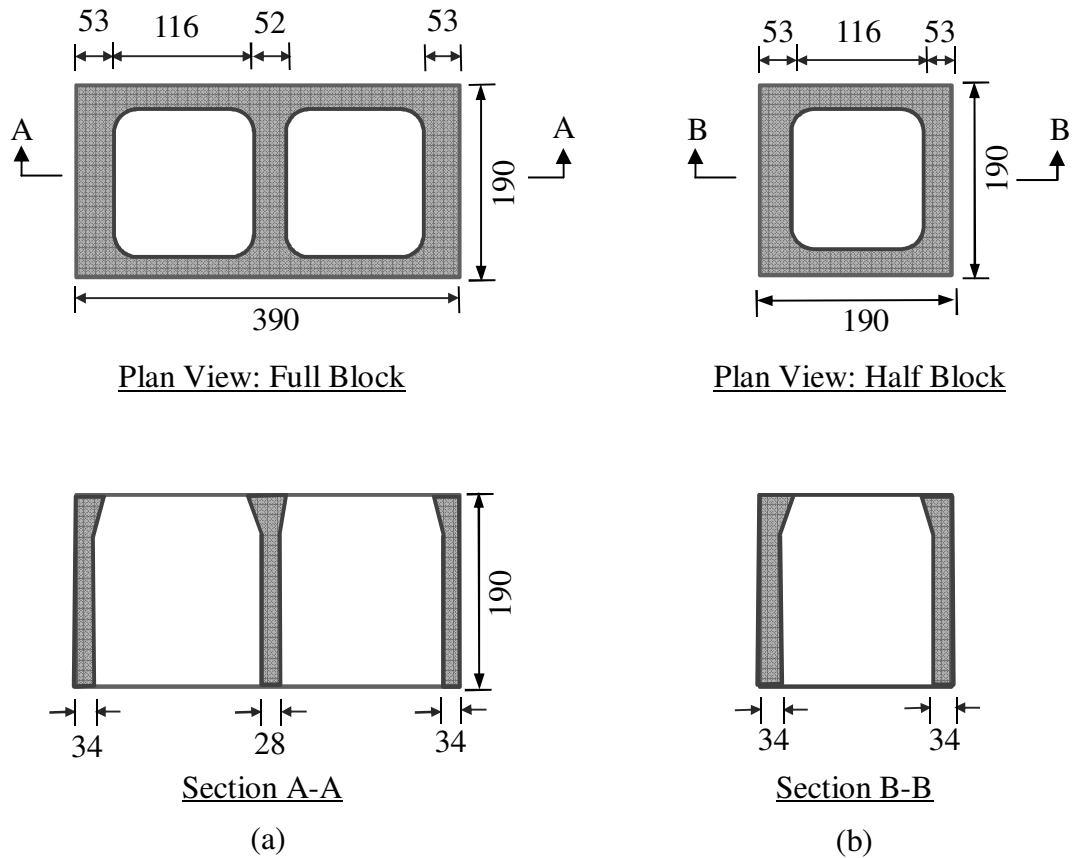
Figure 3.3: Typical concrete masonry blocks: (a) full block units, and (b) half block units. (Dimensions are established from averaging the measured values)

### 3.5.2 Mortar

Mortar is a mixture of sand, cement, and water, and is provided between the concrete blocks as a joining material. Locally available masonry sand was supplied and then stored in a steel bin in the laboratory. Table 3.1 shows the masonry sand gradation from a sieve analysis performed in accordance with CSA test method A23.2-2A (CSA, 2004d). The sand met the aggregate gradation requirements for mortar as specified in CSA A179-04 (CSA, 2004c). Type "S" Lehigh masonry cement was supplied in 40 lb bags and stored on the laboratory floor.

Table 3.1: Aggregate gradation for masonry sand.

| ISO sieve size | Cumulative % passing | | |
|---|---|---|---|
| | Sample 1 | Sample 2 | CSA A179-04 (2004c) requirements |
| 5 mm | 98 | 100 | 100 |
| 2.5 mm | 93 | 99 | 90-100 |
| 1.25 mm | 83 | 98 | 85-100 |
| 630 µm | 64 | 93 | 65-95 |
| 315 µm | 28 | 64 | 15-80 |
| 160 µm | 7 | 32 | 0-35 |

Type "S" mortar with a minimum 28-day compressive strength of 12.5 MPa is required for structural masonry as specified in CSA A179-04 (CSA, 2004c). The mortar must also have an initial flow rate of 100 to 115% to maintain workability. A range of grout batches were designed with a 1:3 cement to sand ratio by weight to determine the suitable water content to produce sufficient workability as well as to achieve the specified minimum compressive strength. Based on the obtained data, a 0.7 water to cement ratio was selected to meet all of the specified criteria.

### 3.5.3 Grout

Grout is the mixture of cement and aggregate used to fill the cells of hollow concrete block masonry walls. The grout establishes bond between the reinforcement and the surrounding concrete blocks and so enables the block walls and reinforcing bars to work as a composite element.

High slump grout with a maximum aggregate size of 10 mm was selected for the current program. Locally available masonry gravel that contained a mixture of fine and coarse aggregate was used for the preparation of the grout. CSA A179-04 (CSA, 2004c) provides separate gradation limits for the fine and coarse aggregate and sets a guideline for a 2:3 fine to coarse aggregate mix proportion. The gravel was pre-mixed by the supplier to satisfy CSA A179-04 (CSA, 2004c) and was supplied in two phases and stored on the laboratory floor. The gradation of the gravel samples from both phases is shown in Table 3.2. However, no specifications are provided for premixed grout in CSA A178-04 (CSA, 2004c). Lehigh Type GU (Formerly Type 10) cement was used for grout preparation. Cement was supplied in 40 kg bags and stored in the Structures Laboratory until the time of specimen construction.

Table 3.2: Aggregate gradation for grout gravel.

| ISO sieve size | Cumulative % passing | | | |
| --- | --- | --- | --- | --- |
| | Phase 1 | | Phase 2 | |
| | Sample 1 | Sample 2 | Sample 1 | Sample 2 |
| 5 mm | 77 | 75 | 61 | 64 |
| 2.5 mm | 71 | 69 | 55 | 57 |
| 1.25 mm | 62 | 60 | 46 | 48 |
| 630 µm | 43 | 42 | 33 | 35 |
| 315 µm | 8 | 8 | 8 | 8 |
| 160 µm | 1 | 1 | 1 | 1 |

A cement to gravel ratio of 1:5 was selected for the grout mix design. CSA A179-04 (CSA, 2004c) recommends a slump between 200 to 250 mm to produce sufficient workability, and a minimum 12.5 MPa 28-day compressive strength. Several grout batches were prepared with water content varying from 0.9 to 1.1 to determine the suitable water content to meet the above specifications. The batch mix with a 1.0 water to cement ratio met the compressive strength requirement and produced a slump ranging from 230 mm to 250 mm. This water content was therefore selected for grout batch preparation for Phase 1 specimen construction.

Sieve test results shown in Table 3.2 revealed that the gravel supplied for Phase 2 construction had more coarse aggregate compared to that supplied in Phase 1. A water to cement ratio of 1.0 produced slumps in excess of 260 mm in trial mixes containing the gravel supplied for the second phase of specimen construction. The water content was therefore reduced to 0.95 based on the trial mix test data for Phase 2 construction to reduce slumps to within 240 to 250 mm. The trial mix test data and selection of water to cement ratio for both construction phases is presented in Appendix 3B.

### 3.5.4 Reinforcing bars

Grade 400 standard deformed No.15 bars were used as reinforcement for the test specimens. Bars were supplied from two separate heat batches and stored on the laboratory floor. Bar samples collected from each batch were tested using the Instron 600DX Universal Testing Machine in accordance with ASTM A370 (ASTM, 2008) test procedures to establish the reinforcing bar properties including: the yield strength,

modulus of elasticity, strain and slope at the initiation of strain hardening, and the ultimate stress for each heat batch.

## 3.6 Construction

Construction of both the double pullout and wall splice specimens was performed by an experienced mason in the Structures Laboratory. The mortar and grout required for the construction was also prepared in the laboratory using the predefined mix ratios as described in Sections 3.4.1 and 3.4.2, respectively. The project was completed in two construction phases due to limited space available in the laboratory. Phase 1 was completed between October 6 and 7, 2009 and included six double pullout specimens and two wall splice specimens. The remaining ten double pullout specimens and fourteen wall splice specimens were constructed in Phase 2, which started on January 18, 2010 and was completed on January 26, 2010. Half of both double pullout specimens and wall splice specimens in each construction phase were built with contact and non-contact lap splices, respectively.

### 3.6.1 Splice preparation

The length of the reinforcing bars required for both the double pullout and wall splice specimens was calculated considering the portions extending from both ends of the specimens that were used for coupling with the high strength bars of the test setup for the double pullout specimens and end anchorage as required for the wall splice specimens. The calculated lengths were cut from the 6 m long as-received bars using a mechanical saw. The bars were then inspected for rust and any other manufacturing

defects. For the specimens with contact lap splices, two spliced bars were lapped by 300 mm and tied using tie wires at both splice ends as commonly practiced by masons. Figure 3.4 show the prepared contact lap splices for the double pullout specimens.
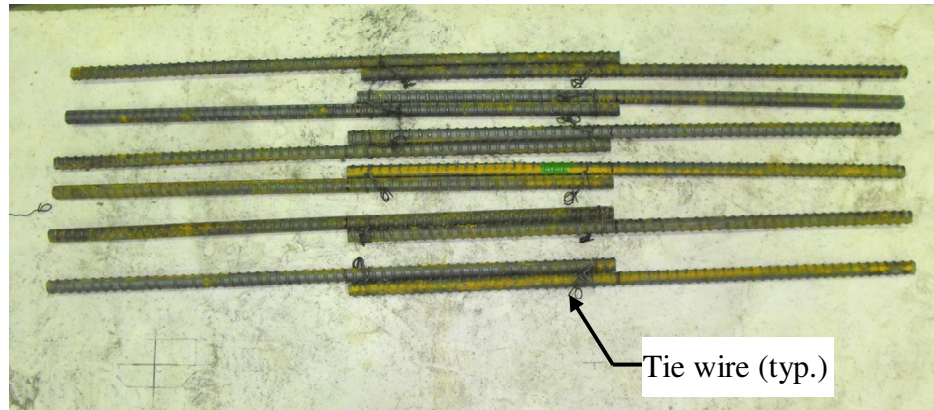


Figure 3.4: Contact lap splice preparation for the double pullout specimens.

### 3.6.2 Mortar preparation

Laboratory prepared mortar was used for the construction of all specimens. The mix proportions for the masonry sand, cement, and water were calculated per batch based on the established mix designs as presented in Section 3.4.1. Figure 3.5(a) shows that half of the sand was first hand mixed with cement and water in a wheelbarrow with a hoe. The remaining sand was then mixed in slowly to prevent the formation of any lumps in the mix. Mortar samples were collected from randomly selected batches for the initial flow test in accordance with CAN/CSA Test Method A3004-C1 (CSA, 2003a) to ensure maintained workability. However, as workability is known to reduce with time, water was added to the mix by the mason as required.

Twelve 50 mm mortar cubes were prepared in construction phase 1: six corresponding to the construction of the double pullout specimens, and the remaining six corresponding with the construction of the wall splice specimens. Twenty four mortar cubes were cast in the second construction phase: 12 cubes each corresponding to the construction of the double pullout specimens and wall splice specimens, respectively. Figure 3.5(b) shows that the cubes were cast in brass moulds in accordance with CAN/CSA A3004-C2 (CSA, 2003b). The moulds were covered with plastic sheets for two days following casting. The cubes were then removed from the moulds and stored in the laboratory environment for curing along with the double pullout and wall splice specimens.

### 3.6.3 Grout preparation

Figure 3.6(a) shows the grout preparation in the Structures Laboratory using a concrete mixer. The amount of material required for a grout batch preparation was calculated from the pre-determined mix design ratio as described in Section 3.4.2. Half of the gravel was first placed with all of the cement in the concrete mixture. Water was added slowly while the machine rotated. After two minutes the rest of the gravel was added to the mixture and the machine continued to rotate for approximately another three minutes. The prepared gravel was then transferred to a wheelbarrow and transported to the construction location. Slump tests were performed for each batch as shown in Figure 3.6(b) to confirm the workability and mix consistency.

Two types of control specimens were prepared for the grout: non-absorbent grout cylinders, and absorptive grout prisms in accordance with CSA A179 (CSA 2004c) and ASTM C1019 (ASTM, 2009), respectively. Figure 3.7(a) shows that four concrete blocks were placed side by side to create 100 mm x 100 mm x 190 mm moulds for the absorptive grout prism test specimens. All mould faces were lined with paper for ease of specimen removal after setting. The grout was placed in two equal layers and rodded 15 times per layer. The control specimens were covered in plastic sheets for two days following casting. Specimens were then removed from the moulds and stored in the laboratory atmosphere for curing along with the double pullout and wall splice specimens.

Figure 3.7(b) shows the non-absorbent cylinders as cast in 100 mm diameter by 200 mm tall plastic moulds. The cylinders were cast in two equal layers rodded 20 times in each layer. The moulds were then covered in plastic sheet for two days. The cylinders were stored in the laboratory atmosphere for curing after removal from the plastic moulds after allowing a minimum of 48 hours period.

A total of six and three non-absorbent cylinders were prepared in construction Phase 1 in conjunction with the double pullout specimens and wall splice specimens, respectively. A total of 24 cylinders were prepared in the second construction phase with 12 cylinders corresponding to the construction of both the double pullout and wall splice specimens. An identical number of absorptive grout prisms were also prepared in both construction phases.

<center>(a)</center>



<center>(b)</center>

Figure 3.5: Mortar preparation: (a) mortar mixing, and (b) mortar cubes.



<center>(a)</center>



<center>(b)</center>

Figure 3.6: Grout preparation: (a) mixing, and (b) slump test.

<center>52</center>
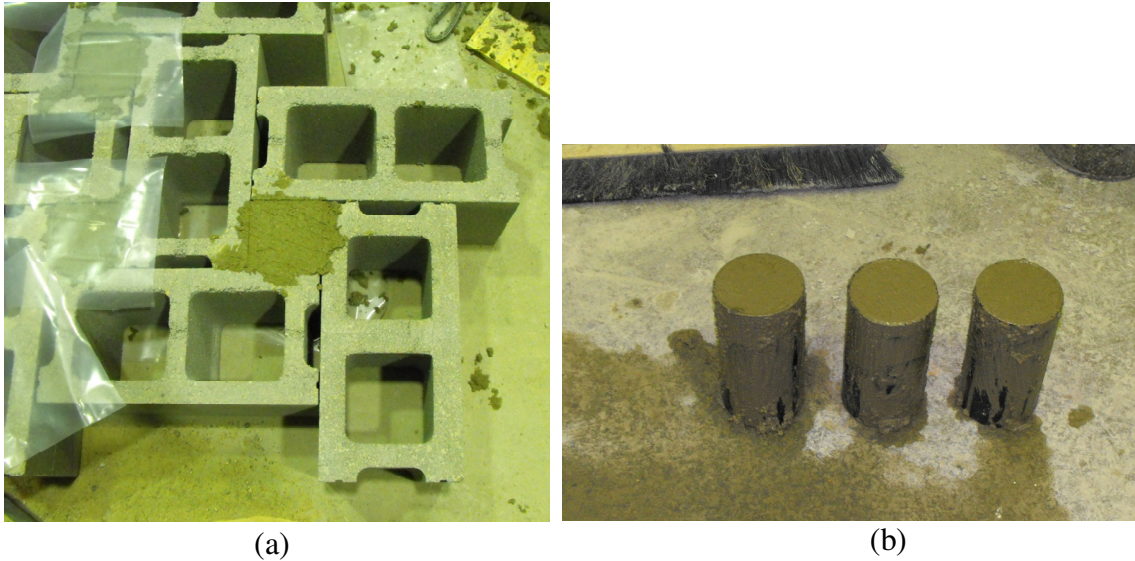
Figure 3.7: Grout companion specimens: (a) absorptive prisms, and (b) non-absorbent cylinders.

### 3.6.4 Double pullout specimens

Figure 3.8(a) shows that the double pullout specimens were built on ¾ inch thick plywood bases supported by three concrete blocks. The dimensions of the plywood bases in plan were 200 mm x 1000 mm with two holes to accommodate the reinforcing bars as they extend below the bottom of the specimens. Eighteen millimeter diameter plastic sheaths were glued inside holes with a 150 mm length projecting above the plywood base. These sheaths debonded the reinforcing bars from the surrounding grout as described in Section 3.4.1 and allowed for their proper positioning. Figure 3.8(b) shows the construction of the double pullout specimens by an experienced mason.
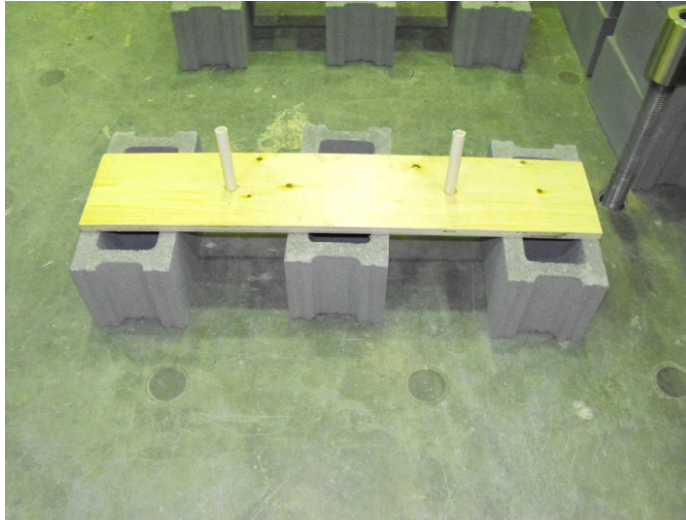
<div align="center">(a)                                 (b)</div>

Figure 3.8: Double pullout specimen construction: (a) base, and (b) block laying by mason.

The three blocks high double pullout specimens were allowed to set for 12 to 24 hours before grouting the cells. The reinforcing bars were inserted into position guided by the holes in the plywood base. Figure 3.9 shows that two plywood strips glued to the top of the double pullout specimens also held the reinforcing bars in position. Plastic sheaths were glued to these plywood strips and extended into the double pullout specimens to again allow the length of the reinforcing bars above the lap splice length to be debonded from the surrounding grout. Figure 3.10(a) shows that the laboratory prepared grout was then hand placed in the cells after reinforcing bar placement. A mechanical vibrator was used to ensure grout compaction [Figure 3.10 (b)].
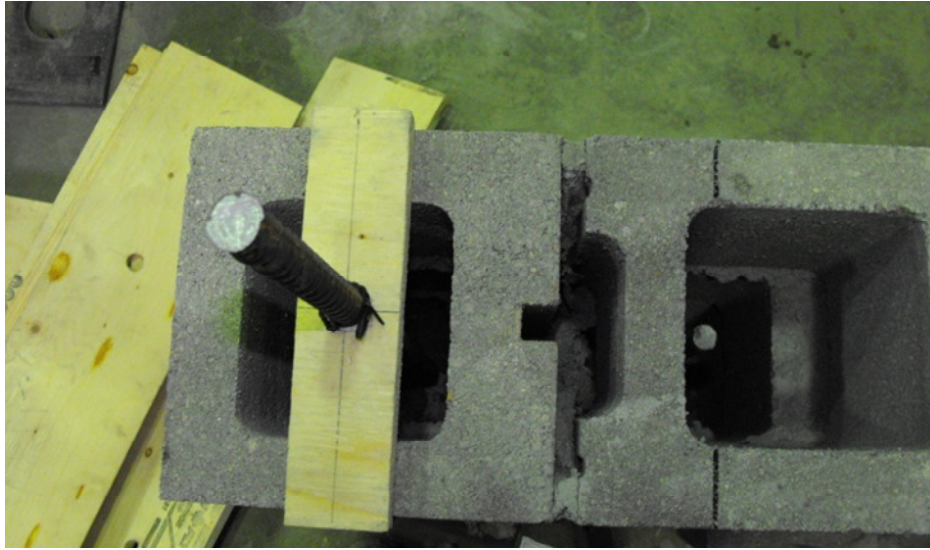
Figure 3.9: Template used for positioning the reinforcing bars.



(a)                                                    (b)

Figure 3.10: Grouting of double pullout specimens: (a) grout placement, and (b) compaction by vibration.

### 3.6.5 Wall splice specimens

Two ¾ inch thick plywood bases, with a geometry identical to those used for the construction of the double pullout specimens, served as the starting point for the construction of the wall splice specimens. The thirteen block high wall splice specimens were constructed in two lifts. Figure 3.11(a) shows that the first lift consisted of eight blocks, was built on the plywood base, and allowed to set for 8 to 12 hours. The reinforcing bars were then inserted from the top of the wall and extended through the holes in the plywood base. Figure 3.11(b) shows the reinforcement positioning at the top of the first lift of the wall construction as maintained by the plywood template that prevented shifting of the bars during subsequent grouting and mechanical vibration. Laboratory prepared grout was then hand placed in the cells of the masonry walls. The grout in all cells was compacted using a mechanical vibrator. Figures 3.12(a) and (b) show the placement of the reinforcing bars extending from the lap splice at mid-height to the top of the wall and the grouting of the first lift, respectively.

Once the grout placed in the first lift set, the second lift of wall construction started with the removal of the plywood templates. Figure 3.13(a) shows the concrete block placement for the remaining construction. The second lift was grouted following an 8 to 12 hours period required for mortar setting. Figure 3.13(b) shows a fully constructed wall splice specimen.

<center>(a)                                       (b)</center>

Figure 3.11: Construction of the first lift - wall splice specimens: (a) block laying, and (b) reinforcing bar placement.



<center>(a)                                       (b)</center>

Figure 3.12: Grouting of the first lift - wall splice specimens: (a) grout pouring, and (b) compaction using mechanical vibration.

### 3.6.6 Masonry prisms

Three block high by one full block wide masonry prisms were constructed in accordance with CSA S304.1-04 (CSA, 2004a). A total of six and three masonry prisms were built during construction Phase 1 in conjunction with double pullout and wall splice specimens, respectively. A total of 24 prisms were built during construction Phase 2 with six prisms for each splice arrangement for both the double pullout and wall splice specimens, respectively. Figure 3.14 (a) shows the block laying for the masonry prisms which were grouted after allowing 8-12 hours for the mortar to set. The completed prisms (Figure 3.14 (b)) were then kept in the laboratory with the test specimens for curing.



(a)                                                    (b)

Figure 3.13: Construction of the second lift - wall splice specimens: (a) block laying, and (b) fully constructed wall splice specimens.

### 3.6.7 Specimen curing

Both the double pullout and wall splice specimens were cured for a minimum of 28 days in the laboratory environment along with all of the companion specimens. The temperature in the laboratory was maintained at 19º C to 21º C with humidity ranging from 14% to 20% as recorded at 7 day intervals during the curing period for both phases. Figure 3.15 (a) shows the fully constructed double pullout and wall splice specimens during the curing period in the Structures Laboratory; and Figure 3.15 (b) shows the companion specimens being cured in the same environment.
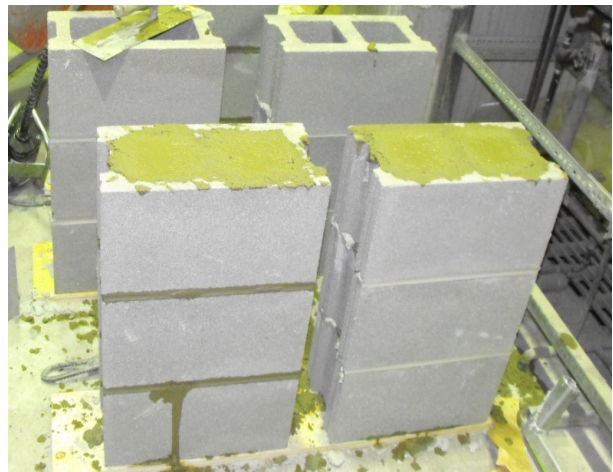


(a)                                                        (b)

Figure 3.14: Masonry prism construction: (a) block  placement, and  (b) completed prisms.
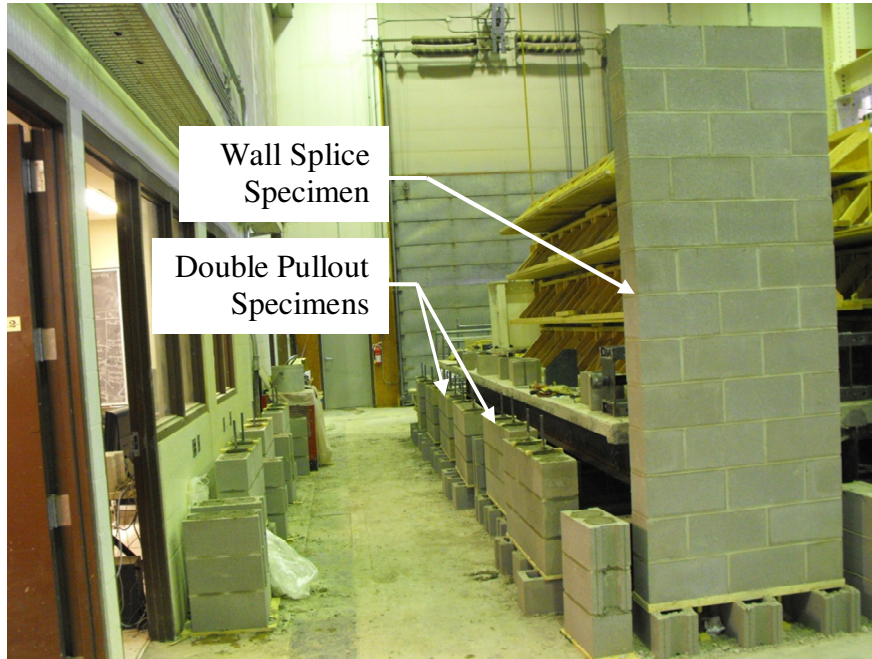
(a)



(b)

Figure 3.15: Specimen curing: (a) double pullout and wall splice specimens, and (b) companion specimens.

## 3.7 Instrumentation and Testing

Specimen testing for each construction phase started shortly after the full 28-day curing period terminated. Companion specimens were tested in conjunction with the double pullout and wall splice specimens to establish the material properties. Table 3.3 summarizes the test schedule followed, along with the number of specimens tested in each construction phase. The following sections describe the instrumentation and testing methods used for both the double pullout and wall splice specimens, as well as for the companion specimens.

Table 3.3: Specimen testing schedule.

| Construction Phase | Test Date | Double pullout specimens | | Wall splice specimens | | Companion specimens | | | |
|---|---|---|---|---|---|---|---|---|---|
| | | CP | NCP | CW | NCW | Mortar cubes | Grout prisms | Grout cylinders | Masonry prisms |
| Phase 1 | Nov. 22-26, 2009 | 3 | 3 | - | - | 6 | 6 | 6 | 6 |
| | Nov. 27-Dec. 1, 2009 | - | - | 1 | 1 | 6 | 3 | 3 | 3 |
| Phase 2 | Mar. 2 - 19, 2010 | 5 | 5 | - | - | 12 | 12 | 12 | 12 |
| | Mar. 22 - Apr. 01, 2010 | - | - | 7 | 7 | 12 | 12 | 12 | 12 |

\* CP and NCP indicate double pullout specimens with contact and non-contact lap splices, respectively. In wall splice specimens, CW and NCW refers to the specimens with contact and non-contact lap splices, respectively. Sections 4.3.1 and 4.4.1 provides more details regarding the identification numbers used for all specimens.

### 3.7.1 Testing of companion specimens

Companion specimens were tested to evaluate the compressive strength of the mortar, the grout, and the masonry assemblage. The Instron 600DX Universal Testing Machine with a 600 kN capacity was used to test the mortar cubes, grout prisms and grout cylinders, while the Amsler Beam Bender with a 2000 kN capacity was used for testing the masonry prisms. The Universal Testing Machine was also used to establish reinforcing bar properties from the tensile tests of bar samples collected from the reinforcing bars used in each construction phase.

#### Mortar cube tests

A total of 12 and 24 mortar cubes were tested during construction Phases 1 and 2, respectively. Compressive strength testing was performed in accordance with CSA A3004-C2 (CSA, 2003b) with a constant loading rate of 10 kN per minute. The load was applied to one of the smooth side surfaces previously lined by the brass moulds to ensure uniform specimen loading. The data acquisition system connected to the testing machine recorded both the applied load and vertical deformation of the cubes throughout the loading range at a rate of 10 Hz.

#### Grout prism tests

Grout prisms were tested in accordance with ASTM C1019-"Standard Test Method for Sampling and Testing Grout"(ASTM 2009) using the Instron 600 DX Universal Testing Machine. Figure 3.16 shows a typical grout prism test arrangement with one fiber board sheets placed both at the top and bottom of the prism to ensure uniform loading over the entire specimen surface. A constant loading rate of 12 kN per minute was applied until
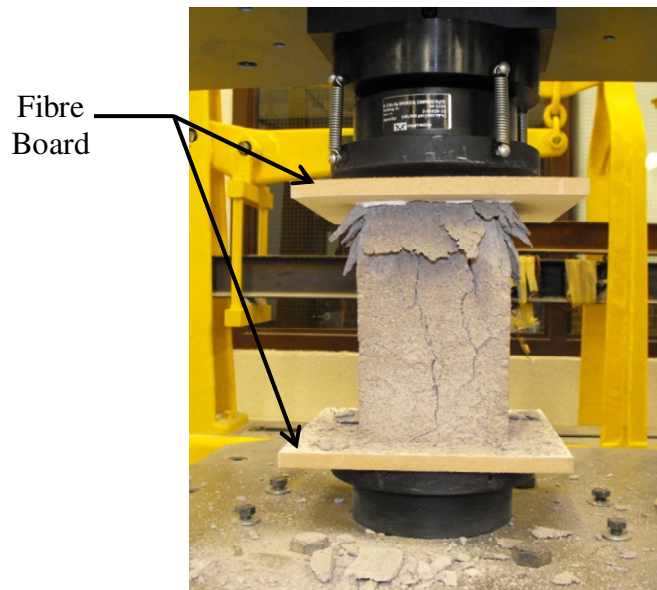
Figure 3.16: Grout prism compressive strength test.

specimen failure. The testing machine's data acquisition system recorded both the applied load and vertical deformation at a rate of 10 Hz. A total of 9 and 24 masonry prisms were tested in conjunction with the Phase 1 and 2 specimens, respectively.

**Grout cylinder tests**

Non-absorptive grout cylinders were tested in accordance with CSA A179-04 (CSA, 2004c). Cylinders were capped with sulfur to ensure uniform loading over the entire specimen surface before placing them in the Instron 600 DX Universal Testing Machine. A constant loading rate of 10 kN/min was applied until failure occurred. The applied load and resulting vertical deformation data was collected by the machine's data acquisition system at a rate of 10 Hz. A total of 12 and 24 specimens were tested in conjunction with the specimens tested in construction Phases 1 and 2, respectively.

**Masonry prism tests**

Masonry prisms were tested in compression in accordance with CSA S304.1-04 Annex D (CSA, 2004a). A total of 9 and 24 masonry prisms were tested during construction Phases 1 and 2, respectively.

Figure 3.17 shows the typical test setup for the masonry prisms. The prisms were lifted from their initial position using the overhead crane in the laboratory and placed under the loading cross-head of the Amsler beam bender. Figure 3.17 (a) and (b) show that fiberboard sheets were placed at both top and bottom of the prisms to ensure uniform distribution of the compressive force. However, it was observed in the first two prism tests in construction Phase 2 that the fiberboard alone was not enough to fill in the gaps at top of the prisms that resulted from the shrinkage of grout in the cells of the concrete blocks. Those prisms were unable to develop a uniform compressive stress. The top of the remaining prisms in Phase 2 tests were therefore leveled with an additional 10 mm layer of mortar 8 to 12 hours before each test.

Figure 3.17(b) shows that two steel angles glued 400 mm apart on a vertical face of the prism were used to obtain displacement measurements during testing using two linear variable displacement transducers (LVDT), each with a 50 mm stroke. The difference in the displacement between the two LVDTs yielded the total vertical deformation between the points. Load was applied at a constant rate of 1 kN/s until failure. The applied load was measured by a load cell with a 1780 kN capacity attached to the loading crosshead.
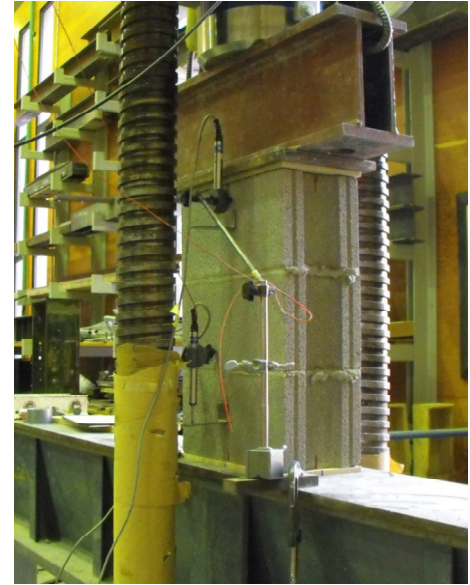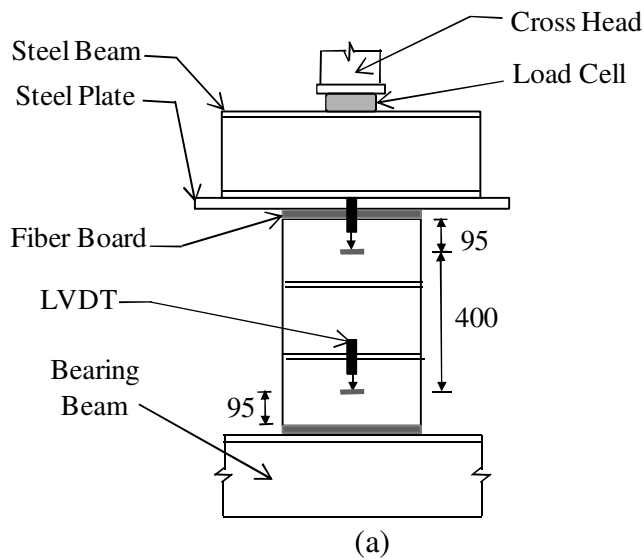
Figure 3.17: Prism test setup: (a) instrumentation, and (b) testing of a masonry prism.

The readings from the load cell and the LVDTs were recorded every second using the data acquisition system manufactured by National Instrument and controlled by LabView$^{TM}$ (2008) software.

**Reinforcing bar tests**

A total of five and four bar samples were tested from reinforcing bars used in construction Phases 1 and 2, respectively. Bars were loaded in tension at uniform rate of 200 N/s in accordance with ASTM A370 (ASTM, 2008) specifications. A strain gauge with gauge length of 50 mm was attached to each reinforcing bar sample to measure the resulting strain in the reinforcing bars. The applied stress and the corresponding strain in the reinforcing bars were recorded at a sampling rate of 10 Hz.

### 3.7.2 Double pullout specimen tests

The double pullout specimens were lifted from the vertical position by an overhead crane in the Structures Laboratory and lowered to the horizontal position. The plywood base, as described in Section 3.6.4 was then removed and the specimens were lifted again to position them into the test frame. Figure 3.18 shows the set up of a specimen in the test frame that applied direct tension loads to the spliced bars using two hydraulic rams.

The rectangular test frame used for the testing of the double pullout specimens consisted of two steel members bolted together using two threaded steel bars. The steel members were built from two 2400 mm long back to back channel sections (C 250×23) welded together with five 12 mm thick steel plates. A 65 mm gap between the channel sections then resulted. The two steel plates that were welded 200 mm from the each end of the channel section allowed two 50 mm diameter threaded bars to be bolted to the steel members after extending through a centrally located hole in the steel plates.

Each double pullout specimen was centered within the test frame and supported on two steel rollers sitting on the test floor to reduce the friction between the specimen and the concrete floor. The reinforcing bars extending beyond each end of the specimen were then connected to the 16 mm diameter high strength (Grade 600) threaded steel bars by Zap Screwlock (Type 2) mechanical couplers. The details of these mechanical couplers are provided in Appendix 3C. The high strength steel bars extended approximately 800 mm beyond the test frame at each end through the 65 mm gap that existed between the
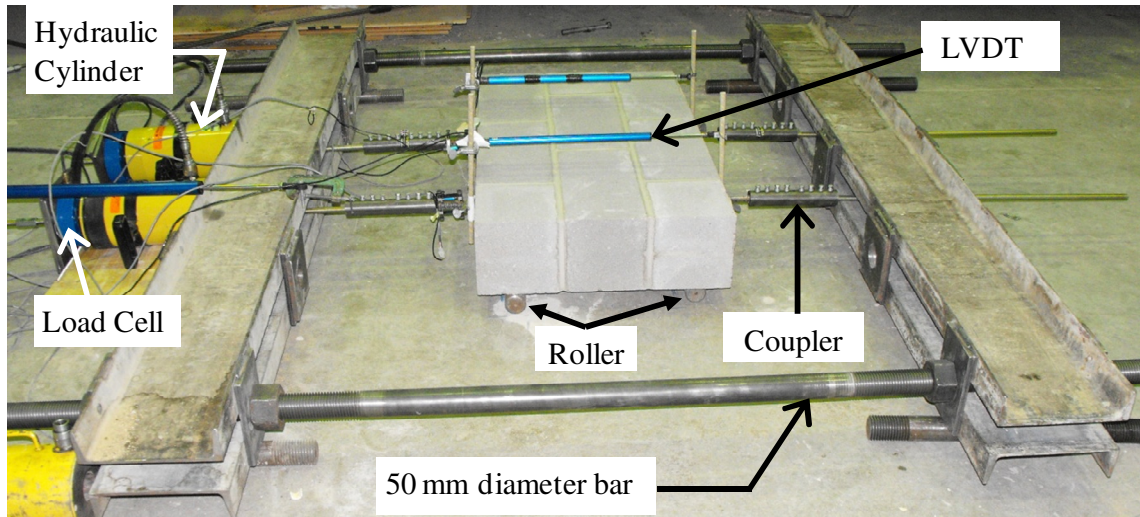
Figure 3.18: Test setup and instrumentation for the double pullout specimens.

two welded channel sections. Two hydraulic rams manufactured by Interface, each with a 300 mm stroke and a 220 kN capacity load cell were used to apply tension to the spliced reinforcing bars. The high strength steel bars were bolted to the frame at their resisting ends using a square steel plate and nut arrangement.

An LVDT with a 300 mm stroke was attached to each set of extended spliced bars using a clamp and stand arrangement as shown in Figure 3.18. The clamps were attached to the reinforcing bars that extended beyond the ends of the specimen. The LVDTs measured the splice extension between the clamps under the applied load.

Direct tension was applied to the reinforcing bars when the hydraulic rams pushed against the test frame. The loading rate was controlled by a data acquisition system manufactured by National Instruments and controlled by a computer running LabView software. The system had two modules: the control module which controlled the

extension of the two hydraulic rams at a constant rate of 0.025 mm/s, and the recording module which logged resulting loads from the two load cells and elongations from the two LVDTs at half second intervals.

The control module consisted of a hydraulic pump and a valve arrangement. High pressure fluid was pumped at a controlled rate using a valve in the two rams. The control mechanism first opened a valve connecting the hydraulic ram attached to Splice 1 to apply an incremental displacement. The valve that connected the loading ram attached to Splice 2 was then opened to apply a similar displacement once the valve attached to ram loading Splice 1 had closed. The load in Splice 1 therefore increased before Splice 2 for each load interval. However, it should also be considered that the slip of either set of spliced bars can result in an increased displacement of the hydraulic ram without any increase in applied load, thus creating a load differential between the two splices with equal displacements of the hydraulic rams. Bolt shear in the mechanical couplers could also add to the displacement of the rams, and may have therefore resulted in a possible unequal splice displacement between the two lap splices at the same displacement of the hydraulic ram.

### 3.7.3 Wall splice specimen tests

The vertically constructed walls were transported to the test bed and lowered to the horizontal position for testing using the overhead crane in the Structures Laboratory. A steel frame consisting of two identical steel horizontal beams connected by four threaded steel bars was used to safely lift and rotate the specimens. Figure 3.19 shows the details of the horizontal beams used in the test frame. The horizontal beams were

built using two back to back channel sections (C 250 × 23) spaced 250 mm apart and welded together by two 12 mm thick steel plates at each end. The plates accommodated a 50 mm pivoting bar through a hole located at their center that allowed the rotation of the frame when supported at the bottom. One of the horizontal beams was lowered to the bottom of the wall allowing the wall to fit within the 250 mm gap in between the channel section of the horizontal beam. This beam was then bolted with two 10 mm thick end bearing steel plates at the flanges of the channel sections as shown in Figure 3.20(a). The other horizontal beam was placed at the top of the specimen using the overhead crane and was then connected to the lower beam with four high strength 16 mm diameter threaded steel bars. When the steel frame was lifted vertically as shown in Figure 3.20(a), the encaged wall was supported on the steel end plates attached to the bottom horizontal beam and was able to be lifted from the casting position.  Figure 3.20(b) shows the rotation of the wall into the horizontal position while being supported by the two pivoting bars at the two ends of the bottom horizontal beam. The wall was lifted horizontally after removal of the test frame and moved to the test bed by the overhead crane as illustrated in Figure 3.20(c).

The specimens were supported by a roller and steel base plate assembly at 100 mm from each end to provide a simply supported clear span of 2400 mm. Figures 3.21(a) and (b) show the front and side views of the support assembly, respectively. The upper portion of the steel support was hinged to the fixed lower portion and was therefore able to rotate about the longitudinal axis of this assembly. A channel section attached to the top
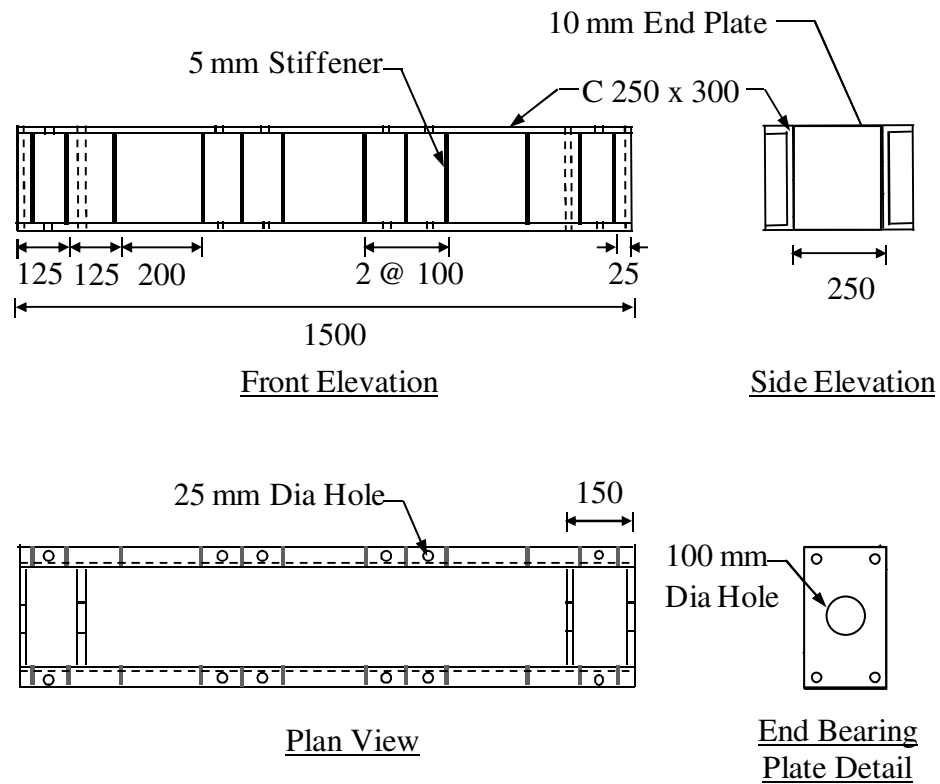
Figure 3.19: Details of the horizontal beam used in the steel moving frame.

of the upper portion supported a 50 mm diameter steel bar spanning across the width of the specimen. The steel bar at the left end support was permitted to translate forming a roller support. Figure 3.21(b) shows that a pin support was created at the right end support by tightening a screw that prevented the translation of the steel bar.

Figure 3.22(a) shows the hydraulic ram at the specimen centreline that was actuated by an MTS servo-controlled hydraulic system at a constant displacement of 0.5 mm/min. A spreader beam positioned below the actuator and supported on two rollers and a steel

Top horizontal beam

High strength steel bar

Bottom horizontal beam

End bearing plate
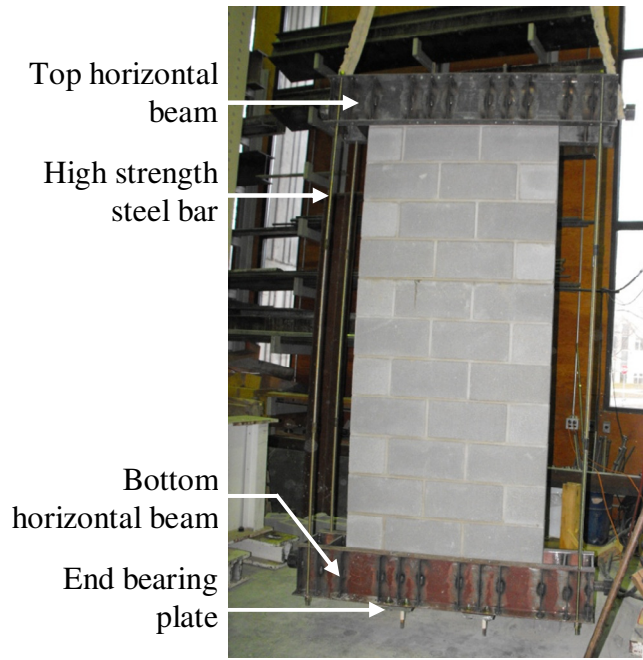
(a)

(b)                                                    (c)

Figure 3.20: Positioning of the wall splice specimens: (a) lifting vertically from the initial as constructed position, (b) rotating in the horizontal position, and (c) lifting the wall in its horizontal orientation.
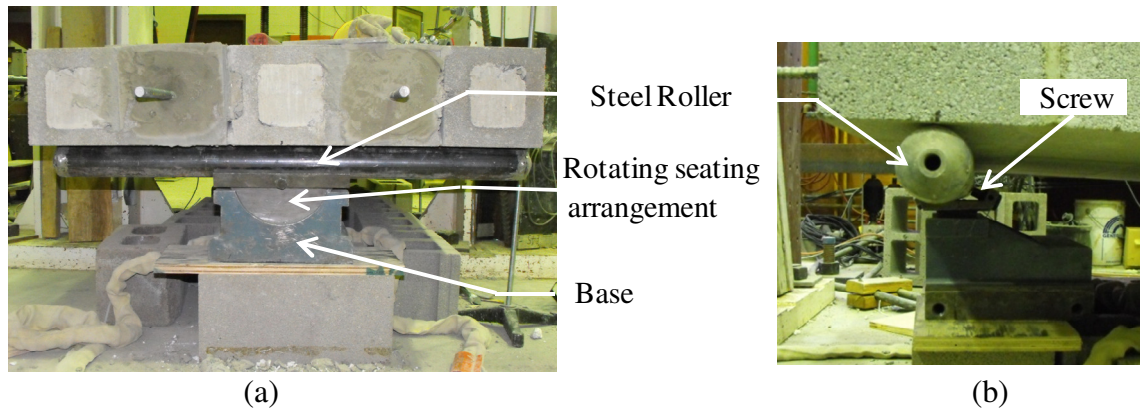
Figure 3.21: Support conditions for the wall splice specimens: (a) front view, and (b) side view.

channel section assembly distributed the applied load equally to two points located 400 mm on each side of the specimen centreline and thus created a four-point loading arrangement.

Figure 3.22(a) shows the anchorage assembly used to prevent bar slip at the wall ends. This assembly consisted of a 12 mm thick, 200 mm square steel plate and anchoring mechanism. The surface of the wall around the reinforcing bars was leveled with a 10 mm thick layer of mortar, and the steel plate was then placed against this uniform surface. A ZAP Screwlock mechanical coupler was then placed on the end of the reinforcing bars extending from the specimen. The couplers were fit snugly against the anchorage plate and tightened.

Figure 3.22(b) shows the location of the six LVDTs used to record the vertical displacement along the length of the specimen during testing. Two LVDTs with a 1000 mm range were placed on the both sides of the specimen at the centreline. Two LVDTs

(a)



(b)
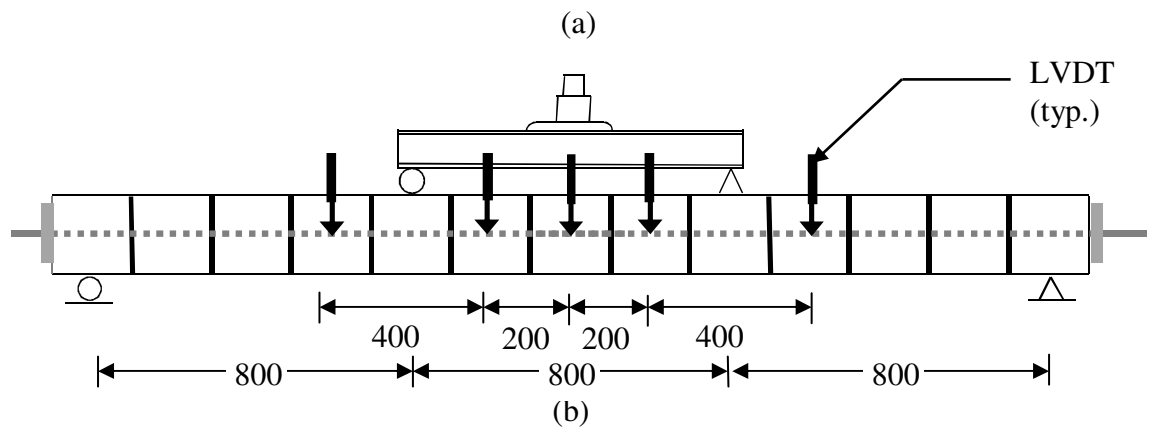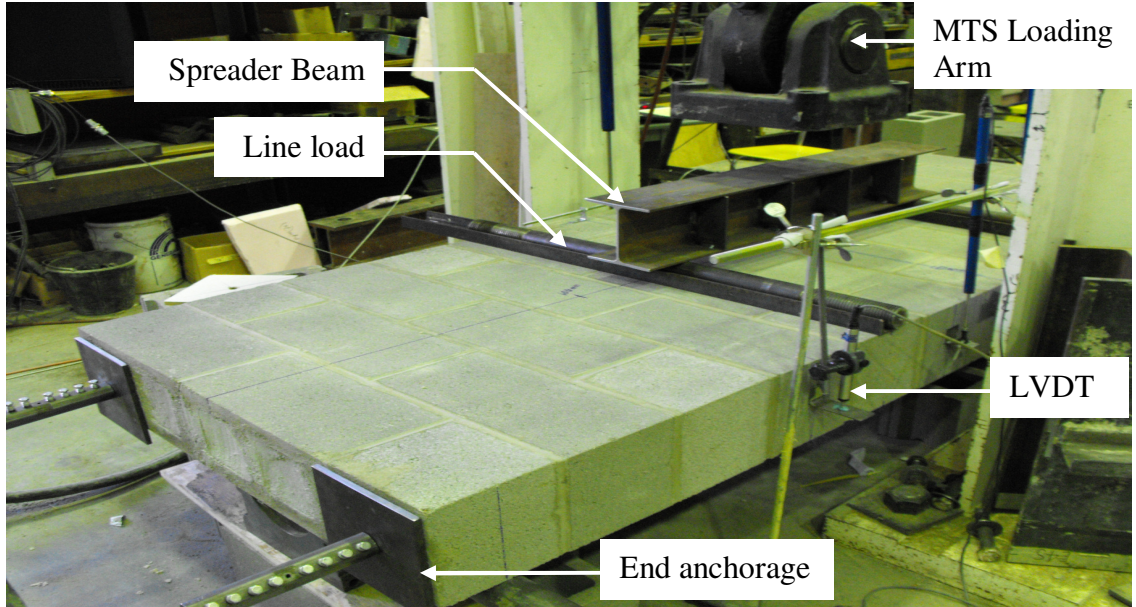
Figure 3.22: Wall splice specimen test setup: (a) loading conditions and instrumentation, and (b) LVDT positions.

with a 300 mm range were placed 200 mm on either side of the specimen centerline, while the remaining two LVDTs with a 50 mm range were placed 600 mm on either side of the specimen centreline. All deflections were measured with respect to the midheight of the wall. A data acquisition system manufactured by National Instruments and controlled by LabView™ software on a personal computer was used to record data

from the MTS actuator load cell and the displacements from the six LVDTs at a rate of 2 Hz until specimen failure. For this purpose, failure was defined as such time when the applied load dropped to 40% of the maximum recorded load.

This chapter described the construction of both the double pullout specimens and wall splice specimens including their test setup and instrumentation. The test results are presented in Chapter 4, which starts with the companion specimens test results and is followed by the results for both the double pullout and wall splice specimens. Chapter 4 then continues with the presentation of the maximum tensile resistance in the lap spliced reinforcing bars for both specimen types with both contact and non-contact lap splices. The failure mode and bond transfer mechanism is also reviewed for both splice arrangements in the double pullout and wall splice specimens.

CHAPTER 4
RESULTS AND ANALYSIS

## 4.1 Introduction

Test results for the sixteen double pullout specimens and sixteen wall splice specimens are presented in this chapter. The load versus displacement behaviour and visual observations of crack propagation are compared for specimens with contact and non-contact lap splices in both double pullout and wall splice specimens. Randomly selected specimens were cut open after failure to reveal internal damage along the lap splice length for both specimen types.

Double pullout specimens were tested under direct tension as described in Section 3.7.2, while Section 3.7.3 described the four-point loading arrangement used to test the wall splice specimens. The tensile resistance of the spliced bars was obtained directly from the data recorded from load cells measurements for the double pullout specimens. A numerical analysis was required to convert the measured applied load in the wall splice specimens to the tensile resistance in the lapped reinforcing bars. The student "t" test was then used to establish if a statistically significant difference existed between the mean maximum splice resistances for the double pullout and wall splice specimens with contact and non-contact lap splices, respectively. The student "t" test was also used to determine whether a statistically significant difference existed between the mean

maximum splice resistance in the double pullout and wall splice specimens with the same splice arrangements. Splice behaviour including the load versus deflection, crack propagation, and internal bond deterioration, was compared for each specimen type with both splice arrangements. Based on the limited test results, a reduction factor is suggested for inclusion in current design standard for the lap splice length when non-contact lap spliced bars are located in adjacent cells.

## 4.2 Material Properties

Table 4.1 shows the mean compressive strength and respective coefficient of variation for: the masonry blocks, mortar, grout, and overall masonry assemblages as established using the specimen types and test procedures outlined in Section 3.7.1. Results are provided for companion specimens tested in conjunction with the double pullout and wall splice specimens in both testing phases. Table 4.2 shows the mean reported values for the dynamic yield strength, modulus of elasticity, strain and slope of the stress versus strain curve at the initiation of strain hardening, and ultimate stress of the reinforcing steel bars used in both phases of specimen construction. These results are reported based upon the specimen types and test methods outlined in Section 3.5.4. Highlights of these material properties are described in the following sub-sections.

### 4.2.1 Masonry block test results

A total of three and six concrete masonry blocks were randomly selected from the supplied blocks used in construction phases 1 and 2, respectively, and tested in compression with a resulting loading rate that ranged from 1.0 to 1.4 kN/sec. The mean

compressive strength and coefficient of variation for both data sets are shown in Table 4.1. No outliers were identified using the procedures outlined in the "Standard Practice for Dealing with Outlying Observations" (ASTM E178, 2000) at the 95% confidence level. The difference between the mean compressive strength of the blocks tested in the two phases is not statistically significant at 95% confidence level, thus indicating that the blocks are from a single normal distribution. Details of the individual test results are provided in Appendix 4A.

Table 4.1: Companion test result summary – block, mortar, grout and masonry prisms.

| Companion Test Type | Test Phase | Double pullout specimens | | | Wall splice specimens | | |
|---|---|---|---|---|---|---|---|
| | | Number of specimens | Mean maximum stress (MPa) | C.O.V. | Number of specimens | Mean maximum stress (MPa) | C.O.V. |
| Masonry Block | 1 | 3 | 22.2 | 6.30% | [1] | [1] | [1] |
| | 2 | 6 | 23.4 | 8.24% | [1] | [1] | [1] |
| Mortar cubes | 1 | 12 | 18.2 | 7.41% | 6 | 17.4 | 6.79% |
| | 2 | 12 | 17.9 | 17.0% | 12 | 12.5 | 18.4% |
| Non-absorbent grout cylinders | 1 | 9 | 20.1 | 4.27% | 3 | 19.7 | 4.30% |
| | 2 | 12 | 27.5 | 12.4% | 12 | 25.6 | 18.7% |
| Absorbent grout prisms | 1 | 5 | 19.7 | 5.28% | 3 | 19.1 | 8.19% |
| | 2 | 12 | 23.9 | 13.6% | 12 | 23.0 | 10.3% |
| Masonry prisms | 1 | 6 | 13.3 | 8.01% | 3 | 14.9 | 8.97% |
| | 2 | 12 | 14.4 | 4.52% | 10[*] | 13.3 | 6.16% |

[1] The masonry block tests represent the material properties for both the double pullout and the wall splice specimens. See values reported for the double pullout specimens.
[*] Two outliers were identified in addition to the value shown above.

Table 4.2: Companion test result summary – reinforcing steel.

| Test Phase | Sample designation | Dynamic yield stress, $f_y$ (MPa) | Modulus of elasticity, $E_s$ (GPa) | Strain at initiation of strain hardening, $\varepsilon_{sh}$ | Slope at initiation of strain hardening, $E_{SH}$ (MPa) | Ultimate steel stress, $f_{ult}$ (MPa) |
|---|---|---|---|---|---|---|
| | 1 | 444 | 199 | n/a[*] | n/a[*] | n/a[*] |
| | 2 | 446 | 205 | 0.014 | 9040 | 603 |
| 1 | 3 | 442 | 207 | 0.014 | 6520 | n/a |
| | 4 | 440 | 205 | 0.015 | 5170 | 616 |
| | 5 | 444 | 220 | 0.014 | 6180 | 613 |
| | 1 | 430 | 199 | 0.015 | 4620 | 608 |
| | 2 | 446 | 195 | 0.014 | 5520 | 635 |
| 2 | 3 | 438 | 193 | 0.014 | 6510 | 642 |
| | 4 | 440 | 218 | 0.014 | 4470 | 617 |

[*] Values were not recorded due to strain gauges malfunction.

## 4.2.2 Mortar cube tests

Table 4.1 presents the maximum stress as averaged from the number of mortar cubes tested in conjunction with the double pullout and wall splice specimens tested in each construction phase. No outliers were identified in the population at the 95% confidence level; also, the difference between the mean values of the compressive strength in the two testing phases was found not to be statistically significant. It should be noted that the mean compressive strengths differed significantly for mortar cubes tested in conjunction with the wall splice specimens as tested in the two construction phases.

Furthermore, an 18% coefficient of variation was reported for the mortar cubes tested in conjunction with the Phase 2 wall splice specimens, while only a 7% coefficient of variation was reported for tests performed in conjunction with the same specimens in construction Phase 1. The mortar was hand mixed in the laboratory, as described in Section 3.6.2. It is therefore likely that a variation in material quantities and mixing effort might have caused a larger variation in the compressive strengths of the mortar cubes prepared in conjunction with Phase 2 of the construction program as samples were taken from a larger number of batches. Moreover, the water content varied depending upon the length of time between batch mixing and cube preparation and would have also resulted in a greater variation in the reported values of the mortar compressive strength. The individual mortar cube test results are provided in Appendix 4A.

### 4.2.3 Grout cylinders and prism tests

Two types of specimens were tested to establish the compressive strength of the grout: non-absorbent grout cylinders, and absorptive grout prisms. The specimen geometry, test setup, and control loading rate for both companion specimen types were provided in Section 3.6.3. A review of the data logged during testing confirmed that the loading rate was accurately controlled by the testing apparatus and was within ±2% of the specified rate as stated in Section 3.7.1.

Table 4.1 shows the mean compressive strengths resulting from a total of 9 and 12 non-absorbent grout cylinders tested in conjunction with the double pullout tests in construction Phases 1 and 2, respectively, and the 3 and 12 non-absorbent grout cylinders tested in conjunction with the wall splice specimens in construction Phases 1

and 2, respectively. Outliers at the 95% confidence rate were not identified in any of the data sets. The mean compressive strength of the grout cylinders tested in construction Phase 2 were 36% and 28% higher than those tested in Phase 1 for the double pullout and wall splice specimens, respectively. The increased mean compressive strength in construction Phase 2 resulted from a change in gradation of the aggregates used in that phase, as described in Section 3.5.3. However, previous researchers (Hamid and Drysdale, 1979) have shown that an increase in grout strength from 20 to 30 MPa only causes a 5% increase in the compressive strength of the masonry assemblage. Tests of double pullout specimens by others (NCMA, 1999) showed an increase of 140% in the compressive strength of the masonry assemblage caused only a 27% increase in splice tensile strength. The resulting difference in the compressive strengths of the grout is therefore presumed not to significantly influence the splice resistance.

Absorptive prism tests were also performed to more effectively capture the compressive strength in the double pullout and wall splice specimens since this value typically increases with a reduction in water content due to water absorption by the masonry blocks (Drysdale and Hamid, 2005). It was interesting to note, however, that the mean compressive strength of the absorptive prisms cast in construction Phase 1 were 2% and 3% less than those reported for the non-absorptive grout cylinders for the double pullout and wall splice specimens, respectively. Similar results were observed for the absorptive prism tests cast in conjunction with Phase 2: values reported were 13% and 10% less than those obtained for the non-absorbent grout cylinders for the double pullout and wall splice specimens, respectively. Specific reasons for this anomaly were not identified.

Only three absorbent grout cylinders were cast and tested in conjunction with Phase 1 wall splice specimens, and, as such, outliers within this data set could not be identified. Outliers were not detected in the other three populations. Individual test results for both the non-absorbent grout cylinders and absorptive grout prisms are included in Appendix 4A.

### 4.2.4 Masonry prism tests

Table 4.1 shows the compressive strength results for the masonry prisms tested in conjunction with the two construction phases and specimen types. The individual test results are shown in Appendix 4A. The test method and setup, instrumentation, and specimen details were described in Section 3.7.1. A review of the logged test data shows that there was a ± 20% variation in the actual loading rate as compared to the target value due to the manual control of the load rate for the testing apparatus.

Outliers were not identified in the sample populations associated with the double pullout specimens tested in conjunction with both construction phases; also, the difference in the mean compressive strength for two construction phases was not statistically significant. The sample size did not allow for the identification of outliers for masonry prism tests performed in conjunction with the Phase 1 wall splice specimens, while two outliers were identified from the results of prisms tested in conjunction with the Phase 2 wall splice specimens. A local failure of the face shell was observed in these two specimens due to a suspected non-uniform distribution of the applied load as described in Section 3.7.1. These specimens have been excluded from the calculation of the mean compressive strength as reported in Table 4.1. The difference between the mean

compressive strengths for the prisms tested in conjunction with the wall splice specimens as cast in both testing phases was not statistically significant.

The mean compressive strengths of all prisms tested in conjunction with the double pullout and wall splice specimens in both construction phases combined were 14 MPa and 13.5 MPa, respectively. The difference between these values is not statistically significant. This suggests that all tested prisms belong to a single normal distribution.

Figure 4.1 shows the experimental stress versus strain curve for a representative masonry prism. Erratic strain measurements were recorded for 21 out of the total 32 tested prisms due to the face shell rotation that occurred during axial compression loading, which, in turn, caused a rotation of the attached angles that served as the datum for the LVDT measurements. Though compressive strengths obtained from these prisms were included in the calculation of the mean strength, the resulting stress versus strain curves was not considered representative. Appendix 4A shows the eleven representative stress versus strain curves for the masonry prisms.

### 4.2.5 Reinforcing bar tests

Table 4.2 shows the tensile properties for the five and four reinforcing bar samples tested in conjunction with construction Phases 1 and 2, respectively. A review of the logged test data shows that the actual loading rate was consistently within ± 1% of the target value of 200 N/s as specified in the test method described in Section 3.5.4. The resulting mean yield stresses were 443 and 441 MPa for those samples tested in

conjunction with construction Phases 1 and 2, respectively. No outliers were identified in either population.

Figure 4.2 shows a representative stress versus strain curve for the steel reinforcing bars. The limitation of the Instron 600DX Universal Testing Machine is that it did not allow for the measurement of strain values greater than 0.03. The ultimate failure stress was, however, recorded regardless of this strain limitation.
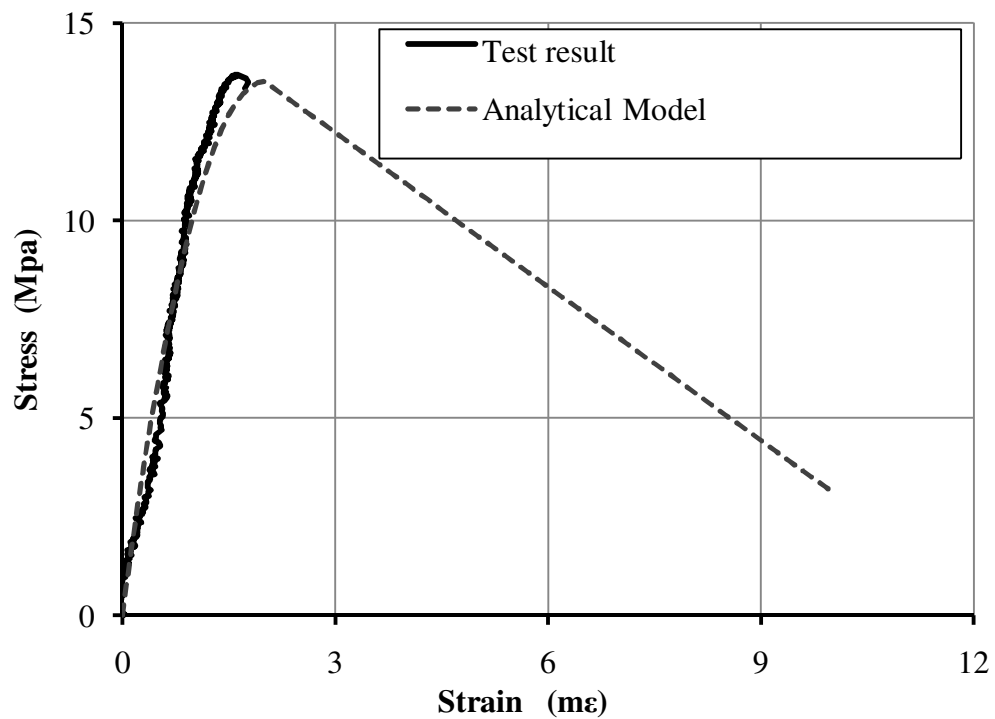


Figure 4.1: Representative stress versus strain curve for a masonry prism.
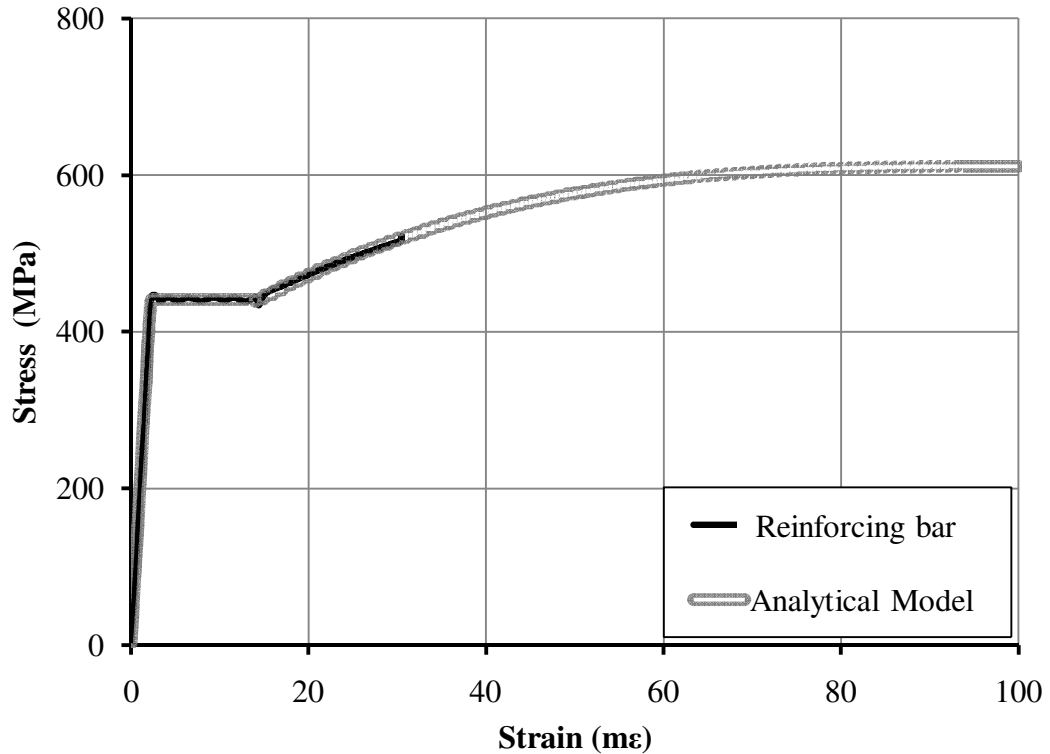
Figure 4.2: Representative stress versus strain curve for the steel reinforcement.

## 4.3 Double Pullout Specimens

Failure loads and behaviour including the load versus displacement response, observed damage, and resulting failure loads for the sixteen double pullout specimens are described herein. The load transfer mechanism for the specimens with non-contact lap splices is also critically reviewed. Section 3.7.2 describes the test procedures and instrumentation of these specimens.

### 4.3.1 Splice tensile resistance versus splice displacement

Figures 4.3 to 4.10 shows the load versus splice displacement curves for the eight double pullout specimens that were reinforced with contact lap splices. Such specimens have been identified as CP-X, where "CP" identifies the specimens as being the double

84

pullout type with contact lap splices, with the numerical "X" designation following the hyphen denoting the specimen number within the test series. Resisted tension in all pullout specimens with contact lap splices exceeded the theoretical yield loads of 88.6 and 87.7 kN established for the specimens tested in Phases 1 and 2, respectively. The theoretical yield loads were established from the mean yield strengths summarized in Table 4.2 as obtained from the results of the tensile tests of reinforcing bar samples supplied for each construction phase.

All of the splice tensile resistance versus splice displacement curves, with the exception of two (Figures 4.7 and 4.10), show that at least one of the lapped bars in the specimens attained the yield plateau as indicated by a horizontal portion at the maximum load, thus suggesting that the 300 mm lap as provided is capable of fully developing the reinforcement. In contrast, Specimens CP-5 and CP-8, shown in Figures 4.7 and 4.10, respectively, do not show the existence of a yield plateau for either of the lapped bars. However, the tensile resistance recorded in at least one of the lapped bars in these two specimens exceeded the theoretically predicted yield load. Failure, in general, was attained when the tensile resistance attained by either spliced bar dropped abruptly. Once failure occurred in one of the spliced bars, which was typically accompanied by a sudden large displacement, the tension in the other splice dropped immediately due to the inability of the load control mechanism to further maintain equal displacements in both splices. In general, higher tensile resistances were recorded for Splice 1 compared to Splice 2 in any given specimen due to the testing methods described in Section 3.7.2. A maximum 8% difference in the recorded tensile resistance between the two spliced

Figure 4.3: Tensile resistance versus splice displacement curve -Specimen CP-1.



Figure 4.4: Tensile resistance versus splice displacement curve - Specimen CP-2.



Figure 4.5: Tensile resistance versus splice displacement curve - Specimen CP-3.



Figure 4.6: Tensile resistance versus splice displacement curve – Specimen CP-4.

86

Figure 4.7: Tensile resistance versus splice displacement curve – Specimen CP-5.
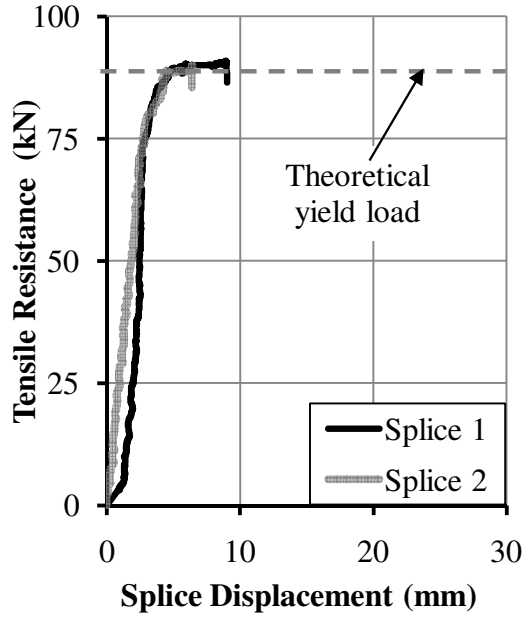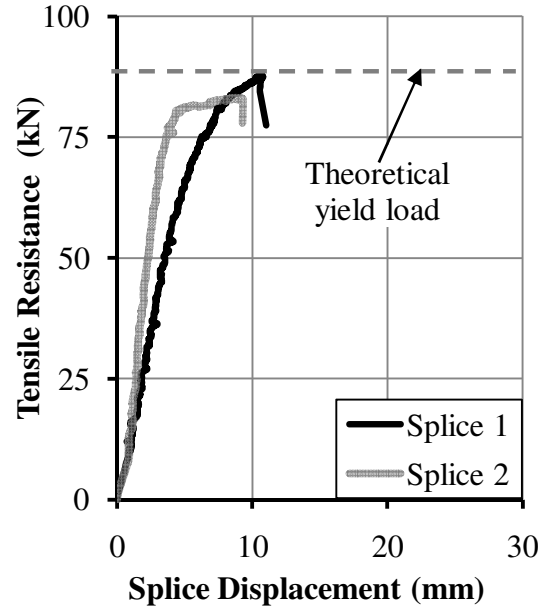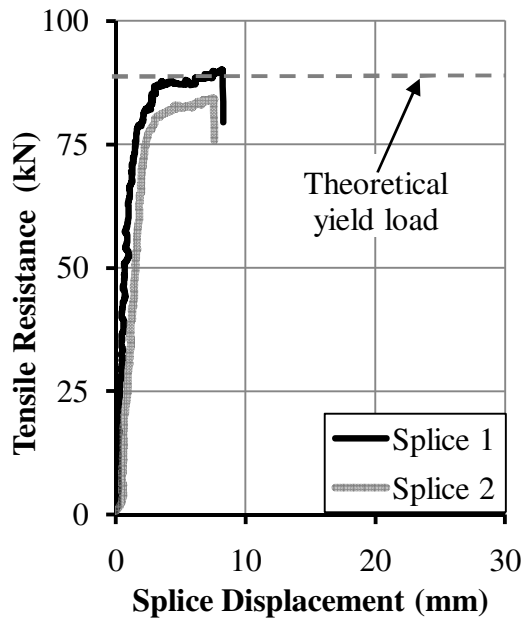


Figure 4.8: Tensile resistance versus splice displacement curve – Specimen CP-6.



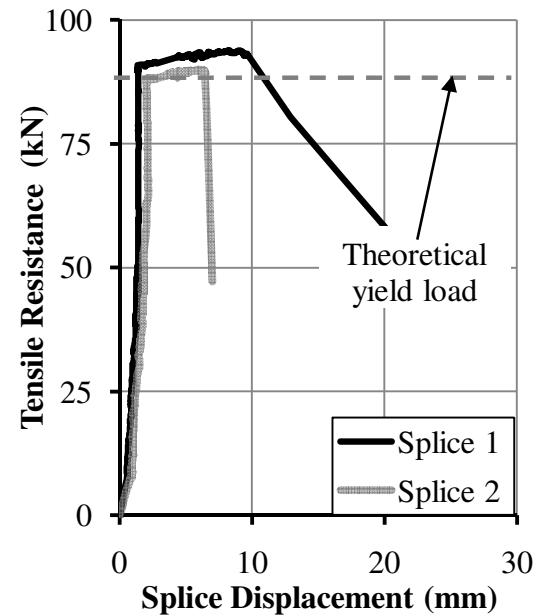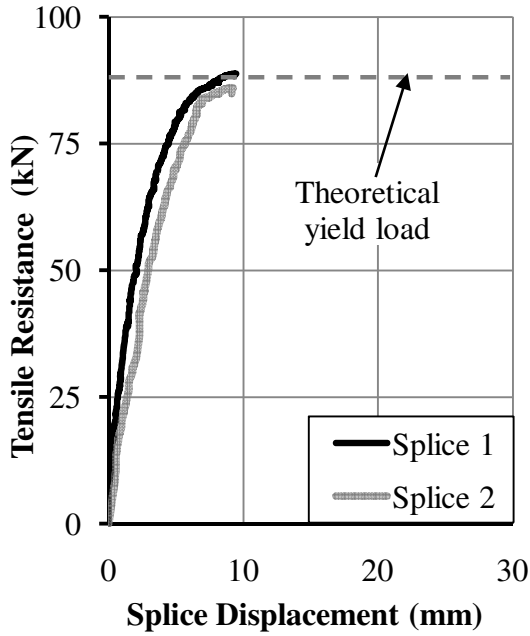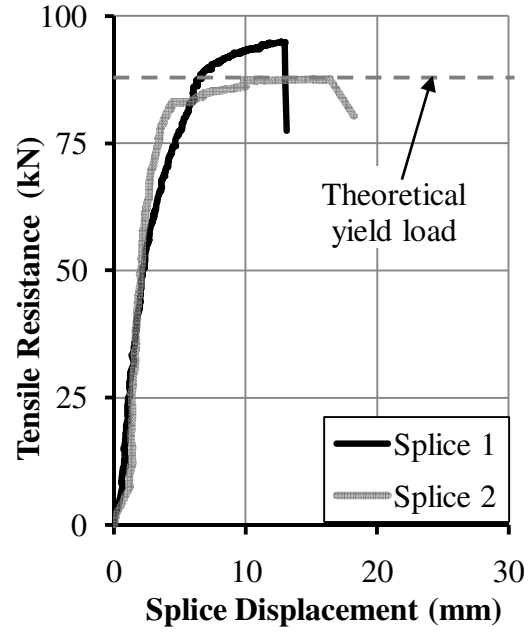Figure 4.9: Tensile resistance versus splice displacement curve - Specimen CP-7.



Figure 4.10: Tensile resistance versus splice displacement curve - Specimen CP-8.

bars was observed at failure for all the specimens. Splice 1 therefore typically achieved a yield plateau before Splice 2, and in some specimens failed before Splice 2 could attained its yield capacity.

Table 4.3 presents the maximum tension resisted by both sets of spliced bars in the double pullout specimens with contact lap splices. The representative tensile resistance of the spliced bars in a specimen is identified by the asterisks in Table 4.3 and based on the result from the lapped bars for which visual evidence of failure was observed. The absence of such evidence of failure in either of the splices as observed for specimens CP-1, CP-3, and CP-5 resulted in the selection of the higher of the two measured tensile resistances as the representative value in these specimens. The mean tensile resistance of lapped bars as obtained from averaging the results attained for all specimens in a given population were 89.6 and 89.7 kN for the Phase 1 (CP-1, CP-2 and CP-3) and Phase 2 (CP-4 to CP-8) specimens, respectively. Outliers were not identified at the 95% confidence level suggesting that the tensile resistance recorded from all eight specimens belonged to a single population, irrespective of the differences in material properties reported for the two construction phases. The combined mean tensile resistance for the contact spliced bars was 89.7 kN, with a coefficient of variation of 2.37%.

Figures 4.11 to 4.16 shows the load versus splice displacement curves for the double pullout specimens reinforced with non-contact lap splices. These specimens have an NCP designation, where "NCP" identifies the specimens as being the double pullout type with non-contact lap splices with the numerical designation "X" following the

hyphen referring to the specimen number within the series. The load versus displacement response for Specimens NCP-3 and NCP-6 are not shown, as errors in testing resulted in loading rates that were nine and eleven times the target value, respectively. The test results from these two specimens were therefore excluded from the reported mean tensile resistance of the spliced bars.

Table 4.3: Tensile resistance of the spliced bars for the double pullout specimens with contact lap splices.

| Specimen ID | Splice No. | Tensile resistance (kN) | Failure mode |
|---|---|---|---|
| CP-1 | Splice 1 | 91.0[*] | Loading halted after both bars yielded. |
| | Splice 2 | 90.1 | |
| CP-2 | Splice 1 | 87.8[*] | Pullout of Splice 1 bar. |
| | Splice 2 | 83.2 | |
| CP-3 | Splice 1 | 90.1[*] | Loading halted after both bars yielded. |
| | Splice 2 | 84.3 | |
| CP-4 | Splice 1 | 93.9[*] | Splice 1 bar pullout with longitudinal splitting. |
| | Splice 2 | 90.0 | |
| CP-5 | Splice 1 | 88.8[*] | Mechanical coupler failure. |
| | Splice 2 | 86.1 | |
| CP-6 | Splice 1 | 95.1 | Splice 2 bar pullout. |
| | Splice 2 | 87.7[*] | |
| CP-7 | Splice 1 | 94.3 | Splice 2 bar pullout in conjunction with mechanical coupler failure. |
| | Splice 2 | 87.8[*] | |
| CP-8 | Splice 1 | 90.1[*] | Splice 1 bar pullout. |
| | Splice 2 | 82.9 | |

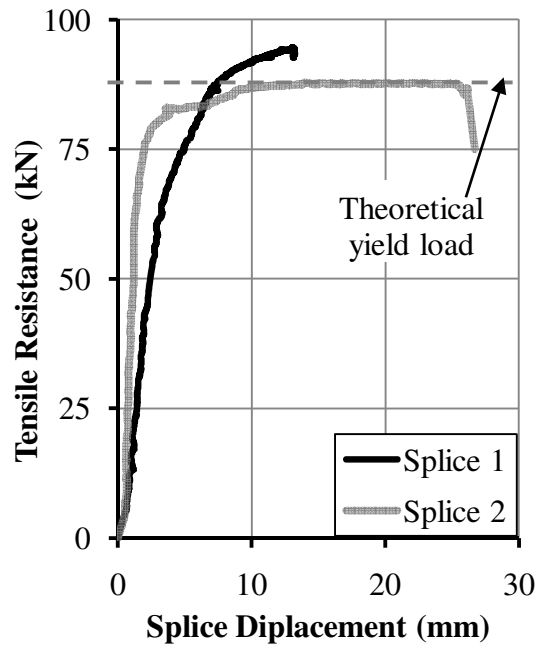[*] Representative tensile resistance of the spliced bars in a specimen as described in the text.
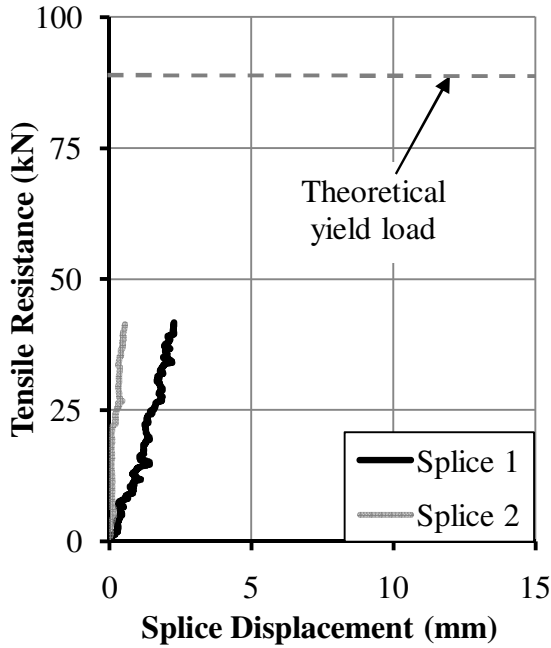
Figure 4.11: Tensile Resistance versus
splice displacement curve -
Specimen NCP-1.
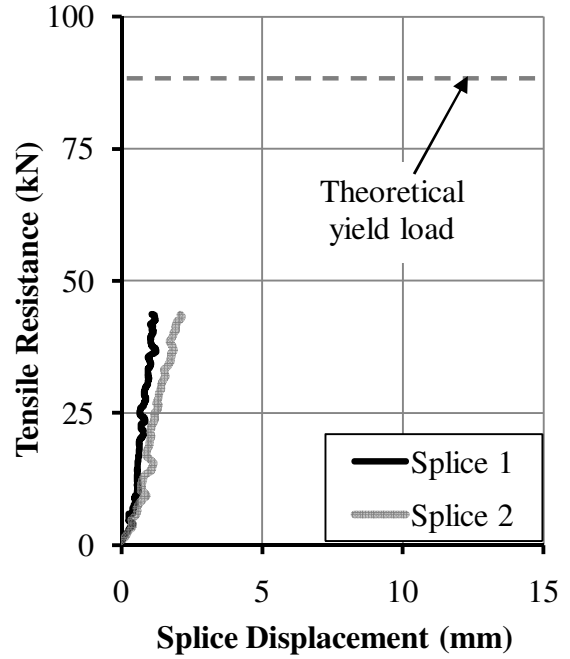


Figure 4.12: Tensile Resistance versus
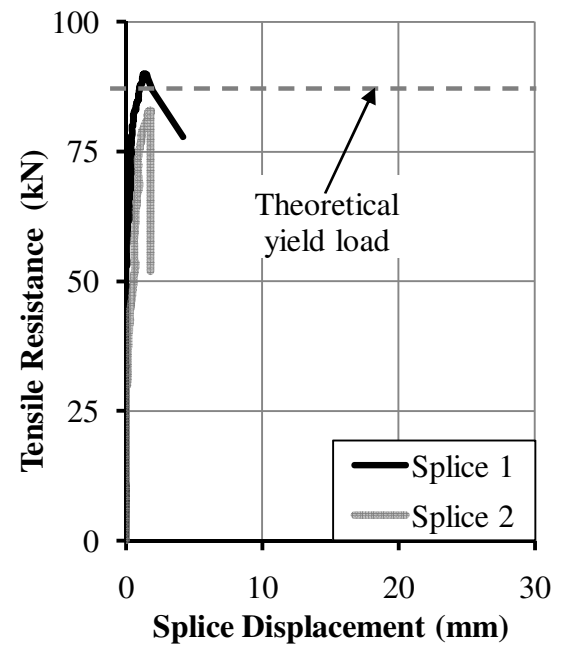splice displacement curve -
Specimen NCP-2.
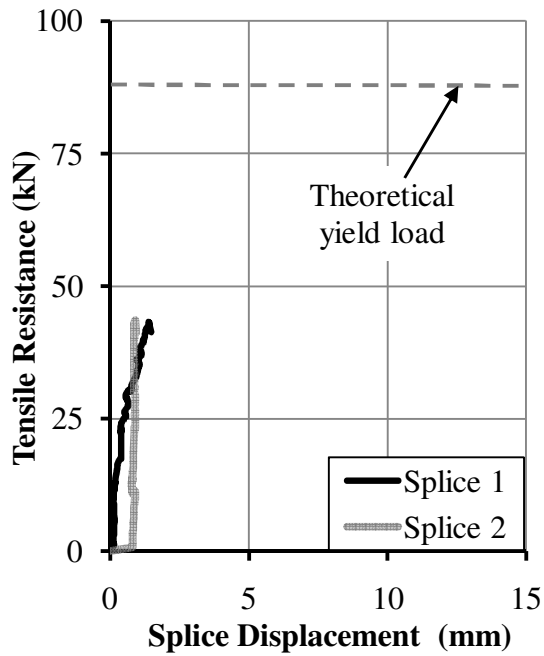


Figure 4.13: Tensile Resistance versus
splice displacement curve -
Specimen NCP-4
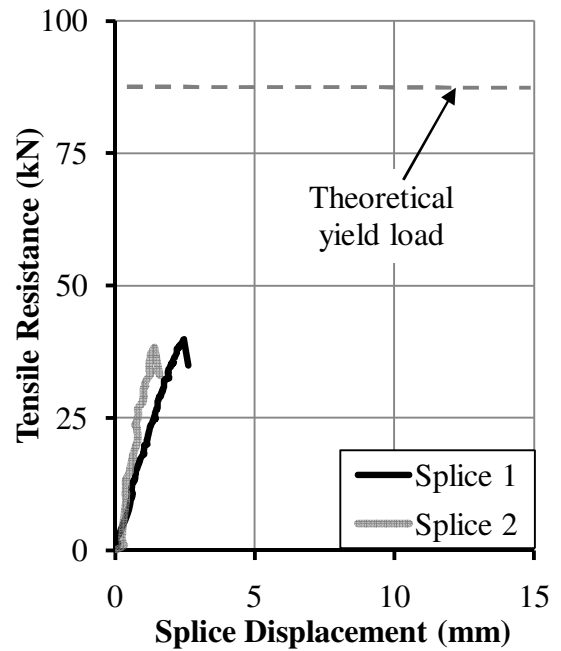


Figure 4.14: Tensile Resistance versus
splice displacement curve -
Specimen NCP-5.
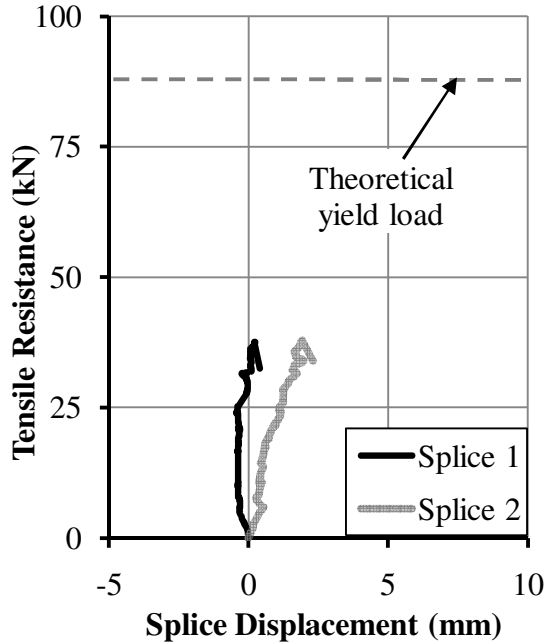
Figure 4.15: Tensile Resistance versus
splice displacement curve -
Specimen NCP-7.
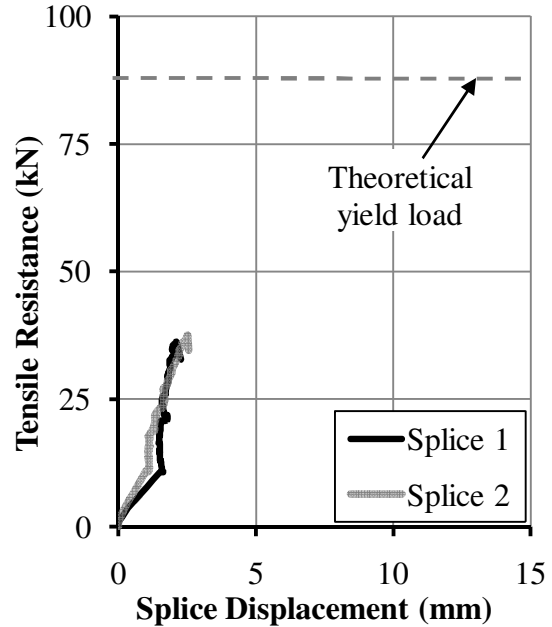
Figure 4.16: Tensile Resistance versus
splice displacement curve -
Specimen NCP-8.

In general, a nearly identical linear load versus displacement relation is observed in both sets of spliced bars in a given specimen, except for specimens NCP-1 and NCP-7. Horizontal rotation of these specimens was observed during loading initiation that might have been caused by the unsymmetrical bar arrangement resulting from a slight shifting of the reinforcing bars from their intended position that may have occurred during grout consolidation. The previously discussed uneven load application between the two loaded bar ends caused by the load control mechanism might also have contributed to this phenomenon. The shortening of the measuring arms attaching the LVDTs to the specimens that occurred as a result of the specimen rotation and caused a zero measured displacement in Splice 2 of Specimen NCP-1 until a load of 18 kN was attained, as well as the initial negative displacement in Splice 1 of specimen NCP-7 that gradually increased to a zero displacement before failure.

Table 4.4 presents the recorded maximum tension resisted by each set of spliced bars for the six double pullout specimens with non-contact lap splices. Unlike their counterparts with contact lap splices, these specimens failed well before the theoretical yield load of the reinforcing bars and splice failures were not observed in any of the specimens. Instead, these specimens failed by splitting of the mortar and concrete blocks starting at the ends connected with the hydraulic rams, as is discussed in detail in Section 4.3.2. The tensile resistance of the spliced bars was therefore determined from the average maximum tension recorded from the two sets of spliced bars in a given specimen. The combined mean tensile resistance of the spliced bars calculated for all six specimens (i.e. excluding the two outliers as identified earlier) constructed with non-contact lap splices was 40.7 kN, with a coefficient of variation of 7.57%. All six specimens appeared to be from a single normal distribution as no outliers were detected at the 95% confidence level.

### 4.3.2 Failure mode and external crack propagation

In general, very little damage was observed during testing of the double pullout specimens with contact lap splices. Table 4.3 summarizes the observed failure mode in each of the double pullout specimens with contact lap splices. As reported, bar pullout from the masonry assemblage at the ends connected with the hydraulic rams was the typically observed failure mode. In some specimens, bar pullout was accompanied by splitting of the masonry assemblage or a failure in the mechanical bar couplers. Figure 4.17 shows the typical hairline bed joint cracking along with fine cracking of the header joint adjacent to one of the spliced bars in these specimens observed after failure.

Table 4.4: Splice resistance of the double pullout specimens with non-contact lap splices.

| Specimen | Splice No. | Tensile Resistance (kN) | Average Tensile Resistance (kN) | Failure mode |
|---|---|---|---|---|
| NCP-1 | Splice 1 | 43.7 | 43.6 | Specimen splitting failure with extended head joint crack. |
| NCP-1 | Splice 2 | 43.5 | 43.6 | Specimen splitting failure with extended head joint crack. |
| NCP-2 | Splice 1 | 41.7 | 43.1 | Specimen splitting failure with extended head joint crack. |
| NCP-2 | Splice 2 | 44.4 | 43.1 | Specimen splitting failure with extended head joint crack. |
| NCP-4 | Splice 1 | 43.3 | 43.5 | Specimen splitting failure. |
| NCP-4 | Splice 2 | 43.6 | 43.5 | Specimen splitting failure. |
| NCP-5 | Splice 1 | 39.9 | 39.1 | Specimen splitting failure with longitudinal splitting crack along a reinforcing bar. |
| NCP-5 | Splice 2 | 38.3 | 39.1 | Specimen splitting failure with longitudinal splitting crack along a reinforcing bar. |
| NCP-7 | Splice 1 | 37.6 | 37.8 | Specimen splitting failure. |
| NCP-7 | Splice 2 | 37.9 | 37.8 | Specimen splitting failure. |
| NCP-8 | Splice 1 | 36.3 | 36.9 | Specimen splitting failure. |
| NCP-8 | Splice 2 | 37.5 | 36.9 | Specimen splitting failure. |

Figures 4.4 and 4.10 show that specimens CP-2 and CP-8 failed before a reduction in slope in the load versus deflection curve occurred. This provides indication that these splices did not attained a definite yield plateau. However, the tensile resistance of the spliced bars in these specimens exceeded their theoretical yield load. A sudden pullout of one of the lapped reinforcing bars was observed in Splice 1 for both of these specimens at failure. Figure 4.18 shows a similar bar pullout failure in Splice 2 of specimen CP-6, where pullout of the bar occurred well after yielding of the reinforcement.
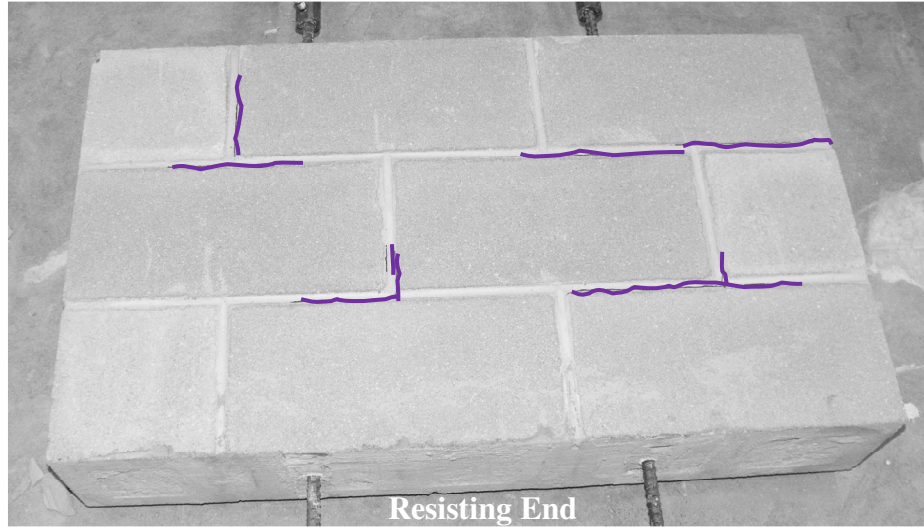
Figure 4.17: Typical surface crack propagation in a double pullout specimen with
contact lap splices – Specimen CP-6.

The bar pullout in Figure 4.18 is evident due to the markedly larger displacement recorded for Splice 2 as compared to that recorded for Splice 1. In fact, a 16 mm difference in displacement between the two ends of the failed splice was recorded. No additional tensile splitting cracks at the surface of these specimens were observed, suggests that a shearing failure between the pulled out reinforcing bar and the surrounding grout lead to this failure mode.

Figure 4.19 (a) shows a splitting failure of the grout and masonry block adjacent to lapped reinforcing bars of Splice 1 in Specimen CP-4 that ultimately led to bar pullout. The longitudinal splitting crack in the middle block adjacent to the Splice 1 lapped bar, as shown in the figure, extended through the two header joints adjacent to both ends of the specimen. The evidence of the resulting bar pullout is shown in Figure 4.19(b) from the displacement of the steel clamp that was in contact with the specimen
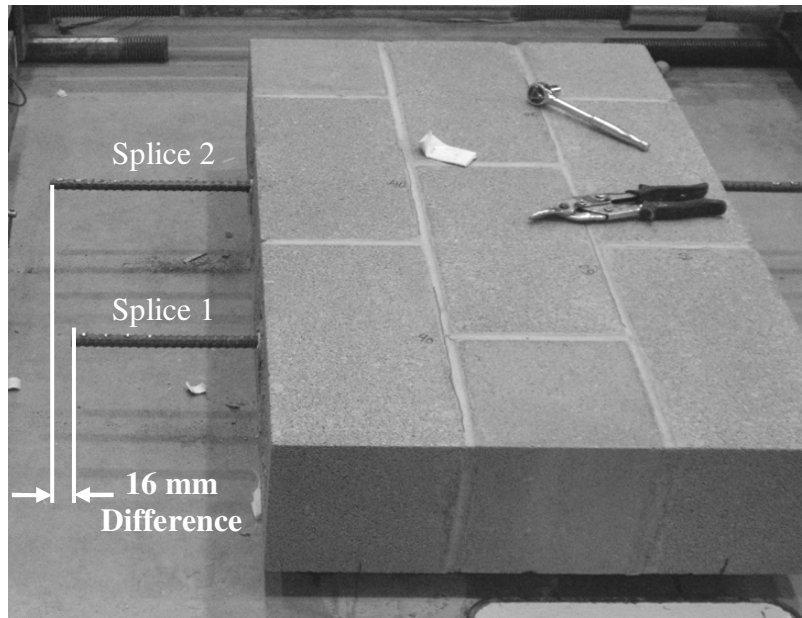
Figure 4.18: Bar pullout failure in - Specimen CP-6.

prior to loading. This failure mode has been observed by other researchers (NCMA,1999; Cheema and Klingner, 1985a) with the mechanism presented in Section 2.2.

Figure 4.20 (a) shows that bolt shearing occurred in the mechanical coupler attached to one of the resisting bar ends in Specimen CP-7, which ultimately leaded to the uncoupling of the reinforcing bars from the high strength bars. As a result, no resistance in the loading ram occurred and a drop in the applied load resulted. A Similar failure occurred at the end of one of the reinforcing bars that was attached to the hydraulic ram in Specimen CP-5. However, visual evidence of bar pullout as shown in Figure 4.20(b) was also observed in both specimens, suggesting that bond loss in the lapped bars occurred that coincided with the bar/coupler failure. Specimen CP-5 failed shortly after
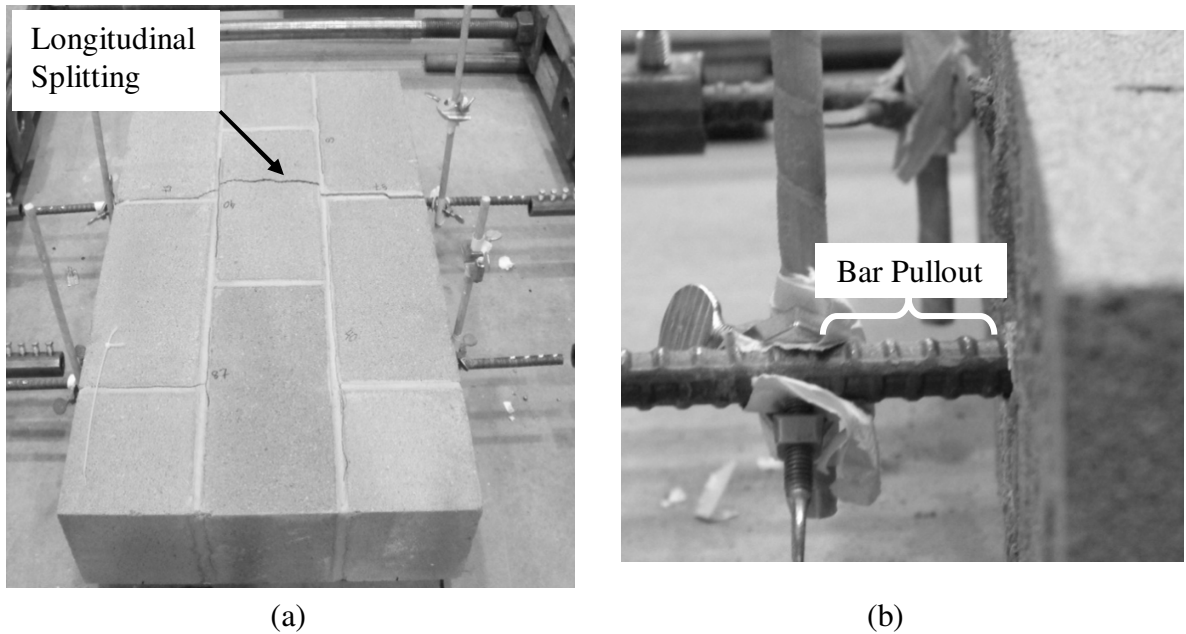
Figure 4.19: Bar pullout failure with longitudinal splitting - Specimen CP-4:
(a) longitudinal tensile splitting crack, and (b) bar pullout.

achieving the theoretical yield load of the reinforcement in Splice 1 at a recorded splice displacement of 9 mm, while a similar failure at a much larger splice displacement of 13 mm occurred in Splice 2 of Specimen CP-7.

Loading was halted for Phase 1 specimens CP-1 and CP-3 once the yield plateau was obtained (i.e. no increase in applied load was recorded with any further increase in the splice displacement), in order to prevent the failure of the mechanical couplers and allow for their reuse for the testing of subsequent specimens.

In contrast, all of the double pullout specimens with non-contact lap splices failed by splitting of the specimen initiating from the end attached with the loading ram. There was no indication of any visible bar pullout, thus suggesting that a bond failure between the reinforcing bars and the surrounding grout did not occur in these specimens.

<div align="center">(a)                                              (b)</div>
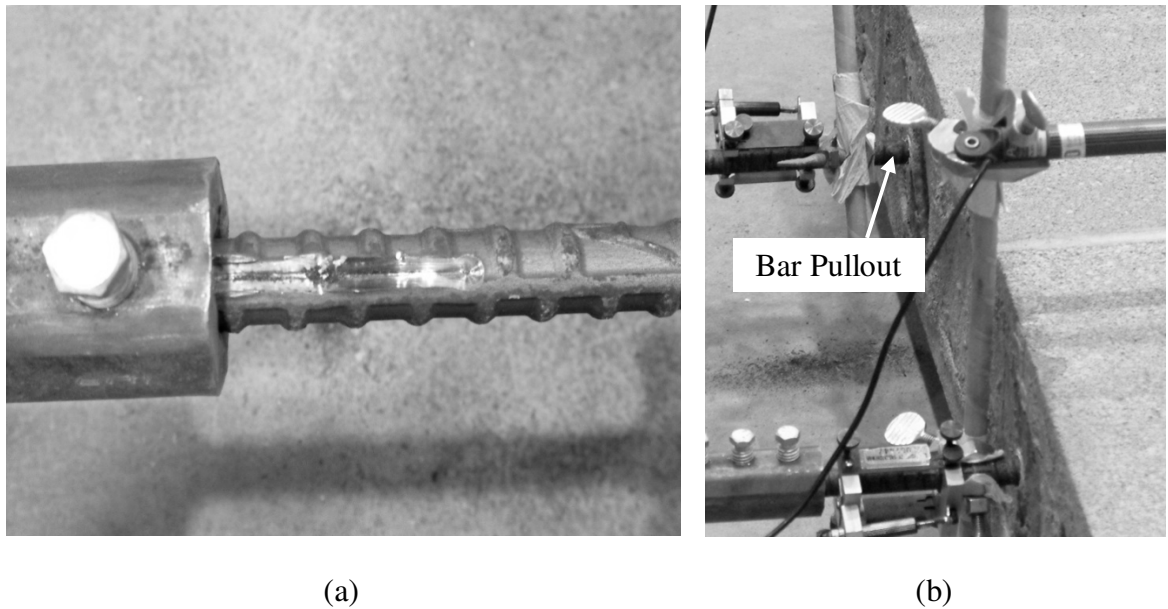
Figure 4.20: Bar pullout with mechanical coupler failure - Specimen CP-7: (a) mechanical coupler bolt shearing at resisting end, and (b) bar pullout at the loading end.

Figure 4.21 shows the typical failure mode and external cracking as observed in Specimens NCP-1 and NCP-2 tested during the first construction phase. A fine crack in the header joint adjacent to the loaded end of the two spliced reinforcing bars typically formed at a relatively low load of roughly 10 to 15% of the theoretical yield load. Bed joint cracks at the resisting end were simultaneously observed. The header joint crack in the weaker of the two splices then tended to continue into the adjacent bed joints with increased load, and eventually started to widen.  Figure 4.21 shows that the header joint crack ultimately extended into the adjacent blocks, and the specimen failed by splitting. In contrast, header joint cracking did not extend through the adjacent block in the specimens tested in the second construction phase, as shown in Figure 4.22. These specimens failed suddenly as a result of splitting at the loaded end similar to that observed for the specimens tested in Phase 1. A higher tensile resistance of the grout as

Figure 4.21: Typical splitting failure and surface crack pattern observed in a Phase 1 double pullout specimen with non-contact lap splices.

reported for the companion specimens tested in conjunction with the Phase 2 specimens might have prevented the extension of the header joint cracks.

### 4.3.3 Visual observation following the removal of face shell and grout

The face shell and grout surrounding the reinforcing bars was removed from representative specimens with both contact and non-contact lap splices following testing to reveal internal crack patterns and potential evidence of bond deterioration.

Following testing, the face shell was first locally removed from above the spliced reinforcing bars for Specimen CP-6; a representative specimen with contact lap splices that failed due to bar pullout. No additional cracks at the block-grout interface were identified. However, removal of the grout surrounding the lapped reinforcing bars then
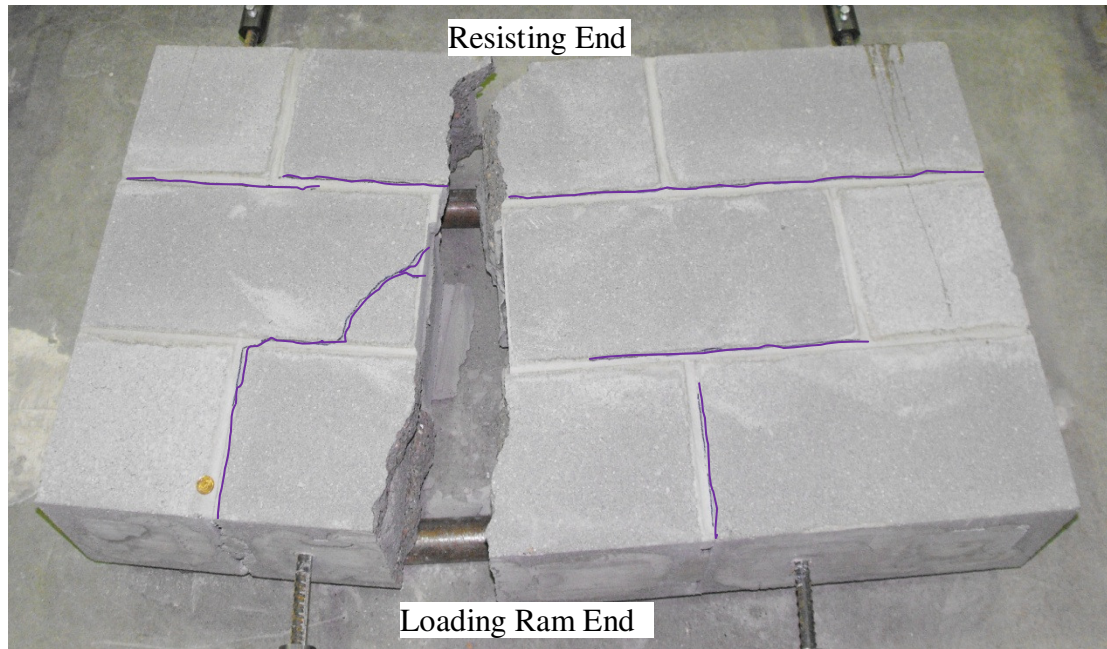
98
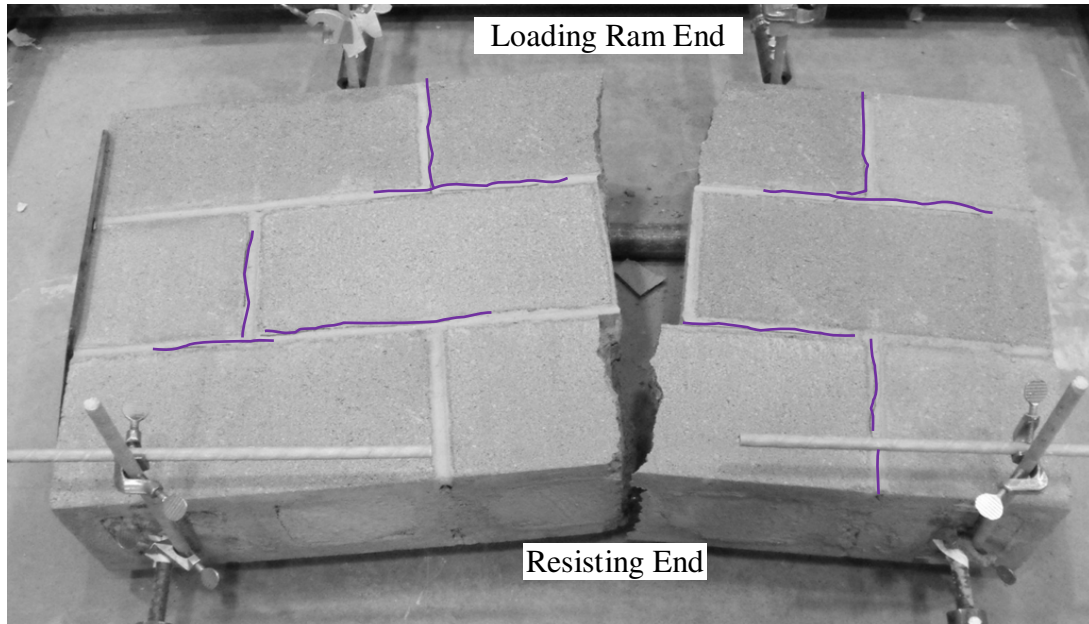
Figure 4.22: Typical splitting failure and surface crack pattern observed in a Phase-2 double pullout specimen with non-contact lap splices.

revealed end slip of the reinforcing bar as shown in Figure 4.23, with significant crushing of the grout keys that formed between adjacent ribs. This evidence of crushing confirmed the pullout failure mode as previously suspected for this specimen.

A distinct splice failure was not observed for Specimens CP-1 and CP-3. However, Figure 4.24 shows that the removal of first the face shell, and then the grout surrounding the reinforcement for Specimen CP-3 revealed a combination of longitudinal splitting cracking adjacent to the loading end of one bar in a given splice and bar slip adjacent to the resisting free end of the same bar. This suggests that the spliced bar was approaching failure when loading of this specimen was halted.
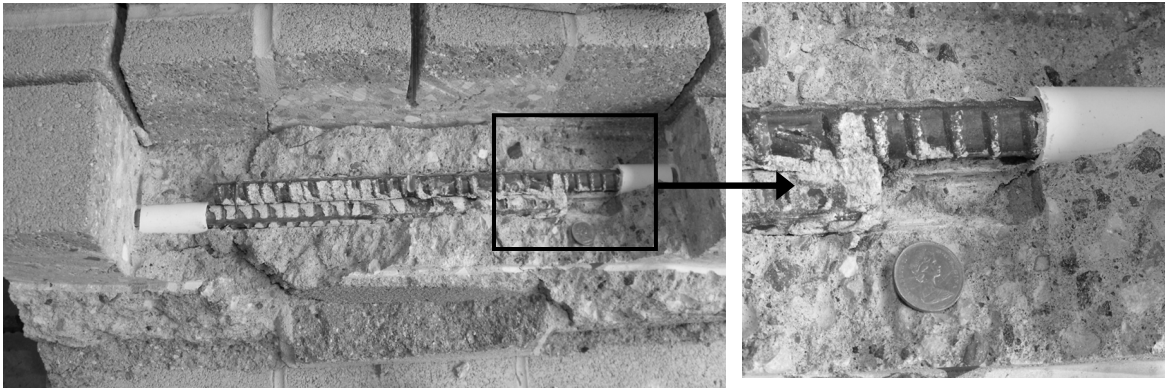
Figure 4.23: Bar pullout by shearing from the surrounding grout - Specimen CP-6.
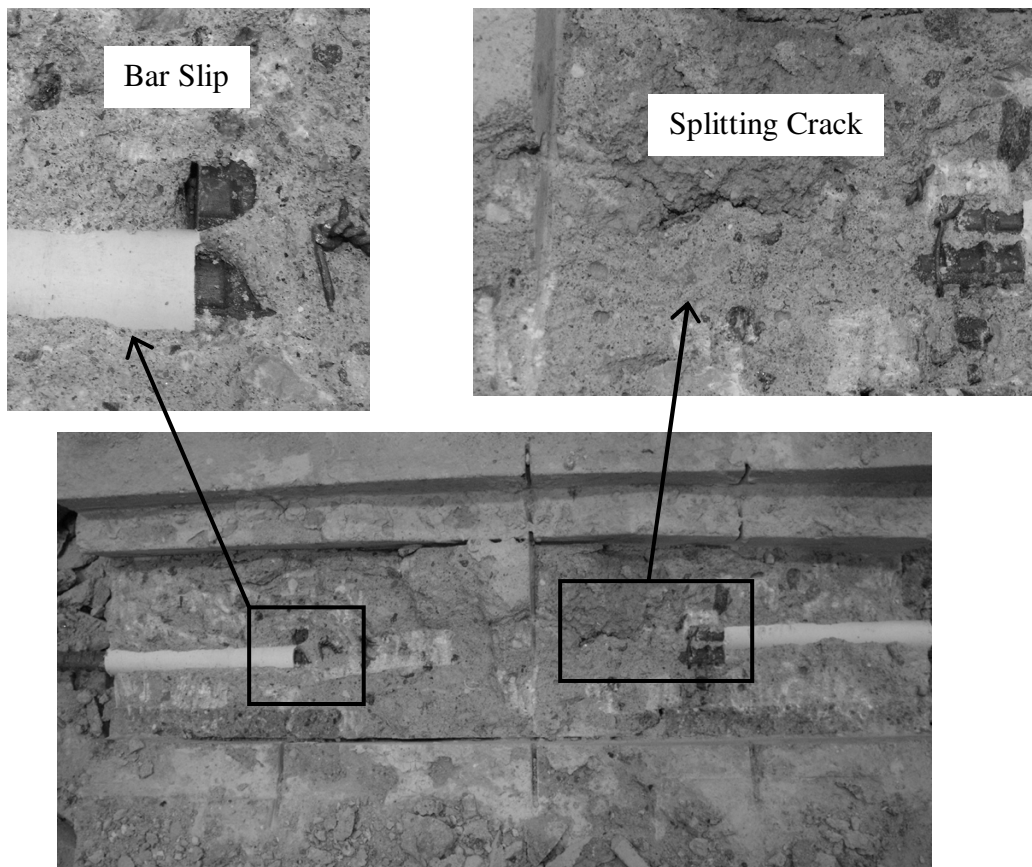


Figure 4.24: Bar pullout and splitting crack - Specimen CP-3.

Figure 4.25(a) shows that the grout in Specimen NCP-4, a representative double pullout specimen with non-contact lap splices, separated from the adjacent concrete block at the loaded end of a lapped bar. Figure 4.25(b) shows the widely spaced diagonal cracks observed upon further removal of the grout surrounding the reinforcing bar for this same specimen. The diagonal cracks extended only to the adjacent web of the concrete block and then changed orientation such that they ran along the grout/block interface as a result of poor bond between the grout and the concrete blocks. Crushing of the grout keys as well as significant slip of the lapped bars at their free ends was absent in this specimen suggesting little or no bond loss between the grout and the reinforcing bar.

Based on the observed damage, the splitting failure of the double pullout specimens with non-contact splices can be explained using basic mechanics and considering the internal bond transfer mechanism as described by Sagan et al. (1991). The arrangement of the reinforcing bars in double pullout specimens is such that the tension forces in each pair of lapped bars is separated by a lever arm and thus creates an external moment couple that acts on the specimen. Though this moment couple is quite small for the case of the specimens with contact lap splices, Figure 4.26(a) shows that the moment couple becomes more significant for specimens with non-contact lap splices. This external moment couple must be resisted by an equivalent internal moment couple in order to maintain force equilibrium.
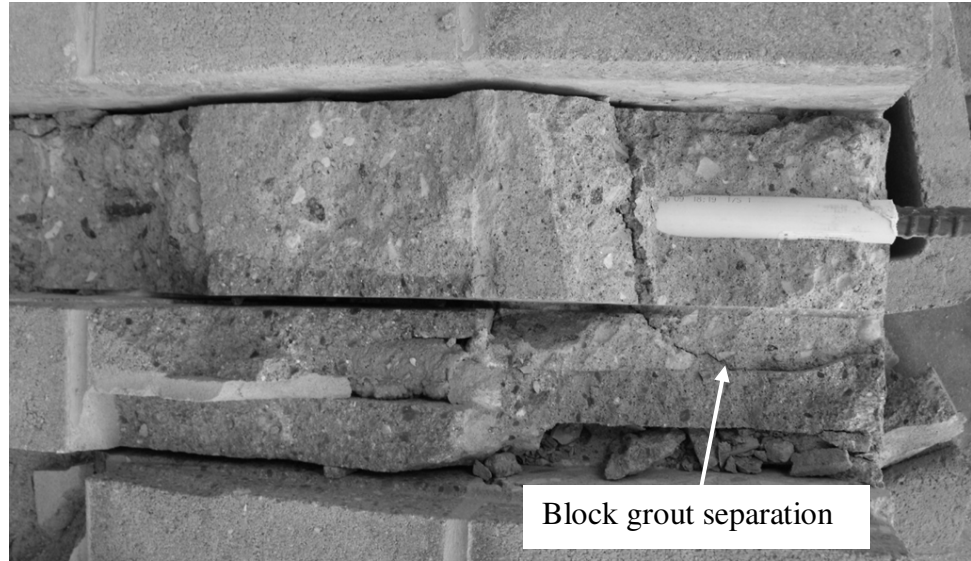
(a)



(b)

Figure 4.25: Damage observed in double pullout specimen NCP-4 after removal of: (a) face shell, and (b) grout.
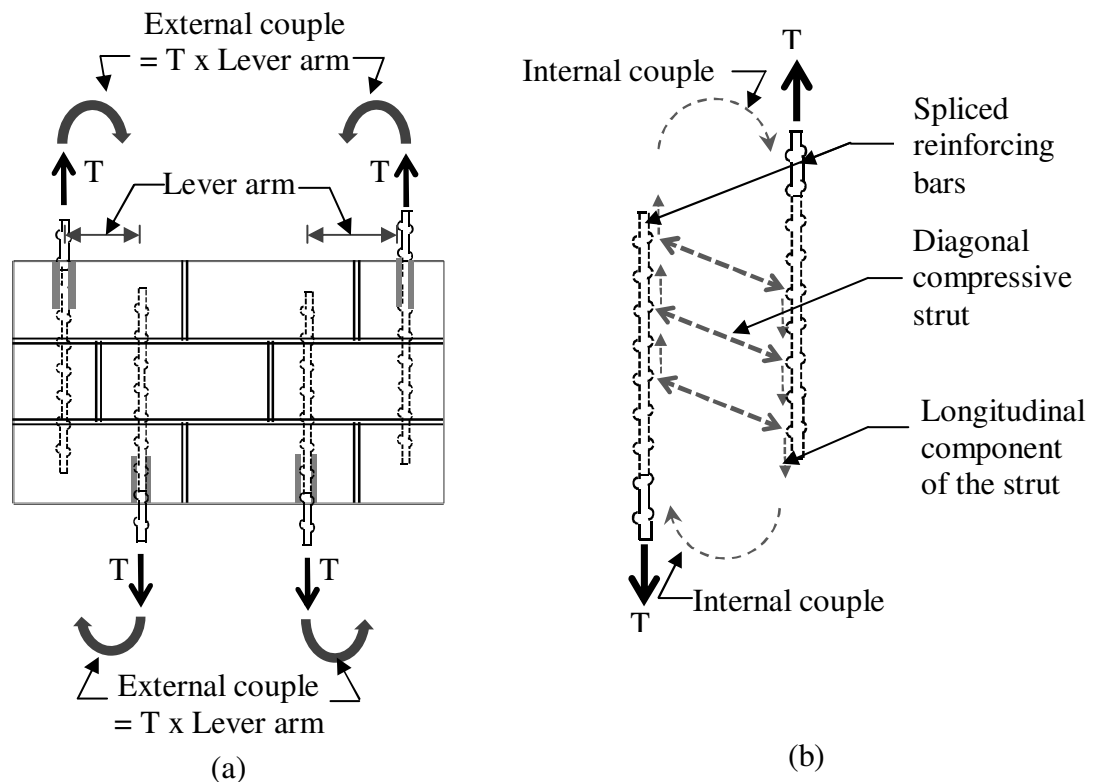
Figure 4.26: Load transfer mechanism for double pullout specimens with non-contact lap splices: (a) external forces and resulting moment couple, and (b) internal forces.

Sagan et al. (1991) showed that the formation of diagonal compressive struts between non-contact lapped reinforcing bars in reinforced concrete slabs created such a resisting internal moment. Figure 4.26(b) shows the identical mechanism for the resisting moment as created by the component of the diagonal compressive force that acts along the length of the spliced reinforcing bars in double pullout specimens. However, poor bond between the grout and the webs of the concrete blocks in masonry specimens as discussed previously, combined with the visual observations made after face shell and grout removal in these specimens, shows that the formation of an effective diagonal compressive strut was interrupted in these specimens: the magnitude of the resisting

internal moment that developed could not counteract the external moment couple in masonry specimens with non-contact lap splices when the lapped bars were located in adjacent cells. The resulting unbalanced opposite external and internal moment couples for the two splices created a lateral tension force at the loaded end of the specimens and caused splitting once the tensile capacity of the masonry assemblage was overcome.

### 4.3.4 Summary

The double pullout specimens with contact lap splices generally failed in bond with pullout failure observed in most of the specimens. In contrast, the specimens with non-contact lap splices with the lapped bars placed in adjacent cells were unable to transfer bond between the pairs of bars effectively, resulting in a sudden tensile failure for these specimens. Poor bond at the grout/block interface that was visually observed upon the removal of the face shell and the grout surrounding the reinforcement was the probable cause of the failure in these specimens.

All double pullout specimens with contact lap splices developed, as a minimum, the theoretical yield capacity of the reinforcement, while specimens with non-contact lap splices developed, on average, 46.0% of the theoretical yield capacity. The mean maximum tensile forces resisted by the No. 15 bars with 300 mm long lap splices in the double pullout specimens were 89.7 and 40.7 kN, when lapped bars were placed in contact with each other and in adjacent cells, respectively. The difference between the mean values is statistically significant at the 95% confidence level as determined from the statistical "t" test. A higher variability in the ultimate splice resistance was recorded for specimens with non-contact lap splices (C.O.V=7.57%) compared to those

constructed with contact lap splices (C.O.V= 2.37%). In contrast to the double pullout specimens with contact lap splices, the failure mechanism of the identical specimens with non-contact lap splices as described in the previous section depended upon on the block/grout bond as well as the tensile splitting strength of the masonry assemblages. These additional factors typically resulted in a higher variability in the recorded failure loads in these specimens.

## 4.4 Wall Splice Specimens

This section describes the recorded test results and observed behaviour for the sixteen wall splice specimens. An equal number of specimens were reinforced with contact and non-contact lap splices. The specimens were tested under the four-point loading system described in Section 3.7.3. The specimen behaviour described includes: the load versus midspan deflection, crack propagation at different load levels, and the observed failure modes. The face shell and grout surrounding the reinforcement were removed from representative wall splice specimens with both lap splice arrangements after testing was terminated to further investigate internal crack patterns and evidence of bond deterioration.

Internal instrumentation, such as strain gauges, was not used in the testing of the wall splice specimens. As such, the force in the reinforcing bars was not directly measured and so could not be directly compared with the results reported for the double pullout specimens. A numerical sectional analysis was therefore performed to establish the splice resistance of the longitudinal reinforcement in these specimens that corresponded

to the ultimate load reported for each of the wall splice specimens. The mean splice resistance was then computed for both specimen populations (i.e. the double pullout and wall splice specimens); the statistical "t" test was then used to determine whether the difference between the mean splice resistances for the two specimen types with identical splice arrangements was statistically significant. Theoretical moment curvature and load versus mid-point deflection curves were developed for the wall splice specimens. The theoretical curves were compared with the experimental curves and critically reviewed with respect to both the specimens with contact and non-contact lap splices.

### 4.4.1 Load deflection behaviour

Figure 4.27 shows the load versus midspan deflection for all wall splice specimens with contact lap splices. Separate curves for each of the specimens with the approximate cracking and yield loads clearly labelled are included in Appendix 4B. A summary of these cracking, yield, and the ultimate loads, with comments on the resulting failure mode for all specimens, is recorded in Table 4.5. Wall splice specimens with contact lap splices are provided with an identifying tag of "CW", with the number following the hyphen referring to the specimen number within the series. Figure 4.27 shows that a slope change between the initial two linear portions of the curves for all specimens was evident, and occurred at an average value of 5.83 kN. The point at which the slope change occurred represents a reduction in flexural rigidity of the specimens with first cracking. The average reported value is 2.65 times the theoretical value of 2.2 kN, as calculated in accordance with CSA S304.1-04 (CSA, 2004a) excluding the self-weight of the spreader beam (0.6 kN) and the specimen self-weight (9.4 kN). The higher experimental cracking loads were possibly caused by the higher tensile resistance of the
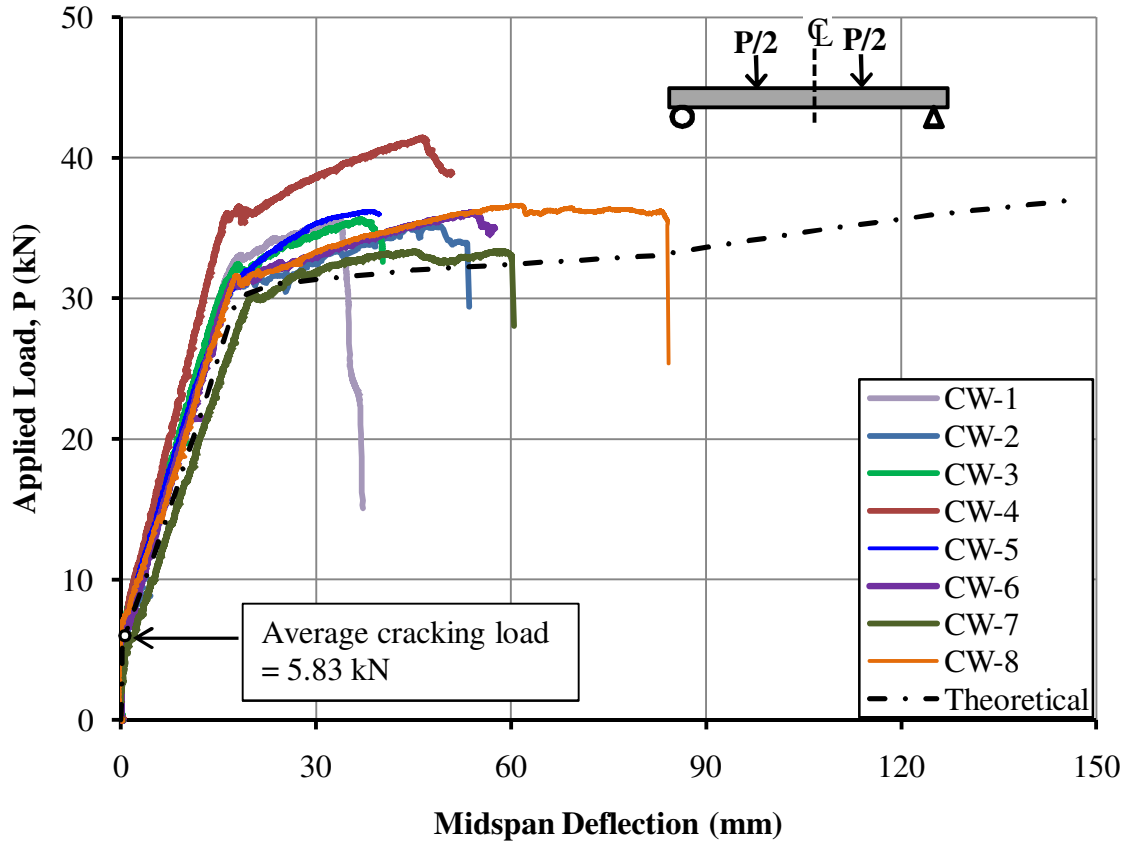
106

Figure 4.27: Load versus midspan deflection for wall splice specimens with contact lap splices.

masonry assemblage compared to that recommended by the design code. Possible frictional resistance of the support rollers may have also caused the increased cracking load by introducing an axial compression force in the walls.

Following cracking, the applied load continued to increase linearly with midspan deflection until the theoretically predicted yield load of 31.0 kN was roughly achieved. A slight load reduction then occurred, suggesting the initiation of reinforcement yielding. The mean recorded experimental load at the initiation of bar yielding was 31.2 kN excluding the value recorded from Specimen CW-4 (36.2 kN). The result for

107

Specimen CW-4 was 117% of the theoretically predicted yield load and was identified as an outlier at the 95% confidence level.

Table 4.5: Summary of loading history and failure mode for wall splice specimens with contact lap splices.

| Wall | Cracking load (kN) | Yield load (kN) | Ultimate load (kN) | Failure mode |
|------|------|------|------|------|
| CW-1 | 5.00 | 32.8 | 35.6 | Longitudinal splitting crack along lapped reinforcing bar at the tension face. |
| CW-2 | 5.30 | 31.1 | 35.1 | |
| CW-3 | 5.90 | 32.0 | 35.6 | |
| CW-4 | 5.10 | 36.2$^*$ | 41.4$^*$ | Transverse splitting crack at the ends of the splice at the tension face with mortar bed joint crushing at compression face. |
| CW-5 | 6.60 | 30.3 | 36.2 | Transverse splitting crack at the ends of the splice at the tension face. |
| CW-6 | 6.20 | 30.9 | 36.1 | Transverse splitting crack at the end of splice at the tension face with mortar bed joint crushing at the compression face. |
| CW-7 | 5.80 | 30.1 | 33.4 | Transverse splitting crack at the end of splice and longitudinal splitting crack along a lapped reinforcing bar at the tension face. |
| CW-8 | 6.70 | 31.3 | 36.6 | Longitudinal splitting crack along a lapped reinforcing bar at the tension face with mortar bed joint crushing at the compression face. |

$^*$ Outlier as established from the statistical "t" test

Loading again began to increase with increased midspan deflection, but with an 88% reduction in slope as compared to the previous linear segment. When the applied load increased to become 113% and 120% of the theoretically predicted yield load, a sudden decrease in load occurred with rapidly increasing midspan deflection signifying specimen failure.

The ultimate failure load was defined as the maximum load resisted by each specimen. The mean ultimate load for wall splice specimens with contact lap splices was 35.5 kN, excluding the ultimate failure load of 41.4 kN from Specimen CW-4 that was identified as an outlier at the 95% confidence level. It is suspected that the bars used in Specimen CW-4 were supplied from a different heat batch, resulting in high failure loads. Figure 4A-4, in Appendix 4A, shows the stress versus strain response of a bar sample collected from Specimen CW-4. The resulting curve did not have any specific yield point. The yield strength determined from the 0.2% offset method was 422 MPa and was reasonably close to the 441 MPa average yield stress of the typical reinforcing bars used in the other specimens and presented in Table 4.2. However, unlike the typical bar samples, a linear yield plateau was not observed. The stress continued to increase for this bar until failure resulting in a higher ultimate load of 677 MPa as compared to the 620 MPa that was typical for the other reinforcing bar samples that were tested.

Figure 4.28 shows the experimental load versus midspan deflection curves for all wall splice specimens with non-contact lap splices. These specimens are provided with an identification tag of "NCW", with a number following hyphen referring to the specimen

number in the series. The load versus deflection curve for Specimen NCW-3 is not shown in Figure 4.28 as it was identified as an experimental outlier due to the pullout of one of the spliced bars that was visually evident just after the first crack appeared in bed joints. A premature failure at a recorded ultimate load of 11.7 kN resulted. Sufficient bond was likely not developed between the grout and the lapped reinforcing bar at the splice location in this specimen. Results from Specimen NCW-3 were therefore excluded from the subsequent analysis. Individual load versus midspan displacement curves with clearly labelled cracking loads and theoretically predicted loads at initiation of bar yielding are presented in Appendix 4B. A summary of the cracking loads and ultimate loads for these specimens with the generally observed failure modes is summarized in Table 4.6.

Similar to the wall splice specimens with contact lap splices, Figure 4.28 shows that the two linear portions of the curves showed a slope change at the cracking load due to a reduction in stiffness once cracks first developed. The mean recorded experimental cracking load for these specimens was 3.60 kN, 1.64 times the theoretically predicted value of 2.2 kN.

Following the cracking load, a linear load versus displacement behaviour was recorded for wall splice specimens with non-contact lap splices until failure occurred. However, a brief and gradual reduction in slope was noticed as the applied load approached the ultimate load. The reduction in slope might have been caused by the reduction in stiffness due to loss of bond along the lap splice length before failure. A gradual

unloading curve following the ultimate load was only observed for Specimen NCW-1. In contrast, all other walls showed a very brief falling curve, suggesting brittle failure in these specimens. No apparent reason for this behaviour was identified except for the higher grout strength used for the Phase 2 specimens. The load versus deflection curve recorded for Specimen NCW-7 showed load drops at two intermediate values of applied load, $P \approx 4.30$ kN and 14.2 kN, but without any noticeable external damage observed during testing. It is therefore presumed that the formation of internal cracks might have caused this to occur. Unlike the wall splice specimens with contact lap splices, neither of these specimens achieved the predicted theoretical load (31 kN) coinciding with yielding of the reinforcement.
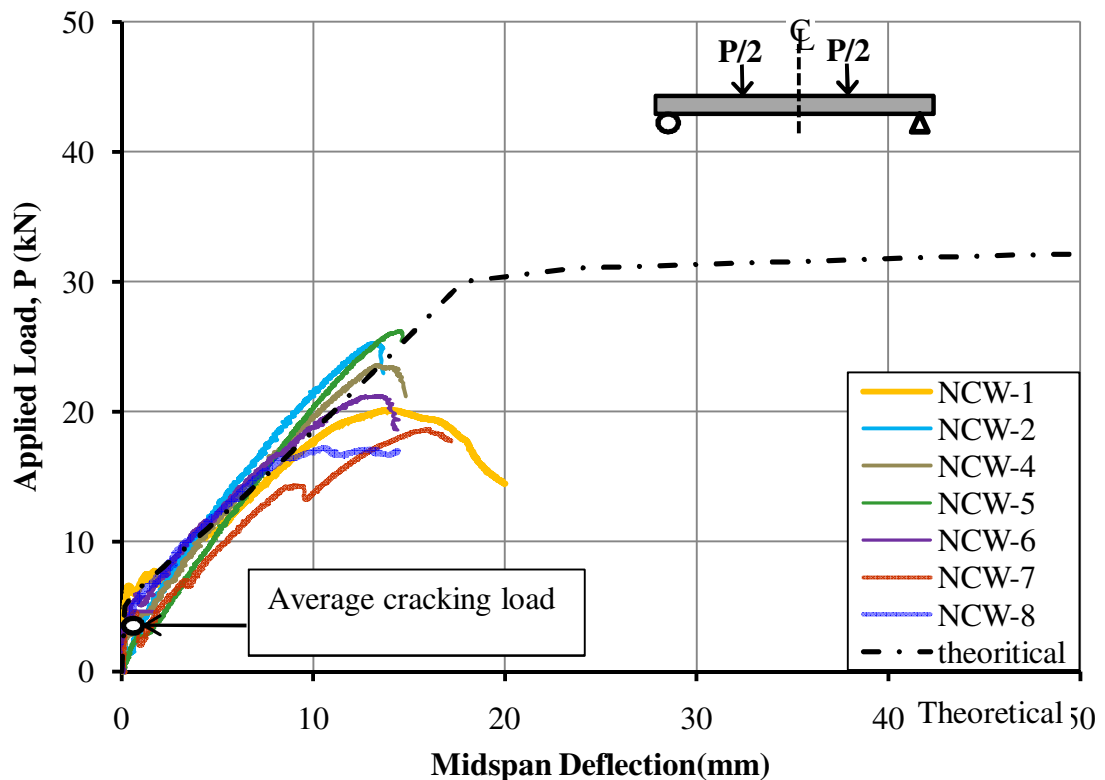


Figure 4.28: Load versus midspan deflection for wall splice specimens with non-contact lap splices.

Table 4.6: Summary of loading history and failure modes for wall splice specimens with non-contact lap splices.

| Wall | Cracking load (kN) | Yield Load (kN) | Ultimate failure load (kN) | Failure mode |
|------|--------------------|-----------------|----------------------------|--------------|
| NCW-1 | 6.11 | n/a | 20.1 | |
| NCW-2 | 1.14 | n/a | 25.3 | |
| NCW-4 | 3.10 | n/a | 23.5 | Flexural crack at the end of a splice leading to failure of the specimen. |
| NCW-5 | 2.40 | n/a | 26.2 | |
| NCW-6 | 5.10 | n/a | 21.2 | |
| NCW-7 | 3.90 | n/a | 18.7 | |
| NCW-8 | 3.40 | n/a | 17.2 | |

## 4.4.2 Visually observed damage as testing progressed

Figure 4.29 shows the crack propagation at various load levels in a representative wall splice specimen with contact lap splices. Load levels are expressed as a fraction of the theoretically predicted yield load, $P_y = 31$ kN. Figure 4.29(a) shows that vertical flexural cracks first appeared in the mortar bed joints adjacent to the load points within the constant moment region, followed by cracks along the bed joint adjacent to load points within the shear span. Lengthening of the two cracks adjacent to the load points was arrested at approximately $0.7P_y$, but the cracks continued to widen thereafter. Figure 4.30 shows such widening of a bed joint crack. A few head and bed joint cracks at the compression face close to the bar anchorage at the ends of the specimen were additionally marked when $P/P_y$ increased from 0.3 to 0.5. However, these cracks did not lengthen with any continued increase in the applied load, proving the effectiveness of the end anchorages.

Figure 4.29(b) shows the initiation of flexural cracks at mortar bed joints on both sides of the middle block as the applied load reached 0.5 $P_y$. These cracks remained shorter and narrower than those that first appeared adjacent to the points of applied load. This observation suggests higher flexural rigidity of the midspan wall section where the spliced bars were located. Other flexural bed joint cracks in the constant shear regions did not appear until the applied load reached approximately $0.5P_y$. These cracks then elongated with an increase in applied load as shown in Figures 4.29(c) and (d) for $P/P_y$ equal to 0.7 and 1.0, respectively.

Crack elongation within the constant moment region for all specimens was arrested once the applied load exceeded the theoretically predicted yield load ($P > P_y$). However, the cracks within the shear span, other than those adjacent to the loading point, continued to lengthen until splice failure occurred. The flexural cracks were limited to the mortar bed joints, and shear or inclined cracks were not observed in any of the specimens.

Figures 4.31(a) and (b) show the typical transverse and longitudinal splitting cracks, respectively, that developed within the spliced region on the tension face at failure for wall splice specimens with contact lap splices. All specimens developed one or both types of splitting cracks at failure as described in Table 4.5. Three out of the eight specimens (CW-4, CW-6 and CW-8) showed crushing of mortar bed joints adjacent to the compression face before failure occurred. However, block crushing was not observed in any of these specimens.
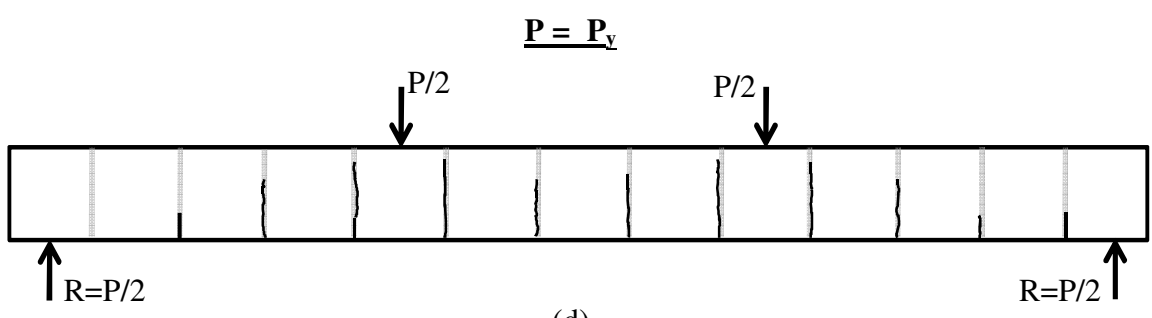
**P = 0.3P$_y$**

(a)

**P = 0.5P$_y$**

(b)

**P = 0.7P$_y$**

(c)

**P = P$_y$**
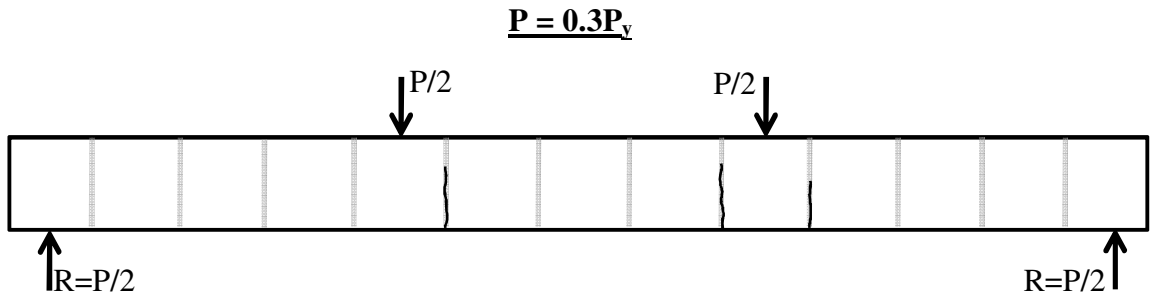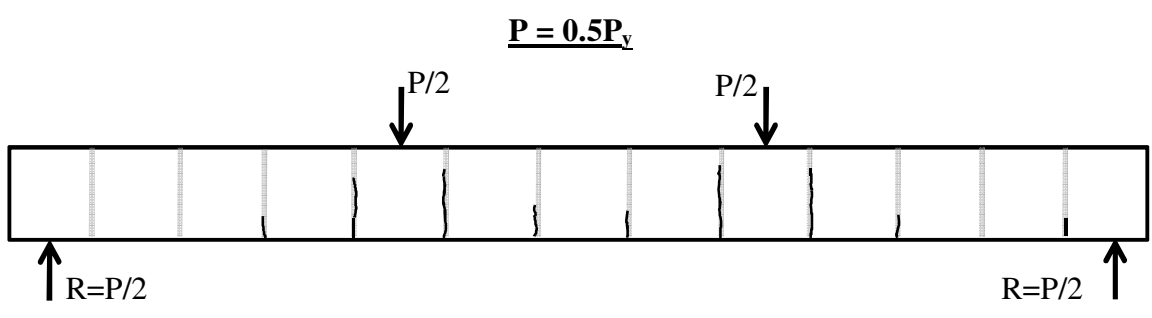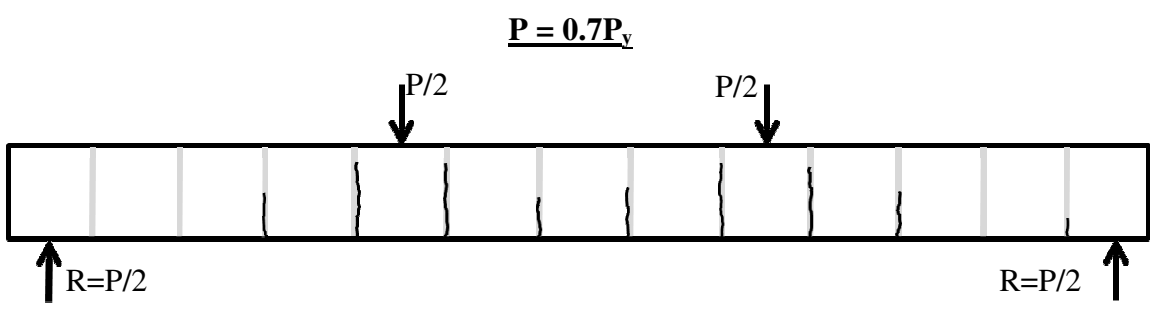
(d)

Figure 4.29: Crack propagation for a representative wall splice specimens – CW-8 at:
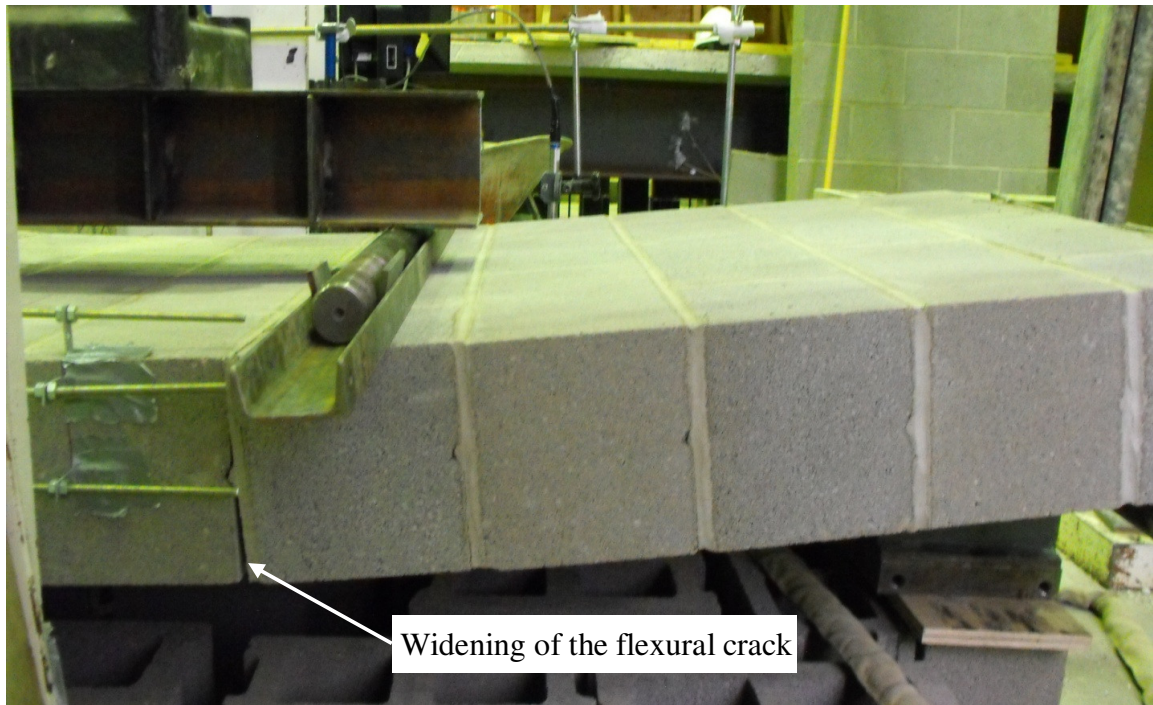(a) P = 0.3 P$_y$, (b) P = 0.5 P$_y$, (c) P = 0.7 P$_y$, and (d) P = P$_y$.

Figure 4.30: Bed joint widening in a wall splice specimen with contact lap splices observed at load level $P/P_y = 1.0$.

Similar crack propagation behaviour was observed in the wall splice specimens with non-contact lap splices at identical load levels; therefore, Figure 4.29 is also relevant for these specimens. In general, wall splice specimens containing non-contact lap splices failed at $0.5 \leq P/P_y \leq 0.7$. The length and width of the cracks in the shear spans were therefore limited for these specimens.

Figure 4.32 shows cracks at failure that typically developed in the wall splice specimens with non-contact lap splices. These specimens failed when a vertical crack in the block at one end of splice developed, followed by the formation of a diagonal crack initiating from this vertical crack to the transverse splitting crack at the other spliced bar end.

These cracks were visible on both the tension and compression faces. Once the first lap splice in a given specimen failed in this manner, the redistribution of forces to the remaining lap splice overloaded the reinforcement that was still effective, causing an immediate failure of the specimen indicated by a sudden drop in the applied load.
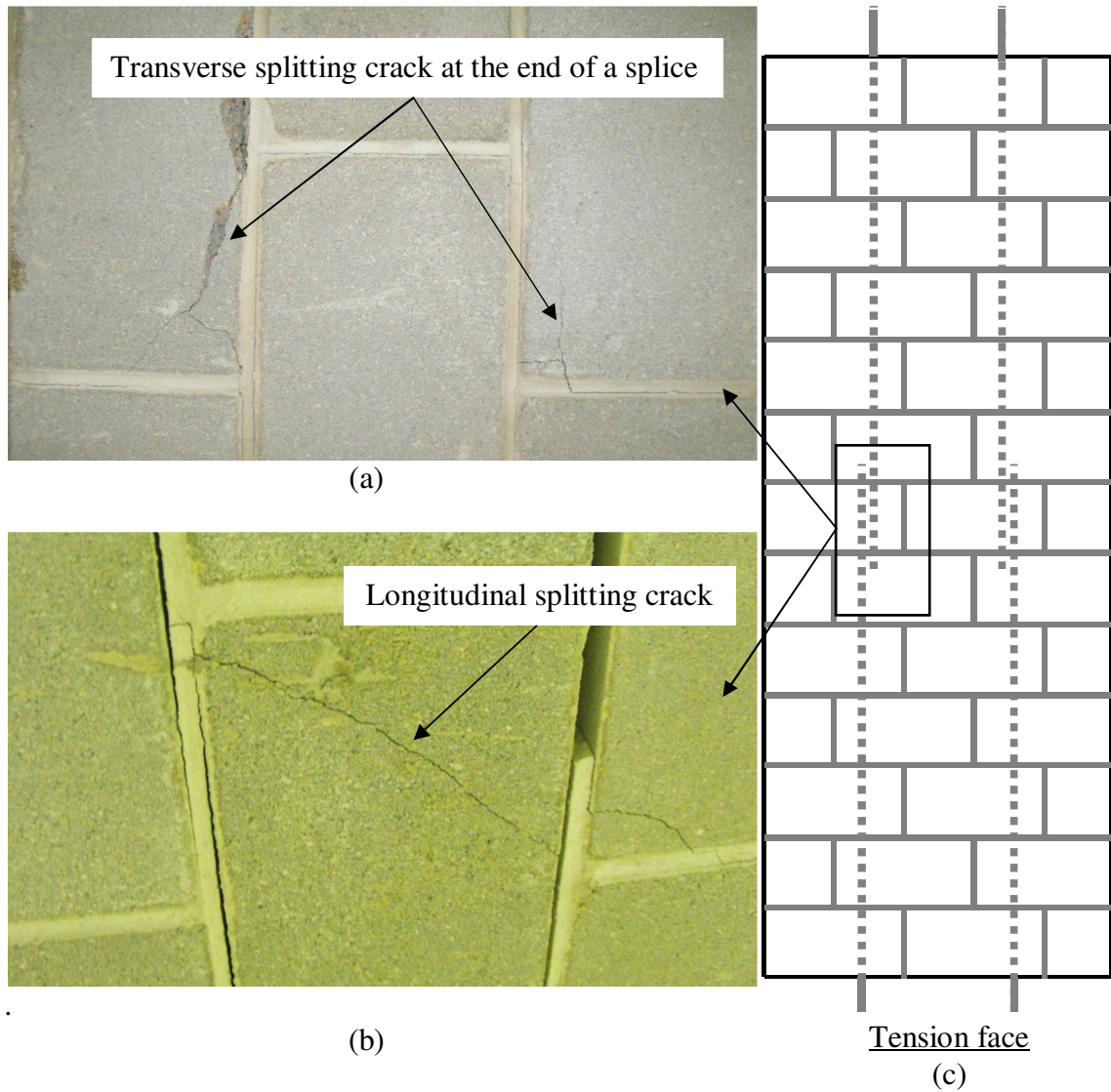


Figure 4.31:Cracking at failure for wall splice specimen with contact lap splices: (a) transverse splitting crack, (b) longitudinal splitting crack, and (c) crack locations.
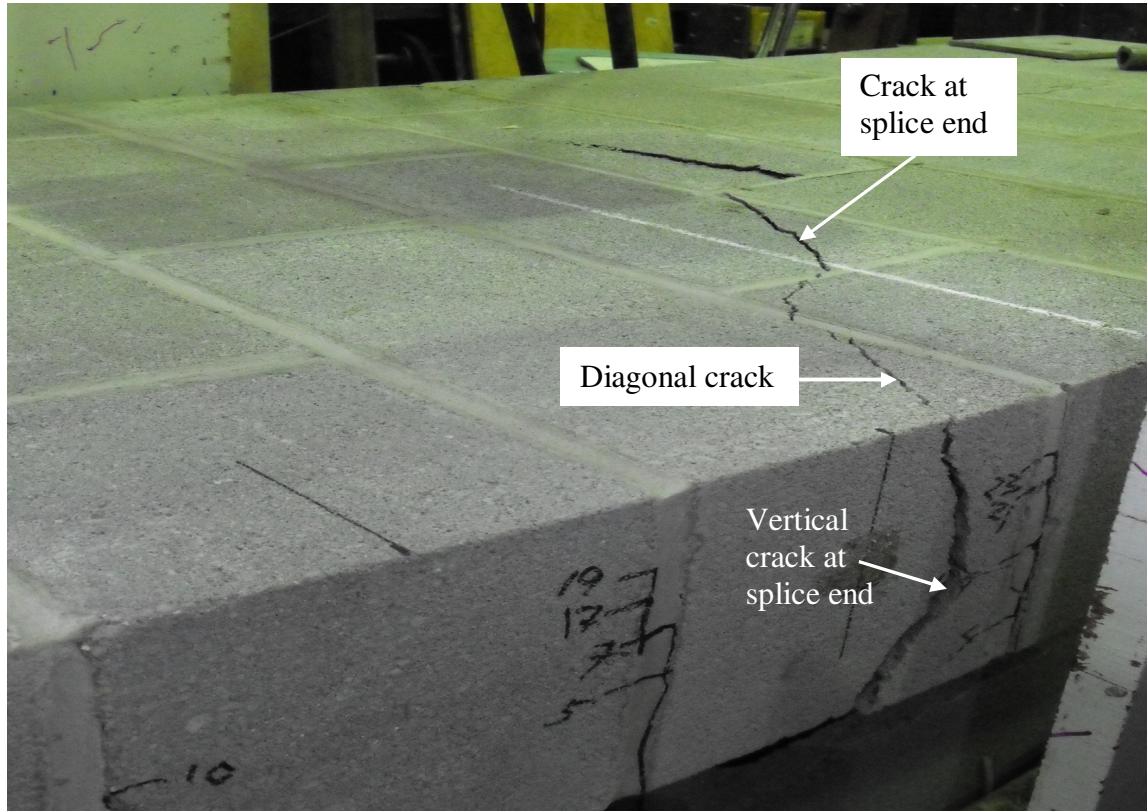
116

Figure 4.32: Typical cracking at failure for a wall splice specimen with non-contact lap splices - Specimen NCW-2.


### 4.4.3 Damage observed upon removal of the face shell and grout

The face shell and grout surrounding the reinforcement was removed from the tension face following testing for two representative wall splice specimens with contact lap splices (Specimens CW- 5 and CW-7) to examine the internal crack propagation and evidence of a possible bond failure. Figure 4.33 shows that, upon removal of the face shell, a longitudinal splitting crack in the end webs of a block was evident and provided an indication of bar pullout. Once the grout surrounding the reinforcing bars was additionally removed, Figure 4.34 shows evidence of crushing of the grout keys between the ribs of the reinforcing bars. This evidence suggests that bond failure

117

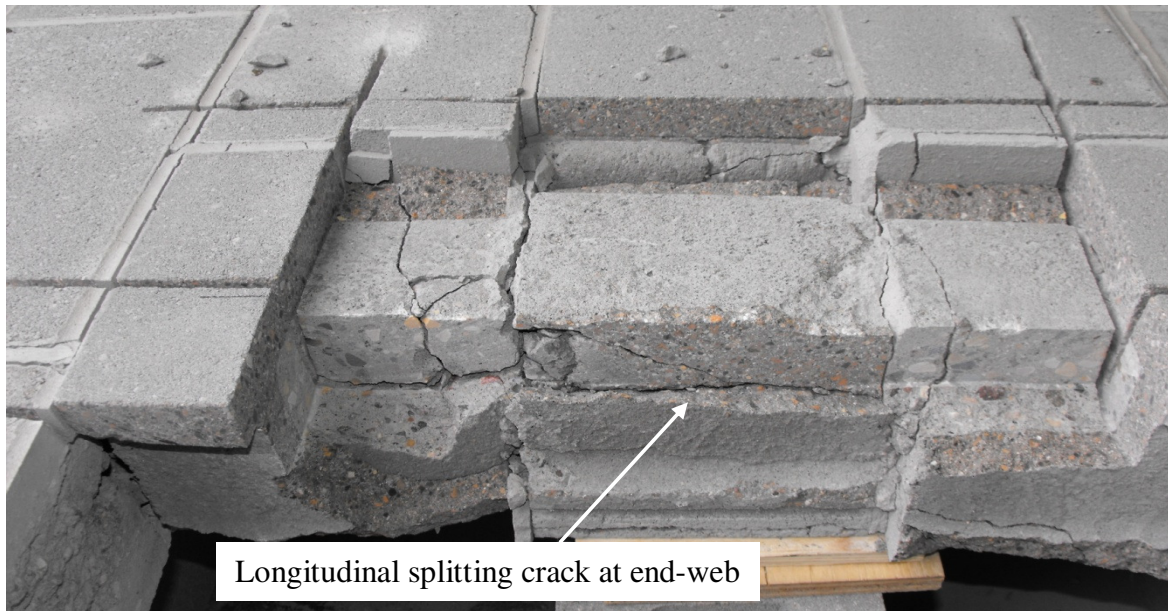Longitudinal splitting crack at end-web

Figure 4.33: Crack propagation revealed after face shell removal – Specimen CW-7.

between the reinforcing bar and the surrounding grout occurred in this specimen. Evidence of a similar failure for Specimen CW-5 was also observed.

Similarly, the face shell and grout surrounding the reinforcement was removed from the tension face of two representative wall splice specimens with non-contact lap splices (Specimens NCW-2 and NCW-6) following testing. Unlike the specimens with contact lap splices, crushing of grout keys between the ribs of the reinforcing bars and slip of reinforcement were not evident. Instead, Figure 4.35 shows that, upon removal of the grout up to the effective depth of the reinforcement, distributed diagonal cracks in the remaining grout existed between the pairs of bars in a given lap splice. These cracks changed orientation once they reached the block that existed between the lapped bars such that they then ran along block-grout interface. This cracking suggests poor bond

between the grout and the concrete blocks. A similar crack pattern was evident in the double pullout specimens with non-contact lap splice as is described in Section 4.3.3.
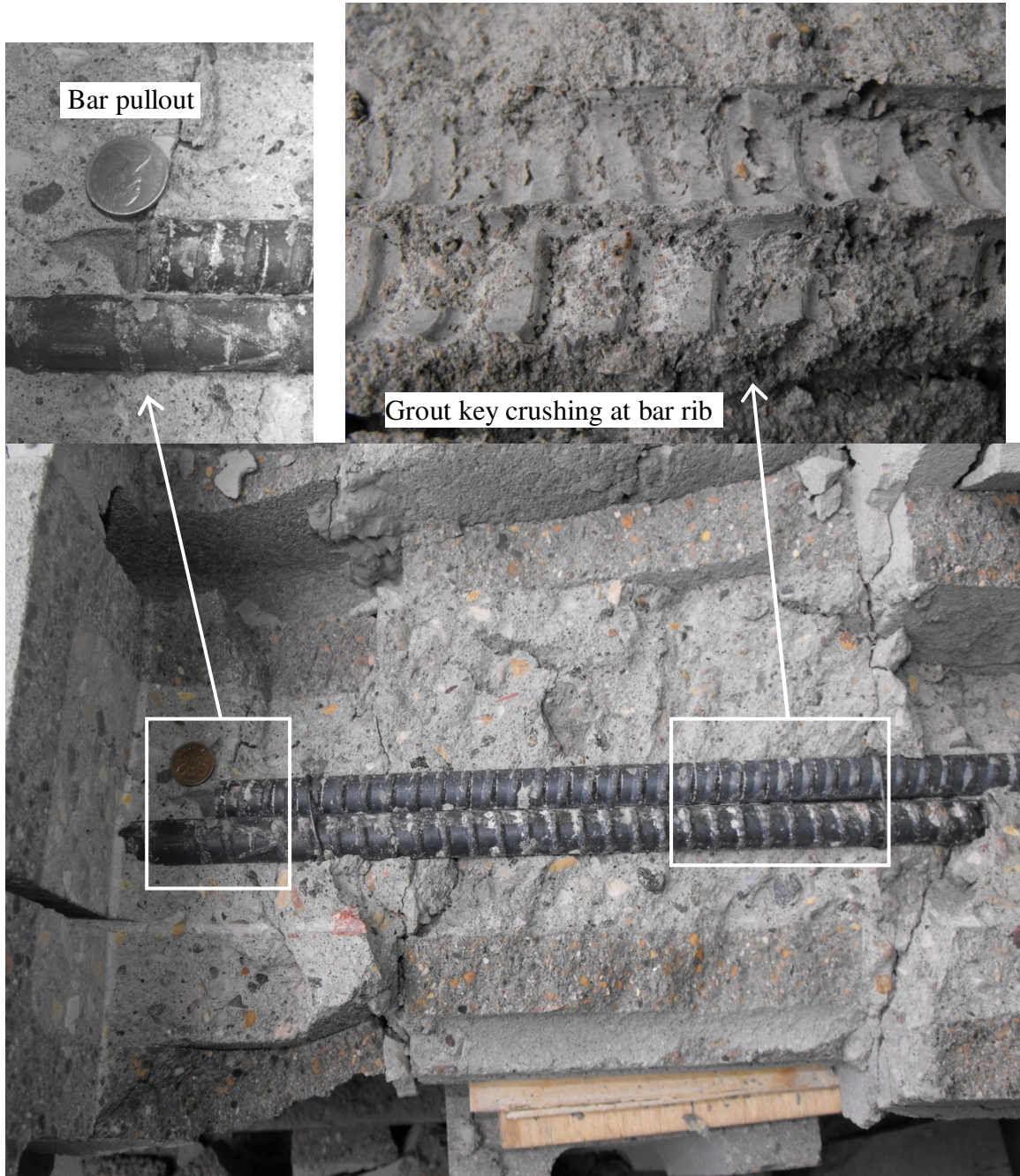


Figure 4.34: Reinforcing bar pullout and bond deterioration as observed after grout removal – Specimen CW-7.
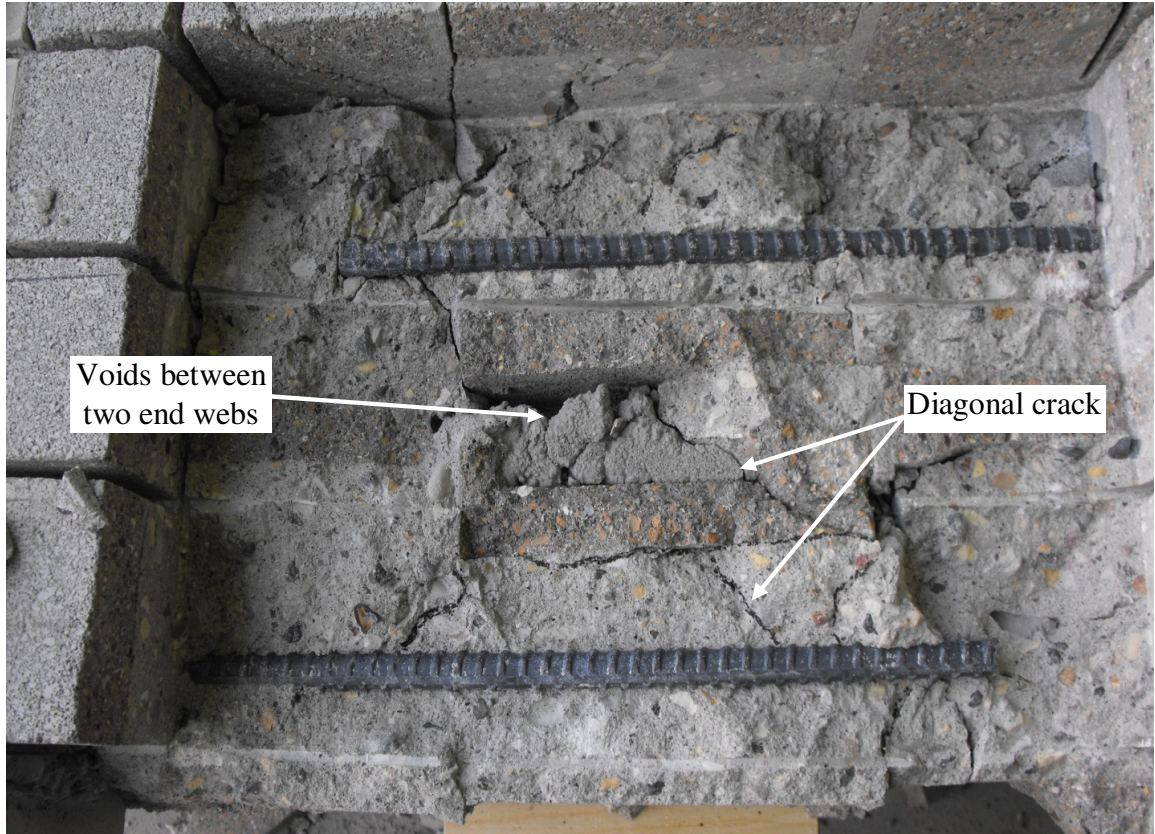
Figure 4.35: Crack propagation revealed after grout removal – Specimen NCW-2.

Figure 4.36(b) shows that removal of the face shell and grout surrounding the reinforcement in the wall splice specimens with non-contact lap splices revealed air voids in the grout adjacent to the reinforcing bars. These air voids may have resulted from the vibration of the isolated non-contact spliced bars in the cells. Figure 4.36(a) shows that such an air void may have resulted in an additional longitudinal splitting crack along the bar in Specimen NCW-6 observed after removal of the face shell alone. Figures 4.35 and 4.36(b) shows additional air voids that typically formed between the two frogged ends of the adjacent concrete blocks as the grout in this region did not get properly consolidated and thus offered a path for crack propagation in these specimens.
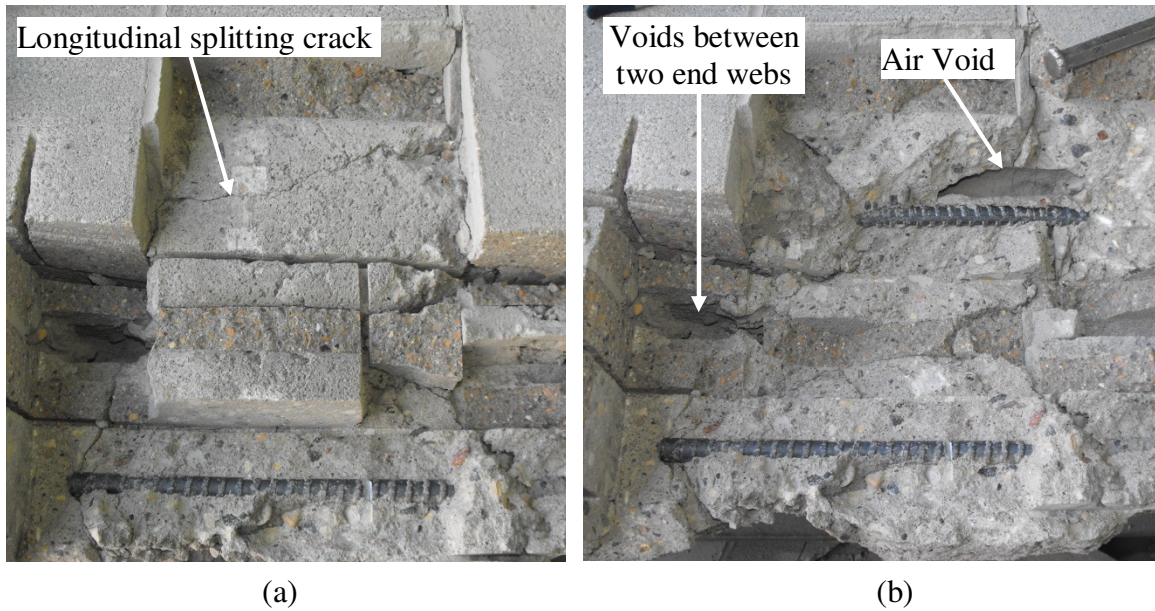
Figure 4.36: Internal crack propagation - Specimen NCW-6: (a) after removal of face shell, and (b) air void detected after grout removal.

The observed crack propagation suggests that poor bond between the grout and the surrounding block, similar to that observed in the double pullout specimen counterparts, resulted in the inefficient transfer of tensile forces between the spliced bars. This occurred due to the ineffective formation of diagonal compressive struts as described in Section 4.3.2. When tension in each of the lapped bars overcame the horizontal component of the ineffective diagonal struts, a net resulting tension force develops in each of the lapped bars. This unbalanced tension force was then transferred to the surrounding grout. Splitting cracks then developed at the bar end when the resulting stress exceeded the tensile strength of the grout. A diagonal crack then travelled towards the other bar end in a given lap splice and splitting cracks formed, resulting in the failure of the splice that was evident by a drop in the applied load.

**4.4.4 Deflection profiles for wall splice specimens**

Figure 4.37 shows the deflection profiles for a typical wall splice specimen with contact lap splices at several load levels: P = 10, 20, 30, and 35 kN. The recorded deflections from the five LVDTs located along the length of the specimen as described in Section 3.7.2 were used for comparison with the second degree parabolic curve fit based on the LVDT data as calculated for each wall splice specimen. The resulting form of the deflected profile for all load levels shown in Figure 4.37 is presented as $y(x) = Ax^2+Bx$, where y is the vertical deflection from the initial position and x is the distance along the specimen with datum at midheight of the section at the left support. The constants A and B are calculated to provide the best fit curve. Figure 4.37 shows that the derived curves showed good agreement with the deflected profile with a root mean square error (RMSE) typically within 10 to 13% of the midspan deflection. The derived equations were also used to calculate the experimental curvature as discussed in the following section.

**4.4.5 Analysis of the wall splice specimens**

The maximum tension resisted by the spliced reinforcing bars could not be obtained directly for the wall splice specimens since the reinforcing bars were not instrumented with strain gauges. A numerical moment-curvature analysis was therefore performed for these specimens based upon the experimentally obtained stress versus strain relations for the masonry assemblage (Section 4.2.3) and the reinforcing bars (Section 4.2.4). The stress versus strain profiles were used to establish the compressive force in the masonry and the tensile force in the reinforcing steel from a linear strain profile corresponding to
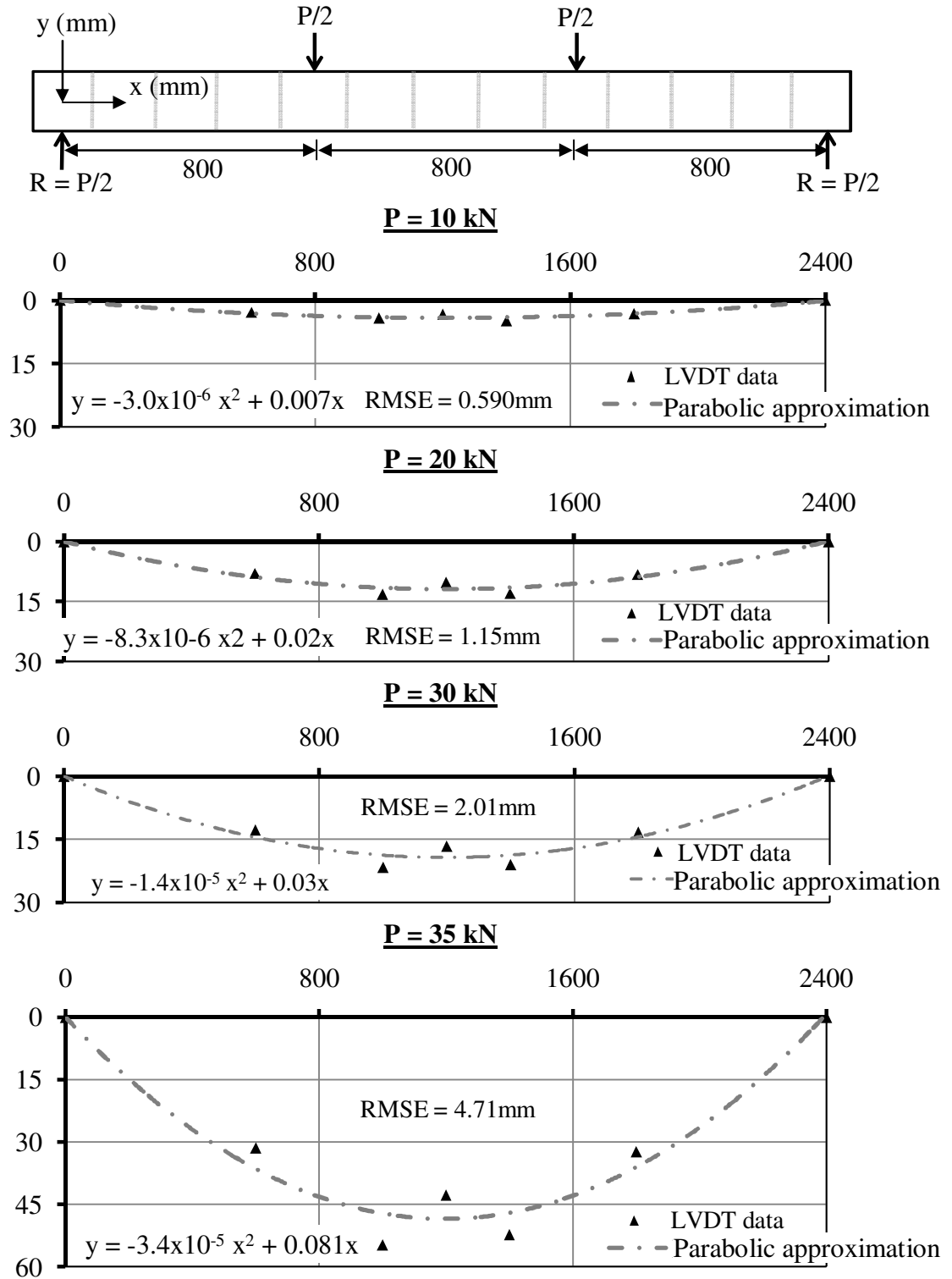
Figure 4.37: Experimental deflection profile and parabolic curve fitting at different load levels for a representative wall splice specimen – Specimen CW-7.

an assumed neutral axis depth. The numerical iterative program developed then established the neutral axis depth such that force equilibrium in the section was attained.

Once the neutral axis was obtained, the theoretical curvature corresponding to the moment was calculated from the neutral axis depth. The theoretical moment-curvature relationship thus developed was then compared with the experimentally obtained moment-curvature curves discussed in Section 4.4.4. The tensile force in the reinforcing bars at the ultimate load was then calculated based upon the theoretical curvature at that load and the resulting force equilibrium in the specimen cross-section. The calculated splice tensile resistance was then directly comparable to that recorded for the double pullout specimens. In addition, a theoretical load versus midspan deflection curve was generated assuming that the longitudinal reinforcement in the specimen was continuous (i.e. not spliced); this then compared with the deflection data recorded by the LVDTs as presented in Section 4.4.4 to critically review the deflection of the tested specimens.

**Moment-curvature analysis**

A compressive stress versus strain profile for the grouted masonry, known as the modified Kent-Park curve (Park et al., 1982), was adopted for the current study. The curve includes a parabolic rising segment from the initiation of loading up to the maximum stress followed by a linearly falling segment. Experimental investigations performed by Priestley and Elder (1983) for unconfined grouted concrete masonry prisms showed good agreement with the modified Kent-Park curve when the model was further modified to allow the strain corresponding to the maximum stress to be set equal to 0.0015 instead of 0.002 as proposed in the original model. A review of the test data

124

obtained in the current investigation, however, shows that the strain corresponding to the maximum stress had a mean value of 0.002. The modified Kent-Park curve (Park et al., 1982) was therefore used for the current study without the further modifications as proposed by Priestley and Elder (1983). Figure 4.1 shows that the generated analytical stress versus strain profile show good agreement with a representative experimental curve. The detailed expression for the curve is provided in Appendix 4C.

The tensile stress versus strain profile for the reinforcing bars was derived from the average tensile properties from bar sample tests as summarized in Table 4.2. The linear-elastic portion of the curve continued up to the yield strain with a slope equal to the modulus of elasticity ($E_s$). The yield plateau then continued up to the beginning of the strain hardening region. A fourth-order parabolic strain curve was assumed for the strain hardening region of the stress versus strain profile and was developed using the boundary conditions as established from the tensile tests of the reinforcing bar samples to find the constants in the parabolic curves. The boundary conditions included: the slope at the beginning of strain hardening, that the yield stress remained constant until the initiation of strain hardening, that zero slope occurred at the ultimate stress, and the value of the ultimate stress corresponding to the ultimate strain. Table 4.2 presents these values for all companion tests of the reinforcing steel bars. The generated theoretical stress versus strain curve is shown in Figure 4.2 and shows good agreement with a representative reinforcing bar sample test result. The detailed expression for the resulting theoretical stress versus strain profile is provided in Appendix 4C.

The curvature of the uncracked section was then calculated from the ratio of the applied moment to the flexural rigidity of the gross section ($M_a / E_m I_g$). Once the applied moment increased beyond the cracking moment ($M_{cr}$) obtained from averaging the experimental values as reported in Table 4.5 and 4.6, the effective flexural rigidity ($E_m I_e$) was reduced and varied with the subsequent increase in the applied moment. The moment corresponding to any curvature for the cracked section was then calculated considering both strain compatibility and force equilibrium.

The analysis assumed that plane sections remained plane after bending and that perfect bond existed between the reinforcing bars and the surrounding grout. The tensile force carried by the concrete blocks and grout was neglected. It was also assumed that friction was not developed at the supports and thus the walls did not experience any axial compressive force.

A finite difference approach was used for the flexural analysis of the cracked section, assuming the neutral axis location for a given curvature value. The compression zone depth was then divided into 100 segments of equal thickness. The error associated with this selection of 100 segments was determined to be 0.06% and is described in Appendix 4D. For any finite segment located at a distance $d_i$ from the neutral axis as shown in Figure 4.38(a), the strain ($\varepsilon_i$) at mid-height of the segment can be computed using the linear strain profile shown in Figure 4.38(b). The compressive stress ($f_{mi}$) corresponding to the resulting strain for the segment was then obtained using the theoretically derived stress versus strain relation for the masonry assemblage. The

126

product of compressive stress in that segment and its cross sectional area gave the compressive force resulted in the segment ($C_i$). Figure 4.38(c) illustrates the calculation of the total compressive force, C, by adding compressive force resulting in all finite segments. The strain in the reinforcement, $\varepsilon_s$, was also established from the linear strain profile in Figure 4.38(b), knowing the centroidal distance of the reinforcing bars from the neutral axis. The total tensile force in the reinforcement, T, as shown in Figure 4.38(c), was then calculated as the product of tensile stress corresponding to the steel strain as derived from the theoretical stress versus strain curve developed for the reinforcement times the nominal steel cross-sectional area.
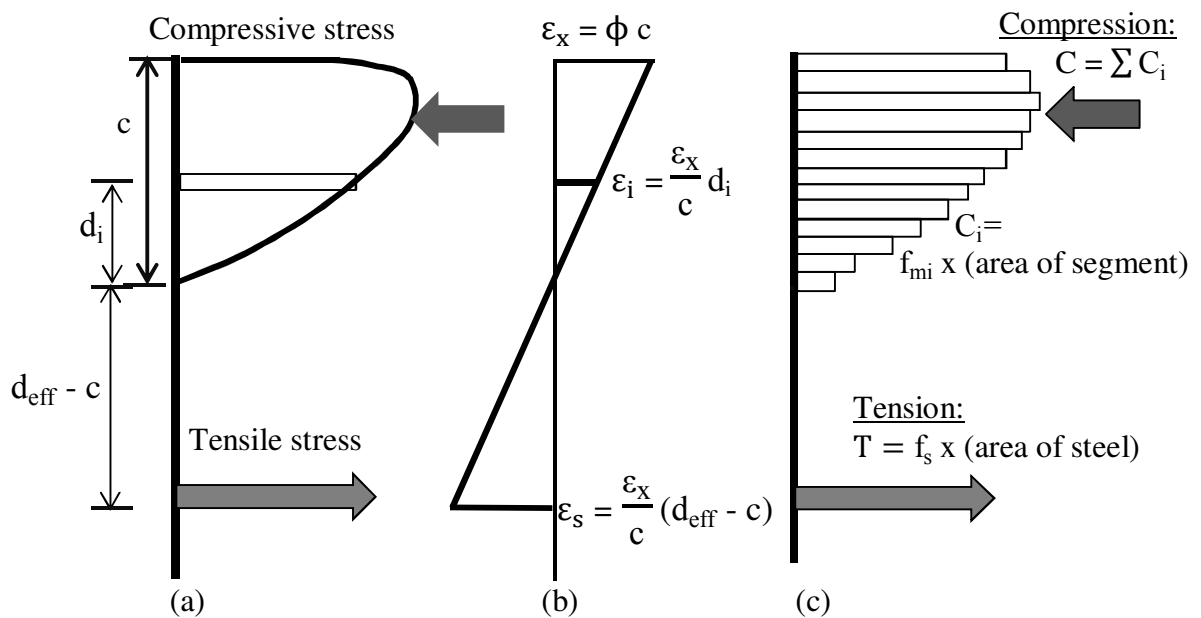


Figure 4.38: Sectional analysis of wall splice specimens: (a) Stress distribution, (b) Strain profile, and (c) Force in masonry and reinforcing bars.

Figure 4.39 shows the procedural flow chart for the iterative program used to establish the neutral axis depth (c), when equilibrium was satisfied between the compressive force

in the masonry and the tensile force in the reinforcement, as defined by allowing a maximum 0.5% difference between the magnitudes of these two forces. The detailed mathematical expressions and the Mathcad program code are described in Appendix 4D. Once the neutral axis depth was established, the resisting moment was then computed by summing the incremental compressive forces in each layer times the distance between the centroid of each layer and the tensile force in the reinforcements. Figure 4.40 shows the theoretical moment-curvature curve developed using the analytical method as described above.

Input ,
Curvature = $\phi$

Assume , **c**

Compute:
Compression , **C**
Tension, **T**

**No**

Check,
**C = T**

**Yes**

Compute Moment, M
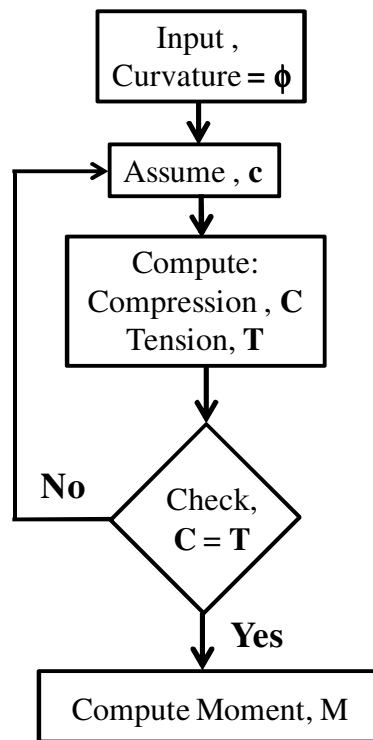
Figure 4.39: Flow chart for the iterative program used to establish neutral axis depth.

Knowing from basic mechanics that curvature is the second derivative of the deflection, differentiating a parabolic deflection profile, $y(x) = Ax^2 + Bx$, twice with respect to x gives the experimental curvature at any load level. The second degree equations

128
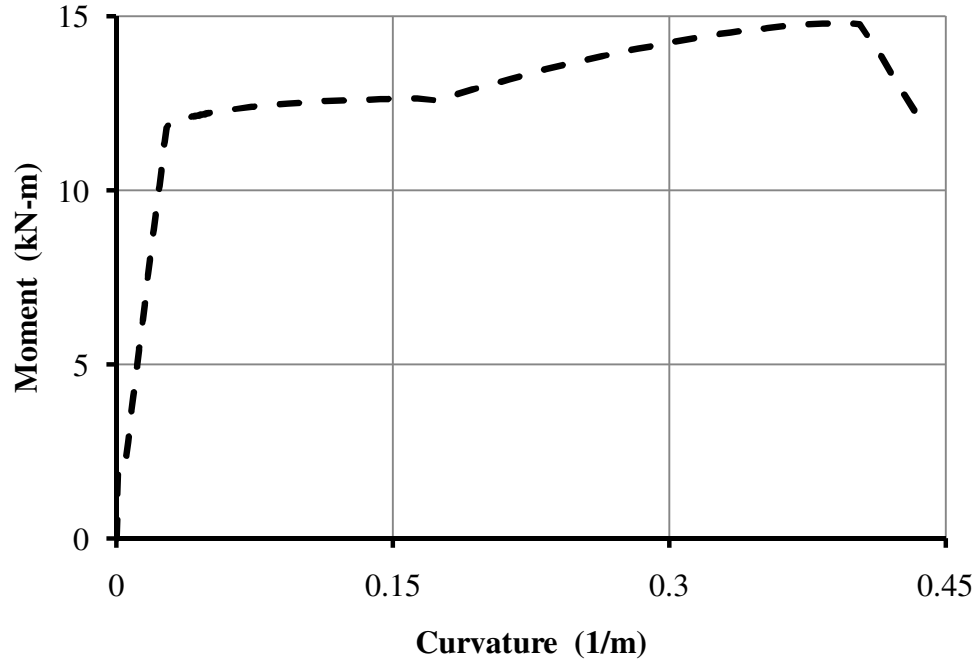
Figure 4.40: Theoretical moment curvature analysis for wall splice specimens.

obtained from the fitted curves in the deflection profiles for different load levels as described in Section 4.4.4 were therefore used to obtain the experimental curvature at each load level. The detailed calculation for a representative specimen with contact lap splices is provided in Table 4D-1 in Appendix 4D. Identical calculations were performed for the wall splice specimens with non-contact lap splices. Figures 4.39 and 4.40 show the experimental and theoretical moment curvature curves for the wall splice specimens with contact and no n-contact lap splices, respectively. The theoretical curves presented in these figures are corrected for the self-weight of the wall splice specimens and the weight of the spreader beam and associated hardware used to establish loading arrangement. The experimental curvature corresponding to moments less than 2 kN-m were not calculated since the very small deflections (less than 0.1mm) recorded by the LVDTs made it complex to fit a parabolic curve to these data. Unlike the theoretically established curves, a sudden change in slope was not observed in the experimental

129

curves as they were derived from the deflection profile of the specimen as a whole: the actual flexural rigidity of the uncracked section therefore changed gradually to that of the cracked section.

Figure 4.39 shows that a linear moment-curvature relationship was observed for all wall splice specimens with contact lap splices until they reached the theoretically predicted yield moment of the reinforcement of 12.4 kN-m. The moment then continued to increase with a reduced slope that, on average, was only 11% of that measured before yielding of the reinforcement. However, the average slope was three times greater than that of the theoretical curve within the same yield plateau region. It is therefore suspected that the reinforcement might have attained some level of strain hardening as will be further discussed in the following section. In contrast, Figure 4.40 shows that wall splice specimens with non-contact lap splices failed before the reinforcement yielded. The linear experimental moment-curvature curves very closely followed the theoretical curves until failure occurred. A deviation from the theoretical curve was observed for Specimen NCW-7, caused by the large deflection of this specimen prior to failure as shown in Figure 4.28. Figures 4.41 and 4.42 show that the experimental moment curvature curves showed good agreement with the theoretical curves for wall splice specimens with both splice arrangements and thus suggests that the forces calculated by the moment-curvature analysis closely approximate the actual forces developed in the wall section.
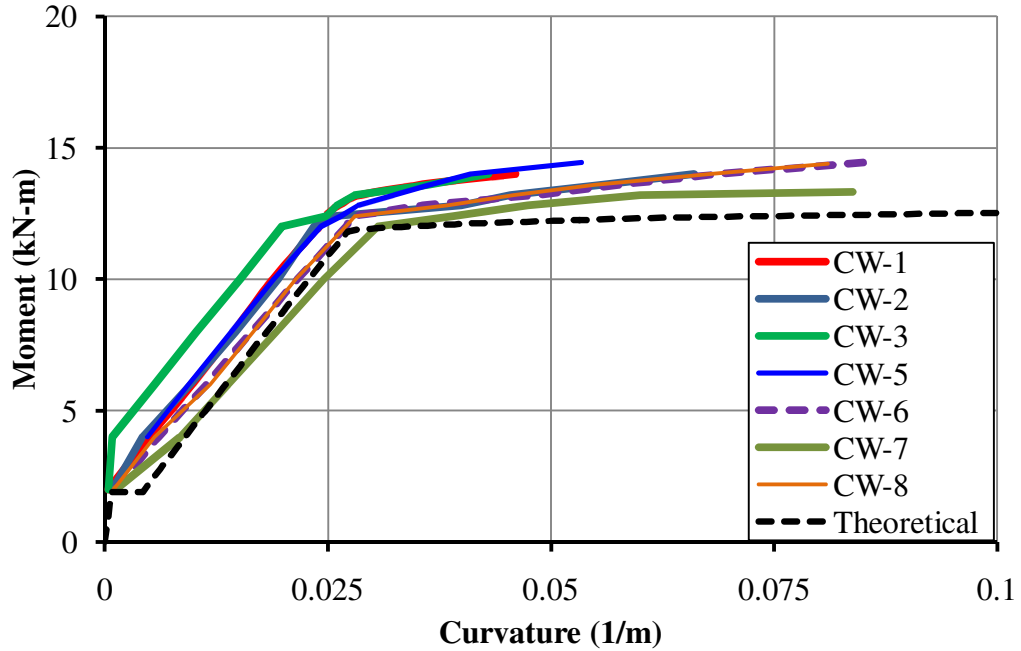
Figure 4.41: Experimental and theoretical moment curvature relationships for the wall splice specimens with contact lap splices.
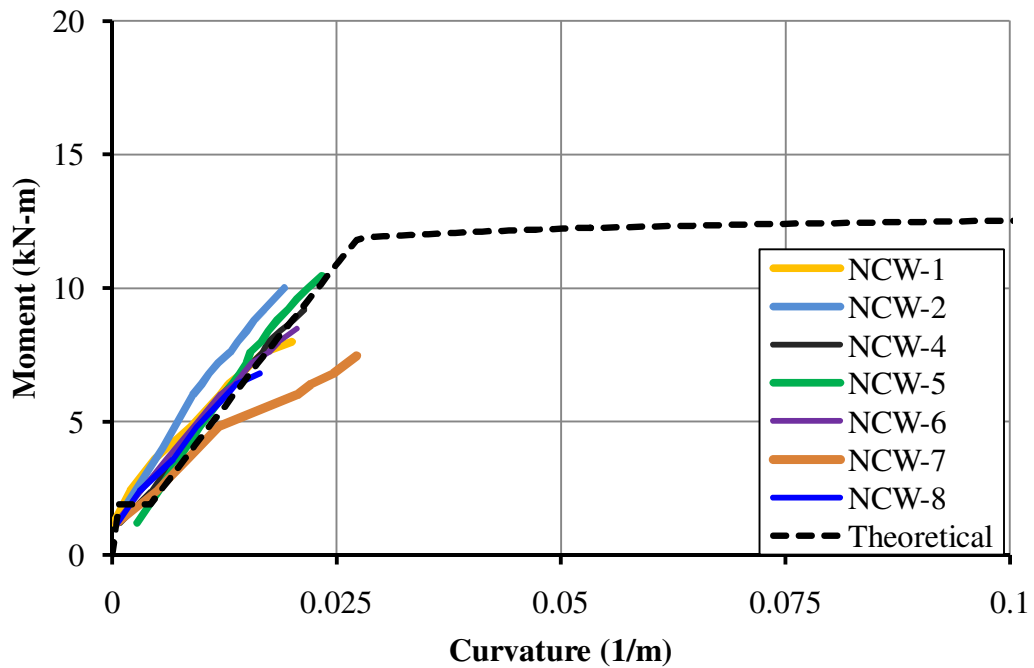


Figure 4.42: Experimental and theoretical moment curvature relationships for the wall splice specimens with non-contact lap splices.

**Development of theoretical deflection curve**

The theoretical deflection at the midspan of the wall slice specimens was calculated from a numerical iteration using the conjugate beam method. According to the conjugate beam method, the deflection at any point is equal to the moment at that point when the beam is loaded with a fictitious load equal to the curvature resulting from the actual load. A finite difference method, in which the length of the beam was divided into 240 equal segments, was used to evaluate the midspan deflection for all wall splice specimens. The resulting average moment in each segment was established from basic mechanics. The curvature corresponding to the resulting moment at the middle of each segment was calculated from an interpolation between the curvatures of the gross uncracked section and the fully transformed cracked section to model the gradual transformation between these section properties. The error associated with the selection of 240 segments was found to be 0.06% with the supporting calculations provided in Appendix 4D.

CAN/CSA S304.1-04 (CSA, 2004a) adopted Branson's (1965) equation for determining the effective moment of inertia used for calculating member deflections. However, Bischoff (2005) showed that Branson's (1965) equation is not suitable for reinforced concrete beams and slabs with reinforcing ratios less than 1%, and proposed a revised equation for such members. Bischoff's proposed equation was therefore adopted for the current analysis as the reinforcement ratio of the wall splice specimens was 0.43%. Appendix 4D shows the derivation of the effective curvature relationship from Bischoff's proposed equation for the effective moment of inertia.

The midspan deflection was then set equal to the midspan moment resulting from the effective curvatures in each segment acting as the fictitious load on the specimen. The theoretical midspan deflection verses applied load curves are shown in Figure 4.27 and 4.28 for the wall splice specimens with contact and non-contact lap splices, respectively, and are compared with the experimental deflection curves. The detailed mathematical expression and the MathCAD program are provided in Appendix 4D.

Figures 4.27 and 4.28 show that the average slopes of the experimental load versus midspan deflection curves before yielding of the reinforcing bars were 8% and 10% higher than the theoretical curves for wall splice specimens with contact and non-contact lap splice, respectively. The reduced deflection that occurred at any load in the experiments likely resulted from the increased stiffness in the actual wall splice specimens caused by the additional reinforcement within the lap splice length. Possible axial restraint due to the presence of friction in the roller or with the support configuration or at the load application points might also have contributed to the higher slope of the experimental curves. Such axial restraint would include a combination of axial loading and flexure in the members which was not considered in the current analysis.

Figure 4.27, that is elaborately shown in Figures 4B-1 to 4B-8 in Appendix 4B show that a very limited yield plateau was observed in the experimental curves for the specimens with contact lap splices. The experimental curves then showed an increase in slope, the average value of which was four times higher than the slope of the theoretical

curve at the same deflection level. This indicates that strain hardening of the reinforcing bars occurred at deflections smaller than those predicted theoretically. This behaviour was also observed by Heisler (1980) during the investigation of ductility in reinforced concrete beams with tension lap splices and described as early strain hardening of the reinforcing bars. The experimental load versus midspan deflection curves showed a decrease in the yield plateau with increasing splice length in the constant moment region (Heisler,1980). The presence of the additional reinforcing bars within the splice length increased the flexural stiffness along the splice length, while reducing the bar length available to yield. This phenomenon resulted in a reduction in the strain, and hence in the deflection before strain hardening (Heisler, 1980). In the masonry walls, this situation is further aggravated since cracks are generally limited to the bed joints. Reinforcement yielding was therefore typically limited to the two bed joints adjacent to the loading points in the constant moment region for the test setup used in this investigation, as was evident from the widening of these cracks as described in Section 4.4.2.

**Calculation of spice tension from the failure loads**

Ultimate moments were calculated from the ultimate loads reported in Tables 4.5 and 4.6 and were further corrected by including the moments due to the specimen self-weight and the weight of the spreader beam. The curvature corresponding to the ultimate moment for each specimen was established using the numerical analysis described previously for establishing the moment-curvature profile. A numerical iteration identical to that for the moment-curvature analysis was then used to satisfy the equilibrium between the compression force in the masonry and the tensile force in the

reinforcing steel. The tensile force thus obtained is the tensile resistance for each specimen as reported in Table 4.7. Outliers were not identified at the 95% confidence level for either the specimens with contact or non-contact lap splices.

Table 4.7: Calculated splice resistance of the wall splice specimens.

| | Specimen Designation | Ultimate Load (kN) | Corrected Ultimate Moment[*] (kN.m) | Theoretical curvature at ultimate moment (1/m) | Tensile resistance (kN) | Mean Tensile Resistance (kN) |
|---|---|---|---|---|---|---|
| Wall splice specimens with contact splices | CW-1 | 35.6 | 17.3 | 0.349 | 101 | |
| | CW-2 | 35.1 | 17.1 | 0.282 | 96.5 | |
| | CW-3 | 35.6 | 17.3 | 0.300 | 97.5 | |
| | CW-4 | 41.4 | 23.7 | n/a | n/a | 98.0 |
| | CW-5 | 36.2 | 17.5 | 0.323 | 99.0 | |
| | CW-6 | 36.1 | 17.5 | 0.323 | 99.0 | |
| | CW-7 | 33.4 | 16.4 | 0.226 | 92.0 | |
| | CW-8 | 36.6 | 17.7 | 0.349 | 101 | |
| Wall splice specimens with non-contact splices | NCW-1 | 20.1 | 11.1 | 0.025 | 66.5 | |
| | NCW-2 | 25.3 | 13.2 | 0.029 | 77.0 | |
| | NCW-3 | 11.7 | 7.72 | n/a | n/a | |
| | NCW-4 | 23.5 | 12.4 | 0.028 | 74.5 | 69.2 |
| | NCW-5 | 26.2 | 13.5 | 0.030 | 79.5 | |
| | NCW-6 | 21.2 | 11.5 | 0.025 | 66.5 | |
| | NCW-7 | 18.7 | 10.5 | 0.023 | 61.5 | |
| | NCW-8 | 17.2 | 9.92 | 0.022 | 59.0 | |

[*]Moments due to the specimen self-weight and weight of spreader beam and roller supports (3.04 kN-m) were added to the experimental moments calculated from the reported failure loads as described in the text.

## 4.4.6 Summary

The mean splice resistance obtained from the theoretical analysis was 98 kN for the wall splice specimens with contact lap splices indicating that these specimens failed by developing, as a minimum, the theoretical yield capacity of the reinforcing bars. In contrast, the mean maximum splice resistance of the wall splice specimens with non-contact lap splice was 69.2 kN, 78% of the theoretical yield capacity of the reinforcing bars. A higher coefficient of variation of 11.4% resulted for these specimens as compared to 3.19% for the specimens with contact lap splices, thus suggesting higher variability in splice resistance when non-contact lap splices are provided. Unlike contact lap splices, the failure mechanism of non-contact lap splices involves the grout/block bond, as well as the tensile strength of the grout, which typically introduced greater variability in these specimens. The poor grout consolidation as suggested by the observed voids within the vicinity of the reinforcing bars might also have contributed to this higher variability. The difference between the mean splice resistance developed in wall splice specimens with contact and non-contact lap splice was found to be statistically significant at the 95% confidence level as established from the student "t" test.

The experimental load versus midspan deflection curves for the wall splice specimens closely followed the theoretical curve until yielding of the reinforcing bars was initiated. Early strain hardening was observed in the specimens with contact lap splices. The specimens with non-contact lap splices failed before bar yielding occurred. Bond loss between the reinforcing bars and the grout was observed once the face shell and grout surrounding the reinforcement was removed for the specimens with contact lap splices.

In contrast, a grout/block bond failure was observed in the wall splice specimens when non-contact lap splices were provided. The ineffective transfer of tensile forces due to bond loss at the grout/block interface was identified as the major cause of failure and resulted in reported ultimate loads for these specimens that were less than the theoretically predicted yield load.

**4.5 Comparison of Double Pullout and Wall Splice Specimens**

The 300 mm contact lap splices in both specimen types developed, as a minimum, the theoretical yield capacity of the reinforcing bars when the contact lap splices were provided. Mean tensile resistances of 89.7 and 98.0 kN were reported for contact lap splices in double pullout and wall splice specimens, respectively. The student "t" test identified that the splice resistance developed by the contact lap splices in the wall splice specimens was significantly different than that of the double pullout specimens at the 95% confidence level. All of the wall splice specimens with contact lap splices developed strain hardening of the reinforcing bars as was evident from the load versus deflection behavior, as well as from the analyzed stresses in these bars at the ultimate loads. In contrast, strain hardening was not observed from the load versus splice displacement records for any of the double pullout specimens with contact lap splices.

In general, contact lap splices in the double pullout specimens failed by bar pullout after shearing from the surrounding grout, as observed in most specimens (i.e. five out of eight specimens) with only one specimen showing splitting of the masonry assemblage before bar pullout. In contrast, all of the wall splice specimens with contact lap splices

failed due to longitudinal splitting along the splice, as well as transverse splitting at the splice ends on the tension face. Bond loss along the lap splice length was identified after face shell and grout removal for both specimen types.

Both the double pullout and wall splice specimens with 300 mm long non-contact lap splices failed before developing the theoretically calculated yield capacity of the reinforcing bars. However, the double pullout specimens with non-contact splices developed a mean tensile resistance of 40.7 kN prior to failure: 41.2% lower compared to the mean maximum tension of 69.2 kN developed by the identical splices in the wall splice specimens. The difference between the mean ultimate tensile forces is statistically significant at the 95% confidence level from the student "t" test.

Similar internal crack distributions were observed when the face shell and grout surrounding the reinforcing bars was removed in both specimen types with non-contact lap splices. Bar slip or evidence of bond loss between reinforcing bars and surrounding grout was absent in these specimens. However, bond loss was observed at the block/grout interface that presumably caused an inefficient transfer of forces between the spliced bars, as described in Section 4.3.3. This inefficient transfer of forces caused a splitting failure at the loaded end when the net external moment couple created sufficient tension to overcome the tensile resistance of the masonry assembly in the double pullout specimens. This is very unlikely to occur in a full-scale structure due to their larger geometry and mass: as a much larger moment couple would be required to cause an identical failure. All wall splice specimens failed due to the development of a

vertical flexural crack at the end of one of the splices when the ineffective transfer of tensile forces created a net tension in the bar that was then transferred to the surrounding grout and exceeded the grout tensile strength.

A review of the results reported for seven full scale wall tests showed that non-contact lap splices can only develop on average, 71% of the tensile resistance of a typical contact lap splice. A correction factor of 1.5 is therefore suggested to calculate the required splice length when the spliced bars are located in the adjacent cells.

CHAPTER 5
CONCLUSIONS

## 5.1 Overview

A total of thirty two specimens were tested: half were double pullout specimens and half were wall splice specimens. Each specimen type had eight replicate specimens with either contact or non-contact lap splice arrangements. The double pullout specimens were tested with direct tension applied to the lap spliced bars, while lateral loads were applied to the wall splice specimens using a four-point loading arrangement so that the spliced bars were located within the specimens' constant moment region. All specimens were reinforced with Grade 400 No.15 deformed reinforcing bars with a lap splice length of 300 mm, and all material properties were kept constant for all specimens. The maximum tensile force resisted by the spliced bars was reported for all specimens in each specimen group. Statistical tests were performed to identify outliers at the 95% confidence level. The mean maximum tensile force resisted by the spliced bars was then established for each specimen type and splice arrangement. The student "t" test was used to determine if the difference between the mean maximum tensile resistances obtained for the two specimen groups was statistically significant at the 95% confidence level. Splice behaviour was also critically reviewed for both specimen types and splice arrangements. The summarized conclusions addressing the three specific objectives of the research program, as presented in Section 1.2, are reported in the following sections.

**5.2 Summary of Findings**

**5.2.1 Contact and non-contact lap splices in double pullout specimens**

All double pullout specimens were tested under direct tension and the maximum tension resisted by the spliced bars was obtained directly from the logged data. The splice displacements corresponding to the recorded loads were obtained from LVDTs attached to each set of spliced bars using a clamp arrangement.  The failure modes and damage corresponding to each splice arrangement were observed and critically reviewed. The following conclusions were noted:

- The contact lap spliced bars in the double pullout specimens developed, as a minimum, the theoretical yield load (87.7 kN) of the reinforcement. The mean tensile resistance of the spliced bars was 89.7 kN with a coefficient of variation of 2.37%. In contrast, the mean splice resistance developed by the non-contact splices in the double pullout specimens was 40.7 kN: 46% of the theoretically predicted yield load of the reinforcement. A higher coefficient of variation of 7.57% resulted for the double pullout specimens with non-contact lap splices due to their failure mechanism that involved a larger number variables, including: the tensile strength of masonry assemblage and the bond strength of the block/grout interface. The difference between the mean maximum tensile resistances developed by the contact and non-contact splices in double pullout specimens was statistically significant at 95% confidence level as evaluated using the student "t" test.

- The double pullout specimens with contact lap splices typically failed by bar pullout at the loaded end, whereas the double pullout specimens with non-contact lap splices exhibited a tensile failure.

- The progressive removal of first the face shell, and then the grout surrounding the lap spliced reinforcing bars provided further evidence of bond loss between the reinforcement and grout for the double pullout specimens with contact lap splices. No such evidence was obtained for the identical specimens with non-contact lap splices. Instead, bond loss at the grout/block interface was deemed to render the required internal struts in these specimens ineffective in resisting the imposed in-plane bending moment induced.

**5.2.2 Contact and non-contact lap splices in wall splice specimens**

The wall splice specimens were tested under a four-point loading arrangement. The tensile resistance of the lapped bars corresponding to ultimate load for a specimen was obtained from a numerical analysis that incorporated the material properties of the masonry assemblage and the reinforcing bars as established from the companion specimen tests. The following conclusions were drawn from the recorded loads and the subsequent analysis, and are based on the visually observed damage in these specimens:

- The theoretical analysis yielded a mean maximum splice resistance of 98.0 kN for the wall splice specimens with contact lap splices and thus confirmed that all specimens developed, as a minimum, the theoretical yield load of the reinforcement. In contrast, the same specimens with non-contact lap splices

developed a mean splice resistance of 69.2 kN or 78% of the theoretical yield load. A higher coefficient of variation of 11.4% resulted in these specimens as compared to 3.19% for the specimens with contact lap splices. The higher variability might have resulted from the tensile force transfer mechanism between the non-contact lap spliced bars that involves the bond at block/grout interface as well as the existence of voids along the lap splice lengths due to poor grout consolidation. The difference between the mean splice resistances is statistically significant at the 95% confidence level as obtained from the student "t" test.

- The measured midspan deflection increased linearly until yielding of the reinforcement in the wall splice specimens with contact lap splices. The experimental curves closely followed the theoretically derived curves until yielding of the reinforcement occurred. Increased flexural stiffness along the splice length due to the presence of the additional reinforcement in this region, and the fact that cracks were limited to the bed joints, resulted in a shorter yield plateau with strain hardening initiating at a smaller corresponding deflection as compared to that predicted theoretically. In contrast, the linear load versus midspan deflection response for the wall splice specimens with non-contact lap splices closely followed the theoretical curve, but failed to develop yielding of the reinforcement prior to specimen failure.

- The wall splice specimens with contact lap splices failed when splitting cracks developed at the tension face within the splice region. A vertical crack at the

splice end was observed at failure in the wall splice specimens with non-contact splices. This crack then travelled towards the splitting cracks at other bar end in a given lap splice. Cracks in both the tension and compression faces were observed for wall splice specimens with non-contact lap splices.

- Bond loss between the grout and the reinforcement was observed when the block face shell and grout was incrementally removed along the splice location for the wall splice specimens with contact lap splices. In contrast, evidence of such bond loss was absent for the identical specimens with non-contact lap splices. Rather, the observed crack distribution within the grout suggests that poor bond existed at the block/grout interface in these specimens.

- A correction factor of 1.5 is suggested for the calculation of the effective splice length when the lapped bars are placed in adjacent cells based upon the results of this experimental program.

### 5.2.3 Comparison of double pullout and wall splice specimens

- The double pullout specimens with contact lap splices, on average, developed 8.47% less tensile resistance compared to that developed by full-scale wall splice specimens with the identical lap splice arrangement. This difference is statistically significant at the 95% confidence level as established from the student "t" test. Lapped bars in the wall splice specimens with contact lap splices developed strain hardening of the reinforcing bars before failure, which was not observed for the double pullout specimens with the identical splice arrangement.

The reinforcing bars sheared away from the surrounding grout without significant observed damage in the double pullout specimens with contact lap splices. Bar pullout following block and grout splitting at the tension face was observed in the wall splice specimens with contact lap splices at failure.

- The mean maximum tensile resistance developed by the non-contact lapped bars in the double pullout specimens was 41.2% lower than that developed in the wall splice specimens with the identical splice arrangement. This difference is statistically significant at the 95% confidence level as established from the student "t" test. Both specimen types with non-contact lap splices failed to develop the yield load prior to failure due to bond loss at the block/grout interface. However, the larger geometry and mass of the wall splice specimens prevented the tensile failure that was the observed typical failure mode for the double pullout specimens with non-contact lap splices. Double pullout tests are not suitable for investigating strength of non-contact lap splices that are lapped in alternate cores based upon both the statistical evaluation of quantitative data and visual observations of failure.

- Coefficients of variation of 2.37% and 3.19% were reported for the tensile resistance of contact lap splices in the double pullout and wall splice specimens, respectively. For non-contact lap splices, double pullout specimens resulted in a coefficient of variation of 7.57% in the tensile resistance of the spliced bars as compared to the 11.4% calculated for the wall splice specimens.

## 5.3 Recommendations for Future Research

The scope of the current research program provided a limited investigation of splice behaviour in reinforced masonry: two specimen types with two bar arrangements were investigated. Valuable information was obtained from this study which suggests the necessity for further investigation related to lap splices in reinforced masonry members. The following are recommendations for relevant future research:

- A parametric investigation of bar size and splice lengths in full-scale reinforced masonry wall splice specimens is necessary to provide a database of test results to effectively evaluate splice lengths for the development of reliability-based design provisions for Canadian reinforced masonry design codes.

- The grout tensile strength appears to have a significant effect on the splice capacity of non-contact lap splices due to the resulting force transfer mechanism between the lapped bars, and the dependence on the bond at block/grout interface. An expansion of the current investigation is therefore necessary to properly evaluate the influence of this parameter.

- In the current study, the distance between the lapped bars in non-contact lap splices was kept constant with the bars placed in two horizontally adjacent cells. Each bar was centered in the common cell grouting width of vertically adjacent cells. The effect of reducing the distance between the lapped bars with these bars placed both in adjacent cells and in the same cell should be investigated.

- Early strain hardening was observed in the wall splice specimens with contact lap splices suggesting that the ductility of the flexural members can be reduced due to the existence of lap splices. Additional research on the ductility of flexural members with spliced reinforcement is therefore necessary.

- The addition of both internal and external instrumentation will help better the understanding of bond behaviour and stress distribution within lap spliced bars in reinforced masonry walls.

- The current experimental program used two and a half block wide specimens that required one of the lapped bars in each non-contact splice to be placed within the end cell. Reinforcing bars in end cells are subjected to reduced confining pressure due to the absence of a continuous block and grout on one side. Wider specimens should be tested so that the reinforcement is not placed within the end cells.

## REFERENCES

1. Abrams, D.A., "Tests of Bond Between Concrete and Steel", *University of Illinois Bulletin No. 71*, University of Illinois Urbana-Champaign, Urbana, IL, 1913.

2. Ahmadi, B.H., "Effect of Loss of Bond in Lap Splices of Flexurally Loaded Reinforced Concrete Masonry Walls", *Materials and Structures*, Vol. 34, October 2001, pp 475-478.

3. ACI 530/ASCE 5/ TMS 402, *Building Code Requirements for Masonry Structures*, American Concrete Institute, Farmington Hills, MI, U.S.A.,1999.

4. ASTM, *ASTM A370: Standard Test Methods and Definitions for Mechanical Testing of Steel Products,* ASTM International, West Conshohocken, PA, USA. 2008.

5. ASTM, *ASTM C1019: Standard Test Method for Sampling and Testing Grout,* ASTM International, West Conshohocken, PA, USA. 2009.

6. ASTM, *ASTM E178-00: Standard Practice for Dealing with Outlying Observations*, ASTM International, West Conshohocken, PA, USA. 2000.

7. Bartlett, F.H., *Pitfalls in Regression Analysis*, University of Western Ontario, London, Ontario. 1999.

8. Baynit, A.R., *Bond and Development Length in Reinforced Concrete Block Masonry,* M. Eng. Thesis, Carleton University, Ottawa, ON, 1980.

9. Bischoff, P.H., "Reevaluation of Deflection Prediction for Concrete Beams Reinforced with Steel and Fiber Reinforced Polymer Bars." *Journal of Structural Engineering*, ASCE, Vol. 131, No. 5, May 2005.

10. Branson, D.E., "Instantaneous and Time Dependant Deflections of Simple and Continuous Reinforced Concrete Beams", *HPR Report No. 7, Part 1*, Alabama Highway Department, Bureau of Public Roads, Alabama, 1965.

11. Canadian Standards Association, *Design of Masonry Structures, S304.1-04*, Canadian Standards Association, Rexdale, ON, 2004a.

12. Canadian Standards Association, *Design of Concrete Structures. A23.3-04*, Canadian Standards Association, Rexdale, ON, 2004b.

13. Canadian Standards Association, *Mortar and Grout for Unit Masonry. A179-04*, Canadian Standards Association, Rexdale, ON, 2004c.

14. Canadian Standards Association, *Methods of Test and Standard Practices for Concrete, A23.2-04*, Canadian Standards Association, Rexdale, ON, 2004d.

15. Canadian Standards Association, *Standard Practice for Mechanical Mixing of Hydraulic Cement Mortars and Test Methods for Determination of Flow, A3004-C1*, Canadian Standards Association, Rexdale, ON, Canada 2003a.

16. Canadian Standards Association, *Test Method for Determination of Compressive Strengths, (A3004-C2)*, Canadian Standards Association, Rexdale, ON, 2003b.

17. Canadian Standards Association, *Masonry Design and Construction for Buildings, CSA Standard S304-77*, Canadian Standards Association, Rexdale, ON, 1977.

18. Cheema,T.S., Klingner, R.E., "Tensile Anchorage Behaviour of Deformed Reinforcement in Grouted Concrete Masonry", *ACI Journal*, May-June 1985a, pp. 372-380.

19. Cheema, T.S., Klingner, R.E., "Failure Criteria for Deformed Reinforcement Anchored in Grouted Concrete Masonry", *ACI Journal*, July-August 1985b, pp. 434-442.

20. Cheema, T.S., Klingner, R.E., "Design Recommendations for Tensile Anchorages of Deformed Reinforcement in Grouted Concrete Masonry", *ACI Journal*, September-October, 1985c, pp. 616-621.

21. Drysdale, R.G., Hamid, A.A., *Masonry Structures: Behaviour and Design,* Canadian Masonry Design Centre, Mississauga, ON, 2005.

22. Hamad, B.S., Mansour, M., "Bond Strength of Non-Contact Tension Lap Splices", *ACI Structural Journal*, V.93, No. 3, May-June 1996.

23. Hamid, A.A., "Design and Construction of Reinforced Masonry in North America", *The 6th Conference of Seismology and Earthquake Engineering*, 2004, pp. 179-196.

24. Hamid, A.A., Drysdale, R.G., "Suggested Failure Criteria for Grouted Concrete Masonry Under Axial Compression", *ACI Journal*, Vol. 76, No.10, 1979, pp. 1047 - 1062.

25. Heisler, T.L., *Performance of Lapped Splices in Reinforced Concrete Beams Loaded Beyond Yielding of Steel*, M.Sc. Thesis, University of Saskatchewan, Saskatoon, SK, 1980.

26. International Conference of Building Officials (ICBO), *Uniform Building Code (UBC)*, International Conference of Building Officials, Whittier, Calif, 1997.

27. Kent, D.C., Park, R., "Flexural Members with Confined Concrete," *Journal of the Structural Division*, ASCE, Vol. 97, No. ST7, Proc. Paper 8243, July, 1971, pp. 1969-1990.

28. Matsumara. A., Igarashi, I. and Takao, H., "Strength and Behaviour of Lap Splices of Reinforcement in Hollow Unit Masonry", *Proceedings of the 11th International Brick/Block Masonry Conference*, Shanghai, Vol.-1, October, 1997, pp. 276-284.

29. MSJC, *Specification for Masonry Structures*, Masonry Standards Joint Committee, Boulder, CO, 1995.

30. NCMA, "Evaluation of Minimum Reinforcing Bar Splice Criteria for Hollow Clay Brick and Hollow Concrete Block Masonry", National Concrete Masonry Association, Report No. MR 12, Herndon, Virginia, July, 1999.

31. Orangun, C.O., Jirsa, J.O., and Breen, J.E., "A Reevaluation of Test Data on Development Length and Splices", *Journal of the American Concrete Institute*, 74(11), March, 1977, pp. 114-122.

32. Paturova, A., *The Influence of Vertical Reinforcement and Lateral Confinement on the Axial Capacity of Masonry Block Walls*, MSc Thesis, University of Saskatchewan, March, 2006.

33. Park, R., Priestley, M.J. Nigel, and Gill, W. D., "Ductility of Square Confined Concrete Columns", *ASCE Proceedings*, V-108, ST4, Apr. 1982, pp. 929-950.

34. Priestley, M.J.N., Elder, D.M., "Stress-Strain Curves for Unconfined and Confined Concrete Masonry", *ACI Journal*, May-June, 1983, pp. 192 – 201.

35. Sagan, B.E., Gergely, P., White, R.N, "Behavior and Design of Non-Contact Lap Splices Subjected to Repeated Inelastic Tensile Loading", *ACI Structural Journal*, V-88, No. 4, July - August, 1991, pp. 420-431.

36. Schuller, M.P., Hammons, M.I., Atkinson, R.H., "Interim Report on a Study to Determine the Lap Splice Requirements for Reinforced Masonry," *ASTM Special Publication STP 1180: Masonry: Design and Construction Problems and Repairs*, eds. J.M. Melander & L.R. Lauersdorf, Philadelphia, PA, 1993, pp.75 – 90.

37. Soric, Z., Tulin, L. G., "Bond Stress Deformation in Pull-out Masonry Specimen", *ASCE Journal of Structural Engineering*, Vol. 115, No. 10, October 1989, pp. 2588-2602.

38. Suter, G.T., Keller, H., "Bond and Development Length in Reinforced Concrete Masonry Beams", *International Journal of Masonry Construction*, Vol. 2, No. 4, 1982.

39. Suter, G.T., Fenton, G.A., "Splice Length Tests of Reinforced Masonry Walls," *International Journal of Masonry Construction*, Arlington, Texas, pp. 68-1-14, 1985.

40. Uniat, D. B., *Lap Splices of Deformed Bars in Reinforced Concrete Block Masonry Walls*, M. Eng Thesis, Carleton University, Ottawa, ON, 1983.

APPENDIX 3A
SELECTION OF NUMBER OF REPLICATE SPECIMENS


This section presents the calculation of the required number of replicate specimens to identify a statistically significant difference in the mean values of two sample populations at a minimum 95% confidence level. The minimum expected difference between the mean splice tension and the assumed coefficient of variation of the two populations were estimated in order to establish this number. The basis of these assumed statistical parameters is presented in Section 3.3.


Assumed number of specimens (samples):                    $N_1 = N_2 = 8$

Degrees of freedom:                    $d.o.f = 2n - 2 = 14$

Expected coefficient of variation in each specimen type:    $C.O.V = 8\%$

Average splice resistance in specimen type 1 (arbitrarily set):    $X_1 = 100$

Based on an expected difference of 10% between the mean values

of the two specimen types, the average splice resistance in    $X_2 = 110$

specimen type 2:

Difference between the average values:    $X_1 - X_2 = 10$

Standard deviation in specimen type 1:    $S_1 = X_1 \times C.O.V$

$= 8$

Standard deviation in specimen type 2: $\qquad$ $S_2 = X_2 \times C.O.V$

$$= 8.8$$

"t" value calculation in accordance with the student "t" test:

$$= \frac{(X_1 - X_2)}{\sqrt{\dfrac{S_1^2(N_1-1)+S_2^2(N_2-1)}{N_1+N_2-2}\left(\dfrac{1}{N_1}+\dfrac{1}{N_2}\right)}} \quad \text{..............................(3A-1)}$$

$$= 2.378$$

The level of confidence for t = 2.378 with 14 degrees of freedom from a two-tailed student "t" table is equal to 96.4%. Eight replicate specimens are therefore sufficient to demonstrate a statistically significant difference between two populations at the 95% confidence level with a minimum 10% difference between their mean values.

APPENDIX 3B
GROUT MIX DESIGN


This appendix describes the grout mix design for both construction phases. Trial batches

were made with a 1:5 cement to gravel ratio while varying the water content to meet the

requirement of CSA A179-04: Mortar and Grout for Unit Masonry (CSA, 2004c) such

that the slump of the mixes fall within 200 and 250 mm while producing a minimum

compressive strength of 7.5 and 12.5 MPa when tested at 7 and 28 days, respectively.

Due to time limitations, the 7-day compressive strength requirement only was used to

establish the water to cement ratio of the grout mix design. Trial mixes were performed

before both construction phases to control the consistency of the grout compressive

strength so that any resulting strength variation would not significantly affect the tensile

resistance of the spliced reinforcing bars.


Table 3B-1 presents the slumps measured in the first trial phase of grout mix evaluation

and the 7-day compressive strengths that resulted from the cylinders prepared from

these trial mixes. Figures 3B-1 and 3B-2 show the water to cement ratio versus slump

and water to cement ratio versus 7-day compressive strengths, respectively. A water to

cement ratio of 1.00 was selected based on the graphs, such that the resulting grout mix

was expected to produce a 7-day compressive strength approximately equal to 9 MPa

with a 218 mm slump. Table 3B-2 shows that the trial mixes for grout in the second

phase of trial batch evaluation yielded a higher 7-day compressive strength with a much lower slump with identical water to cement ratios as compared to the first phase trial mixes. The difference resulted due to a variation in the aggregate proportions supplied during the second phase of construction and described in more detail in Section 3.5.3. A water to cement ratio of 0.95 was therefore selected to prepare the grout mix for construction Phase 2 to yield grout with a target slump of 240 mm and a 7-day compressive strength of 12 MPa.

Table 3B-1: Test results for the first phase of grout batch mix trials.

| Batch No. | Water to cement ratio | Slump (mm) | No. of cylinders tested | 7-day compressive strength (MPa) |
|-----------|-----------------------|------------|-------------------------|----------------------------------|
| 1 | 0.90 | 200 | 3 | 11.5 |
| 2 | 1.05 | 230 | 3 | 8.60 |
| 3 | 1.10 | 260 | 3 | 7.90 |
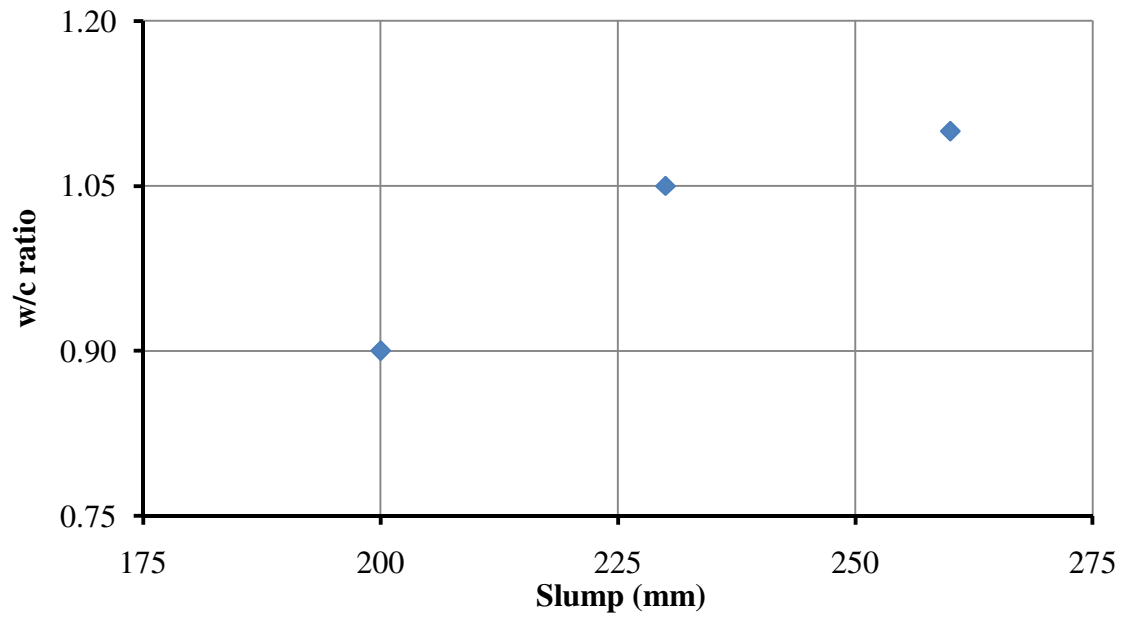
Figure 3B-1: Water to cement ratio versus slump for the first phase of grout batch mix trials.
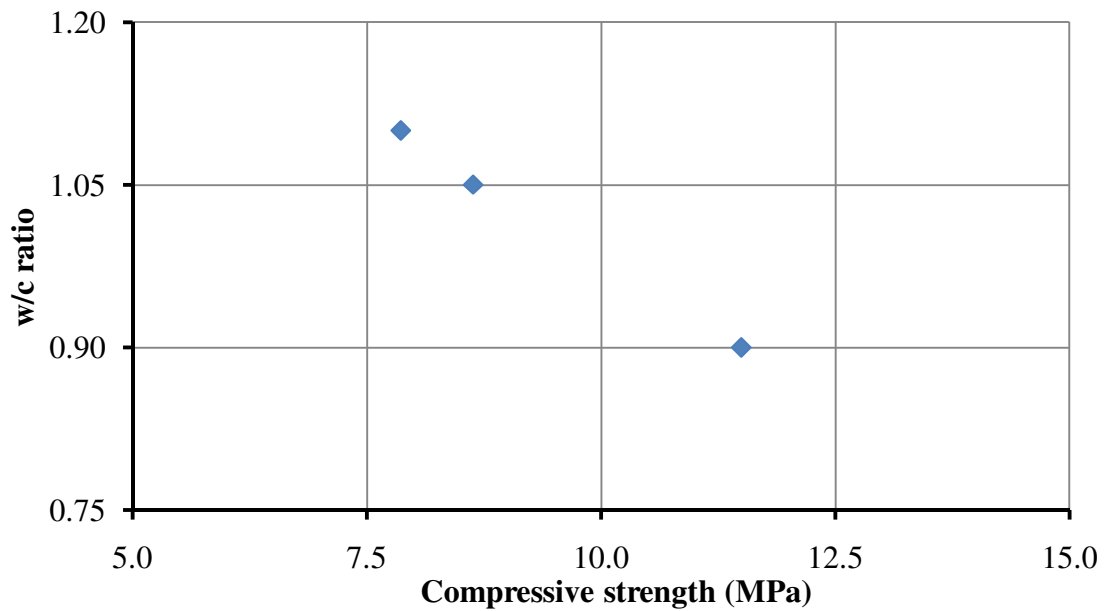


Figure 3B-2: Water to cement ratio versus cylinder compressive strength for the first phase of grout batch mix trials.

Table 3B-2: Test results for the second phase of grout batch mix trials.

| Batch No. | Water to cement ratio | Slump (mm) | No. of cylinders tested | 7 day compressive strength (MPa) |
|---|---|---|---|---|
| 1 | 0.850 | 218 | 6 | 11.5 |
| 2 | 0.950 | 247 | 9 | 8.60 |
| 3 | 0.850 | 267 | 3 | 7.90 |
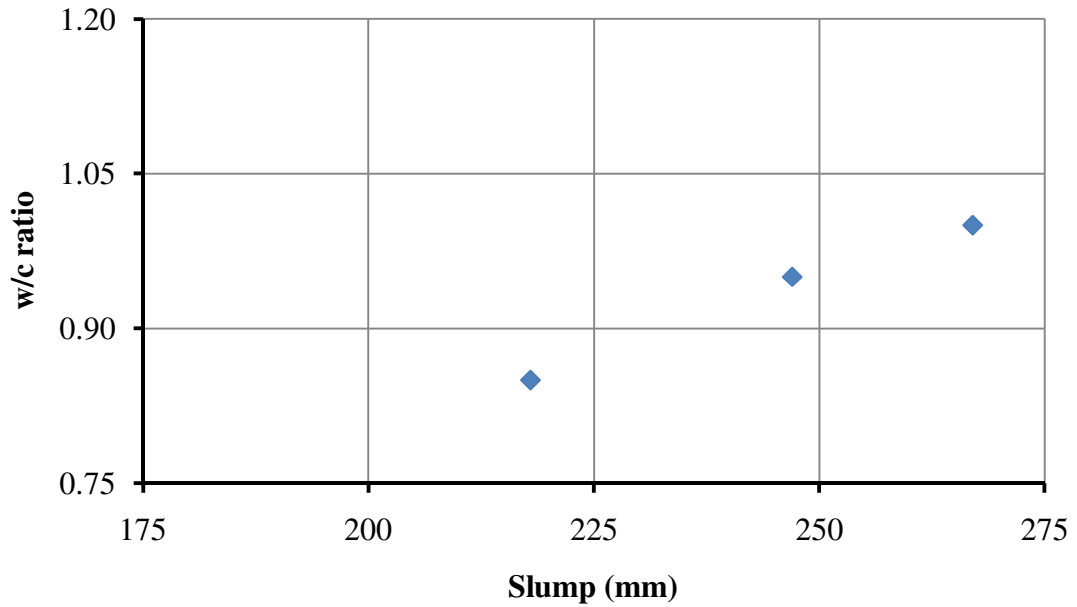


Figure 3B-3: Water to cement ratio versus slump for the second phase of grout batch mix trials.
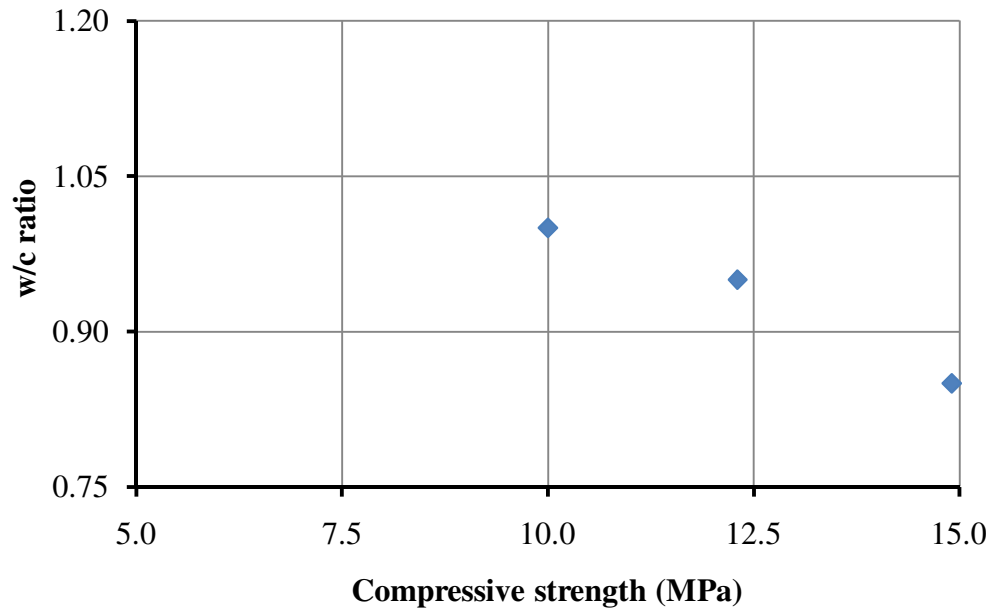
Figure 3B-4: Water to cement ratio versus cylinder compressive strength for the second
phase of grout batch mix trials.

APPENDIX 3C
MECHANICAL COUPLERS


Figure 3C-1 shows the detailed geometry and magnitude of the specified torque for bolts

in the Zap Screwlock Type-2 (Size-5) mechanical couplers that were used in the double

pullout and wall splice specimen test setups as described in Sections 3.7.2 and 3.7.3,

respectively. The recommended torque for the size 5 coupler is 50 ft-lb per bolt in

accordance with the manufacturer's specification in order to resist a tension that is 1.25

times the yield strength of Grade 400 reinforcing bars. However, a lower torque of 40

lb-ft was applied to each bolt for the test setup to ensure that damage did not result. This

allowed for the re-use of these couplers. The torque was found sufficient to resist the

tension up to the yield strength of the reinforcing bars, as confirmed by tensile tests

using the Instron 600DX Universal Testing Machine.

ZAP SCREWLOK TYPE 2 / EPOXY SERIES

(a)

sizes #3 - #11
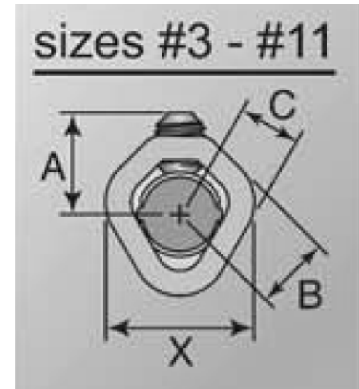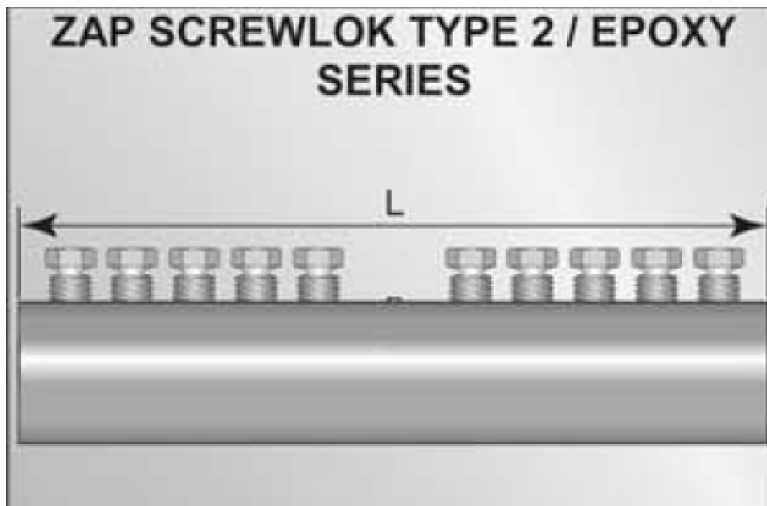
(b)

| Coupler Size | Coupler Weight (lb) | Length 'L' (in) | 'A' (in) | 'B' (in) | 'C' (in) | 'X' (in) | Number Screws per Bar | Average Torque (ft-lbs) |
|---|---|---|---|---|---|---|---|---|
| 3 | 1.0 | 5 | 13/16 | 5/8 | 7/16 | 1 1/8 | 2 | 50 |
| 4 | 2.2 | 7 | 1 1/16 | 11/16 | 1/2 | 1 3/8 | 3 | 50 |
| 5 | 3.4 | 9 | 1 1/8 | 3/4 | 5/8 | 1 5/8 | 4 | 50 |
| 6 | 4.7 | 11 | 1 3/16 | 15/16 | 11/16 | 1 3/4 | 5 | 50 |
| 7 | 7.6 | 13 | 1 1/4 | 1 1/16 | 13/16 | 2 1/16 | 5 | 100 |
| 8 | 10.9 | 15 1/4 | 1 5/16 | 1 1/16 | 7/8 | 2 1/4 | 6 | 100 |
| 9 | 17.6 | 16 3/4 | 1 5/8 | 1 1/4 | 1 1/16 | 2 5/8 | 6 | 200 |
| 10 | 21.4 | 19 1/8 | 1 11/16 | 1 7/16 | 1 1/8 | 2 3/4 | 7 | 200 |
| 11 | 25.4 | 21 1/2 | 1 13/16 | 1 1/2 | 1 1/4 | 2 15/16 | 8 | 200 |
| 14 | 31.7 | 15 3/8 | 2 5/16 | 1 3/4 | 1 1/2 | 3 3/4 | 9 | 350 |

(c)

Figure 3C-1: Zap Screwlock Type-2: (a) front view (b) cross-section view, and
(c) dimensions and magnitude of specified torque.
(Reproduced from brochure published on the following website:
http://www.barsplice.com/zapscrewlok_system.html)

159

APPENDIX 4A
COMPANION SPECIMEN TEST RESULTS


This section presents the individual test results for the material properties reported in Table 4.1. Tests of masonry blocks from both construction phases are presented in Table 4A-1. Tables 4A-2 and 4A-3 report the compressive strengths of mortar cubes tested in conjunction with the double pullout and wall splice specimens, respectively. Tables 4A-4 and 4A-5 show the results for the non-absorbent grout cylinders and Tables 4A-6 and 4A-7 show the same results for the absorptive grout prisms. Tables 4A-9 and 4A-10 provide the masonry prism test results for establishing the compressive strength of the masonry assemblage for both the double pullout and wall splice specimens, respectively. Only eleven compressive stress versus strain diagrams for the masonry assemblages are shown in Figures 4A-1 to 4A-3 as the strain measuring instrumentation malfunctioned for the remaining prisms.


Figures 4A-4 shows the stress versus strain curve for the bar sample collected from the reinforcement used in Specimen CW-4. As previously discussed in Section 4.4.1, this bar shows no definite yield point or any yield plateau, in contrast to the typical stress versus strain response obtained from the bar sample tests used in the remaining seven specimens.

Table 4A-1 : Compressive strength of the concrete masonry block.

| Test Phase | Specimen No. | Compressive strength (MPa) | Average compressive stregth (MPa) | C.O.V. |
|------------|--------------|----------------------------|-----------------------------------|--------|
| 1 | 1 | 23.6 | 22.2 | 6.30% |
|   | 2 | 22.3 |  |  |
|   | 3 | 20.8 |  |  |
| 2 | 1 | 23.6 | 23.4 | 8.24% |
|   | 2 | 23.9 |  |  |
|   | 3 | 20.0 |  |  |
|   | 4 | 21.5 |  |  |
|   | 5 | 25.8 |  |  |
|   | 6 | 25.8 |  |  |

Table 4A-2: Mortar cube tests performed in conjunction with the double pullout specimens.

| Test Phase | Specimen No. | Compressive strength (MPa) | Average compressive Strength (MPa) | C.O.V. |
|---|---|---|---|---|
| 1 | 1 | 16.8 | 18.2 | 7.41% |
| | 2 | 16.9 | | |
| | 3 | 16.5 | | |
| | 4 | 17.6 | | |
| | 5 | 17.8 | | |
| | 6 | 18.1 | | |
| | 7 | 18.5 | | |
| | 8 | 19.7 | | |
| | 9 | 20.7 | | |
| | 10 | 17.1 | | |
| | 11 | 19.6 | | |
| | 12 | 19.2 | | |
| 2 | 1 | 19.1 | 17.9 | 17.0% |
| | 2 | 22.5 | | |
| | 3 | 19.8 | | |
| | 4 | 15.6 | | |
| | 5 | 17.9 | | |
| | 6 | 13.8 | | |
| | 7 | 17.1 | | |
| | 8 | 16.1 | | |
| | 9 | 21.4 | | |
| | 10 | 12.7 | | |
| | 11 | 21.0 | | |
| | 12 | 17.4 | | |

Table 4A-3: Mortar cube tests performed in conjunction with the wall splice specimens.

| Test Phase | Specimen No. | Compressive strength (MPa) | Average compressive strength (MPa) | C.O.V. |
|---|---|---|---|---|
| 1 | 1 | 18.5 | 17.4 | 6.79% |
| | 2 | 17.8 | | |
| | 3 | 17.9 | | |
| | 4 | 15.4 | | |
| | 5 | 16.6 | | |
| | 6 | 18.3 | | |
| 2 | 1 | 12.8 | 12.5 | 18.4% |
| | 2 | 11.1 | | |
| | 3 | 10.6 | | |
| | 4 | 11.2 | | |
| | 5 | 7.4 | | |
| | 6 | 12.3 | | |
| | 7 | 15.2 | | |
| | 8 | 16.1 | | |
| | 9 | 14.5 | | |
| | 10 | 12.9 | | |
| | 11 | 12.3 | | |
| | 12 | 13.2 | | |

Table 4A-4: Non-absorbent grout cylinder tests performed in conjunction with the double pullout specimens.

| Test Phase | Specimen No. | Compressive strength (MPa) | Average compressive strength (MPa) | C.O.V. |
|---|---|---|---|---|
| 1 | 1 | 21.3 | 20.1 | 4.27% |
| | 2 | 21.0 | | |
| | 3 | 21.1 | | |
| | 4 | 19.5 | | |
| | 5 | 19.5 | | |
| | 6 | 18.9 | | |
| | 7 | 19.9 | | |
| | 8 | 19.5 | | |
| | 9 | 20.3 | | |
| 2 | 1 | 28.0 | 27.5 | 12.4% |
| | 2 | 21.6 | | |
| | 3 | 29.4 | | |
| | 4 | 21.9 | | |
| | 5 | 29.5 | | |
| | 6 | 30.6 | | |
| | 7 | 31.6 | | |
| | 8 | 25.1 | | |
| | 9 | 27.5 | | |
| | 10 | 31.7 | | |
| | 11 | 27.9 | | |
| | 12 | 25.6 | | |

Table 4A-5: Non-absorbent grout cylinders tested in conjunction with the wall splice specimens.

| Test Phase | Specimen No. | Compressive strength (MPa) | Average compressive strength (MPa) | C.O.V. |
|---|---|---|---|---|
| 1 | 1 | 20.5 | 19.7 | 4.30% |
| | 2 | 18.8 | | |
| | 3 | 19.8 | | |
| 2 | 1 | 29.0 | 25.6 | 18.7% |
| | 2 | 31.6 | | |
| | 3 | 31.0 | | |
| | 4 | 27.8 | | |
| | 5 | 29.5 | | |
| | 6 | 28.6 | | |
| | 7 | 19.5 | | |
| | 8 | 21.2 | | |
| | 9 | 18.9 | | |
| | 10 | 25.7 | | |
| | 11 | 25.9 | | |
| | 12 | 18.8 | | |

Table 4A-6: Absorbent grout prisms tested in conjunction with the double pullout specimens.

| Test Phase | Specimen No. | Compressive strength (MPa) | Average compressive strength (MPa) | C.O.V. |
|---|---|---|---|---|
| 1 | 1 | 20.9 | 19.7 | 5.28% |
| | 2 | 19.9 | | |
| | 3 | 20.3 | | |
| | 4 | 18.8 | | |
| | 5 | 18.4 | | |
| 2 | 1 | 24.8 | 23.9 | 13.6% |
| | 2 | 29.4 | | |
| | 3 | 26.9 | | |
| | 4 | 24.0 | | |
| | 5 | 23.8 | | |
| | 6 | 25.0 | | |
| | 7 | 25.4 | | |
| | 8 | 23.0 | | |
| | 9 | 23.8 | | |
| | 10 | 18.1 | | |
| | 11 | 17.8 | | |
| | 12 | 24.2 | | |

Table 4A-7: Absorbent grout prism tested in conjunction with the wall splice specimens.

| Test Phase | Specimen No. | Compressive strength (MPa) | Average compressive strength (MPa) | C.O.V. |
|---|---|---|---|---|
| 1 | 1 | 20.7 | 19.1 | 8.19% |
| | 2 | 19.1 | | |
| | 3 | 17.6 | | |
| 2 | 1 | 28.3 | 23.0 | 10.3% |
| | 2 | 20.0 | | |
| | 3 | 23.2 | | |
| | 4 | 21.6 | | |
| | 5 | 25.4 | | |
| | 6 | 21.0 | | |
| | 7 | 24.0 | | |
| | 8 | 21.7 | | |
| | 9 | 24.6 | | |
| | 10 | 21.3 | | |
| | 11 | 21.2 | | |
| | 12 | 23.9 | | |

Table 4A-8: Masonry prisms tested in conjunction with the double pullout specimens.

| Test Phase | Specimen No. | Compressive strength (MPa) | Average compressive strength (MPa) | C.O.V. |
|---|---|---|---|---|
| 1 | P-1 | 14.3 | 13.3 | 8.01% |
|   | P-2 | 14.7 |  |  |
|   | P-3 | 12.9 |  |  |
|   | P-4 | 13.5 |  |  |
|   | P-5 | 12.3 |  |  |
|   | P-6 | 12.1 |  |  |
| 2 | P-7 | 14.8 | 14.4 | 4.52% |
|   | P-8 | 13.8 |  |  |
|   | P-9 | 14.8 |  |  |
|   | P-10 | 13.5 |  |  |
|   | P-11 | 15.1 |  |  |
|   | P-12 | 14.7 |  |  |
|   | P-13 | 13.5 |  |  |
|   | P-14 | 13.5 |  |  |
|   | P-15 | 14.5 |  |  |
|   | P-16 | 15.2 |  |  |
|   | P-17 | 14.5 |  |  |
|   | P-18 | 14.7 |  |  |

Table 4A-9: Masonry prisms tested in conjunction with the wall splice specimens.

| Test Phase | Specimen No. | Compressive strength (MPa) | Average compressive strength (MPa) | C.O.V. |
|---|---|---|---|---|
| 1 | P-19 | 13.3 | 14.9 | 8.97% |
| | P-20 | 15.5 | | |
| | P-21 | 15.8 | | |
| 2 | P-22 | 10.2[*] | 13.3 | 6.16% |
| | P-23 | 13.2 | | |
| | P-24 | 10.2[*] | | |
| | P-25 | 15.2 | | |
| | P-26 | 13.3 | | |
| | P-27 | 13.4 | | |
| | P-28 | 12.5 | | |
| | P-29 | 12.4 | | |
| | P-30 | 12.6 | | |
| | P-31 | 13.7 | | |
| | P-32 | 13.8 | | |
| | P-33 | 13.2 | | |

[*]Outliers as identified from experimental observations described in Section 4.2.3.
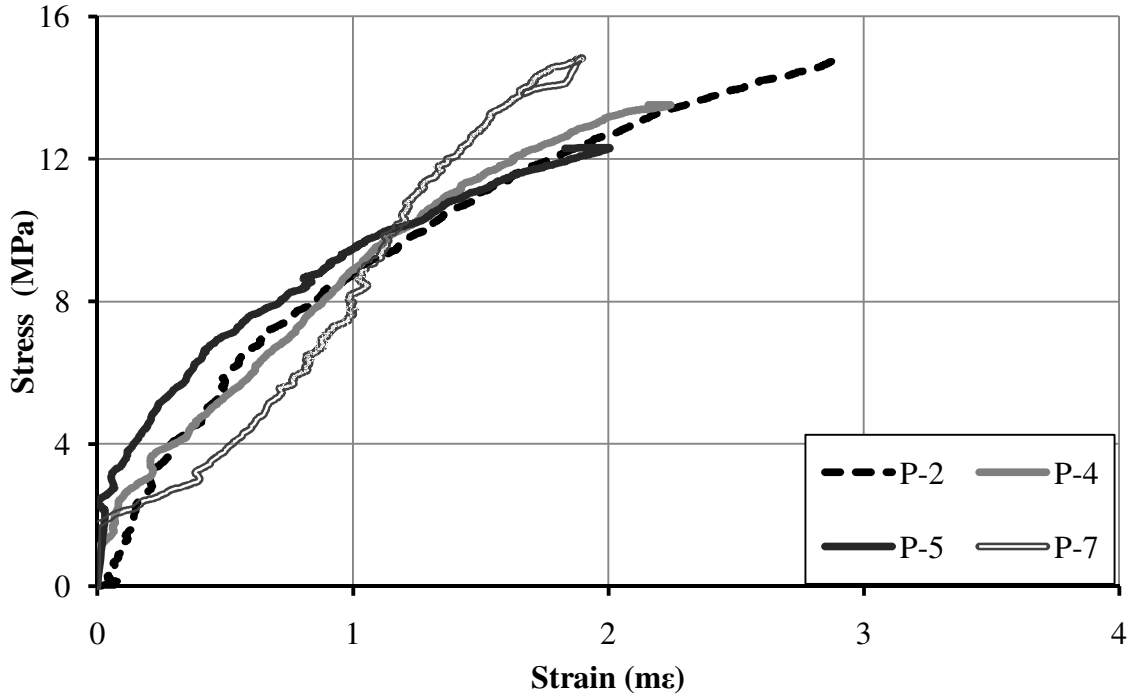
Figure 4A-1: Compressive stress versus strain diagram for masonry prisms: P-2, P-4, P-5, and P-7.
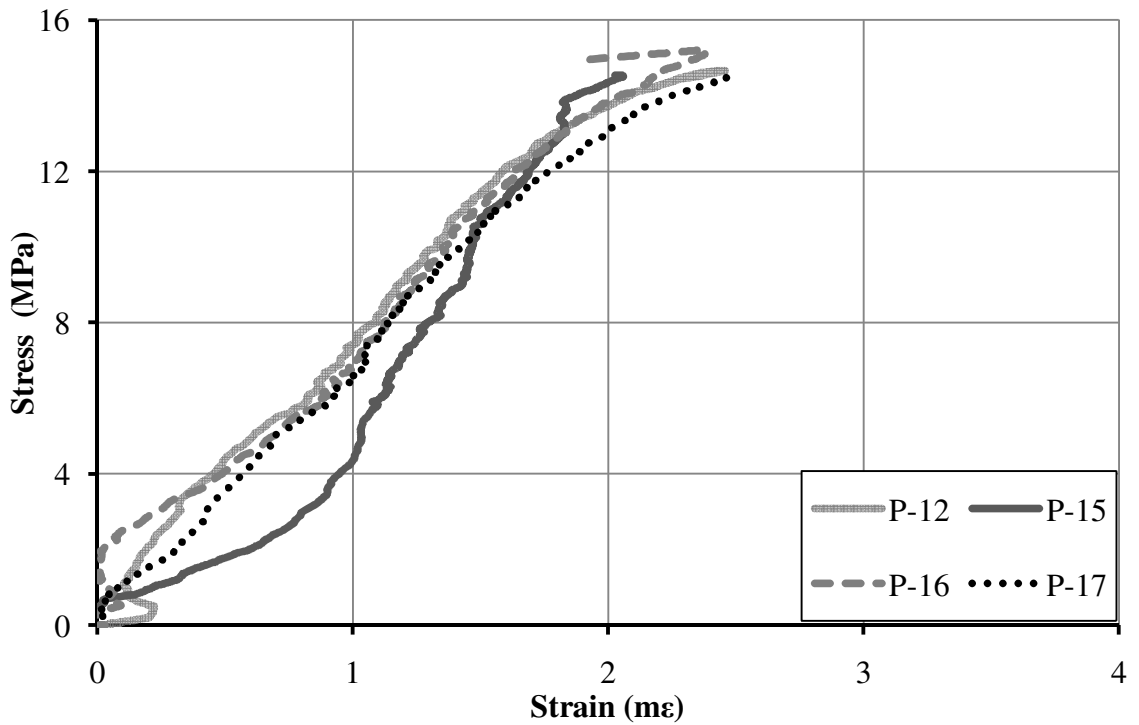


Figure 4A-2: Compressive stress versus strain diagram for masonry prisms: P-12, P-15, P-16 and P-17.
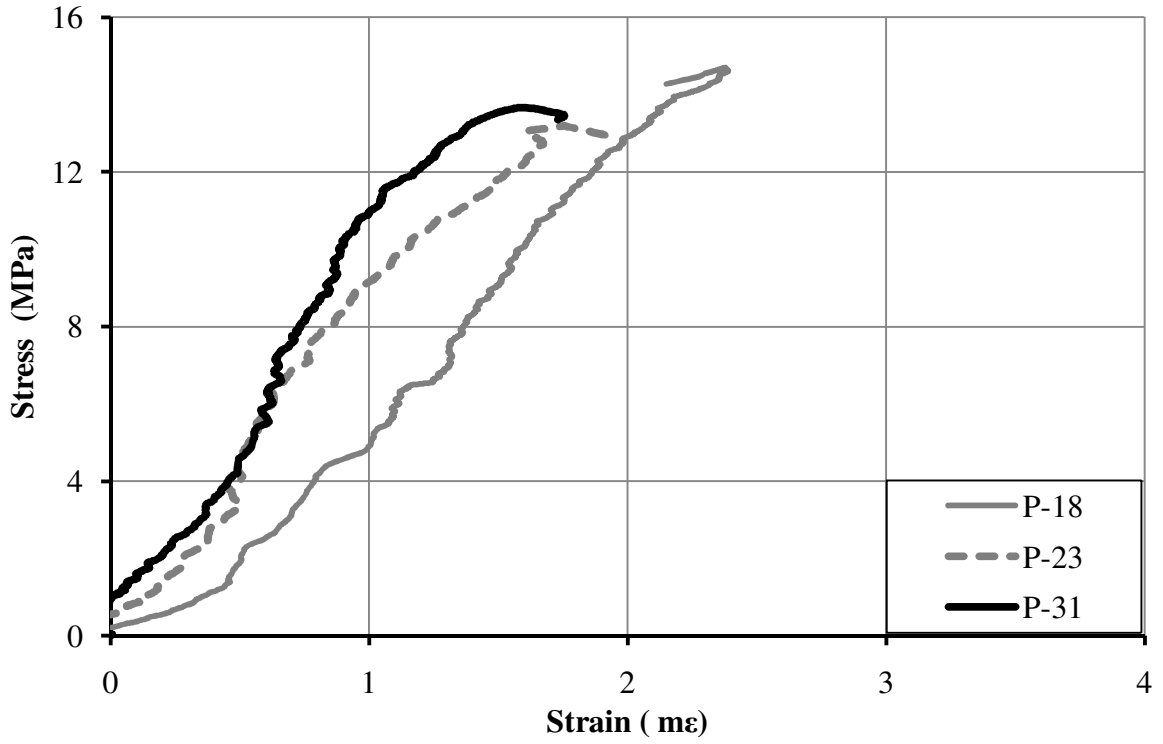
Figure 4A-3: Compressive stress versus strain diagram for masonry prisms: P-18, P-23, and P-31.
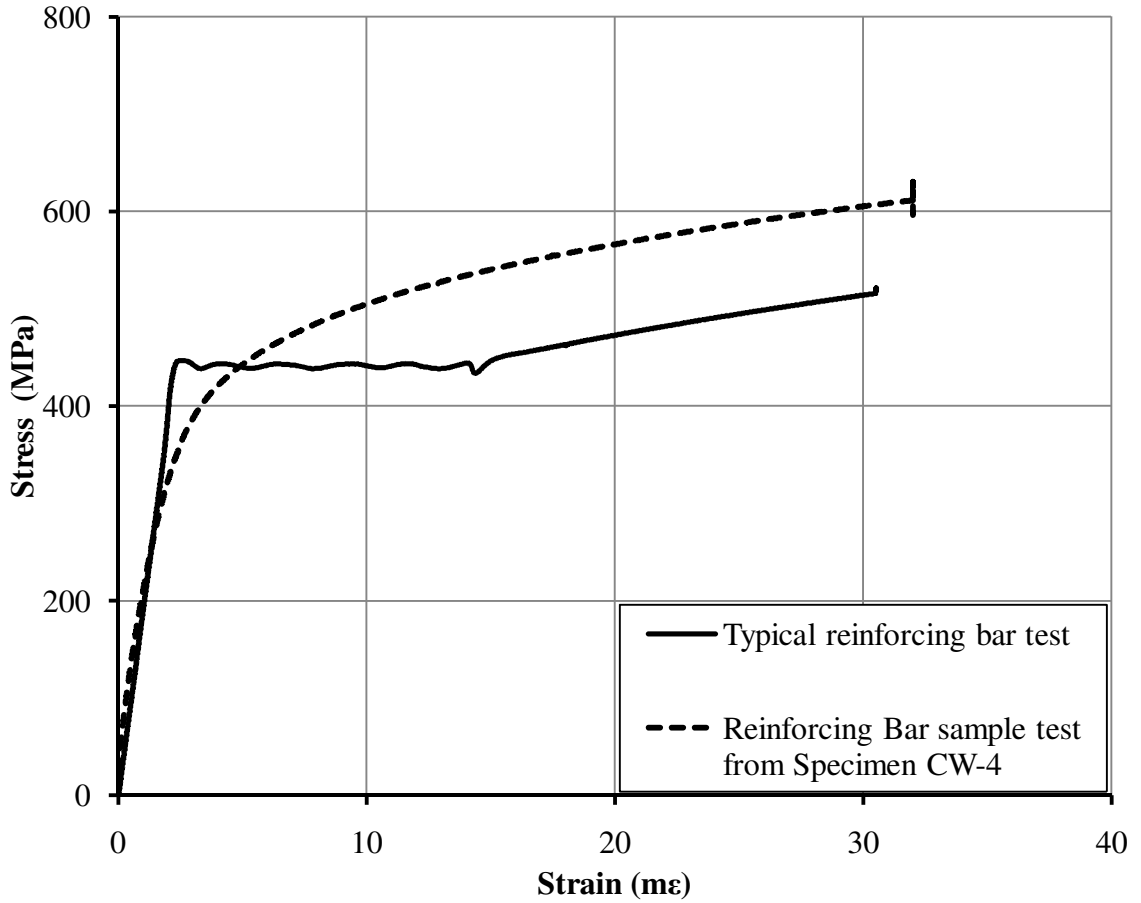
Figure 4A-4: Tensile stress versus strain diagram for reinforcing bar sample collected from Specimen CW-4.

LOAD VERSUS MIDSPAN DEFLECTION CURVES FOR THE WALL SPLICE
SPECIMENS

Figures 4B-1 to 4B-15 present individual load versus midspan deflection curves for the
wall splice specimens with both contact and non-contact lap splices. The experimental
cracking load, $P_{cr}$, and the load at yielding of the longitudinal reinforcement, $P_{Ey}$, are
indicated on each figure. The wall splice specimens with non-contact lap splices failed
well before the longitudinal reinforcement in these specimens yielded.
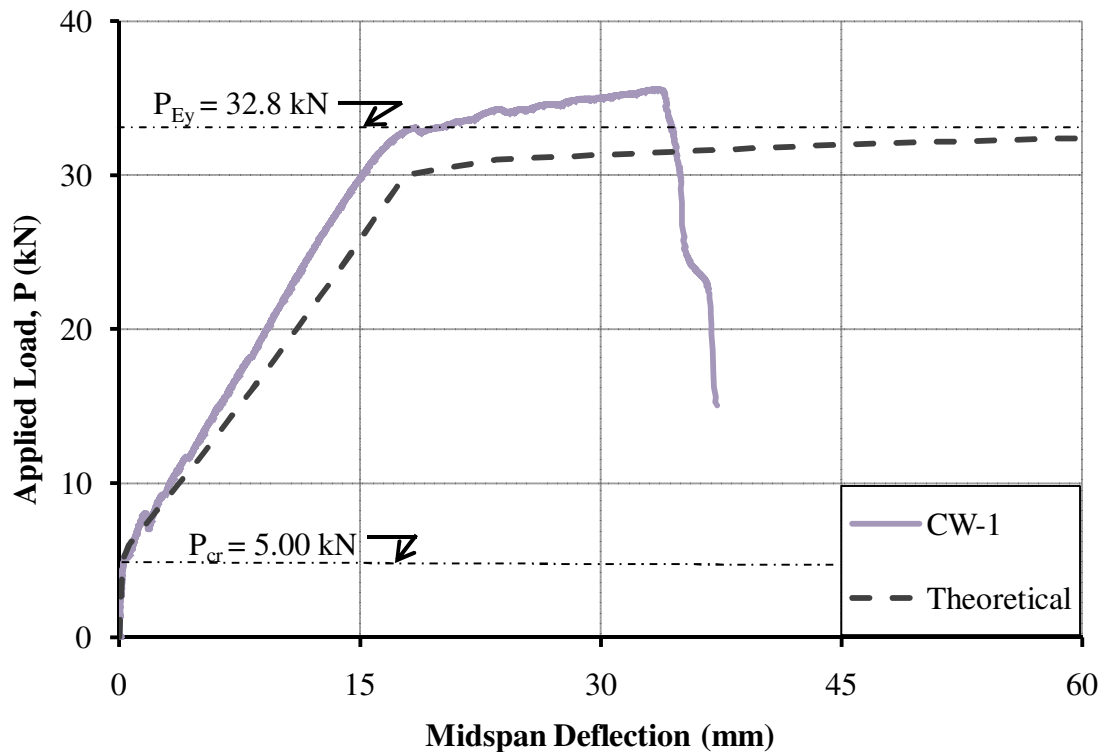


Figure 4B-1: Load versus midspan deflection - Specimen CW-1.
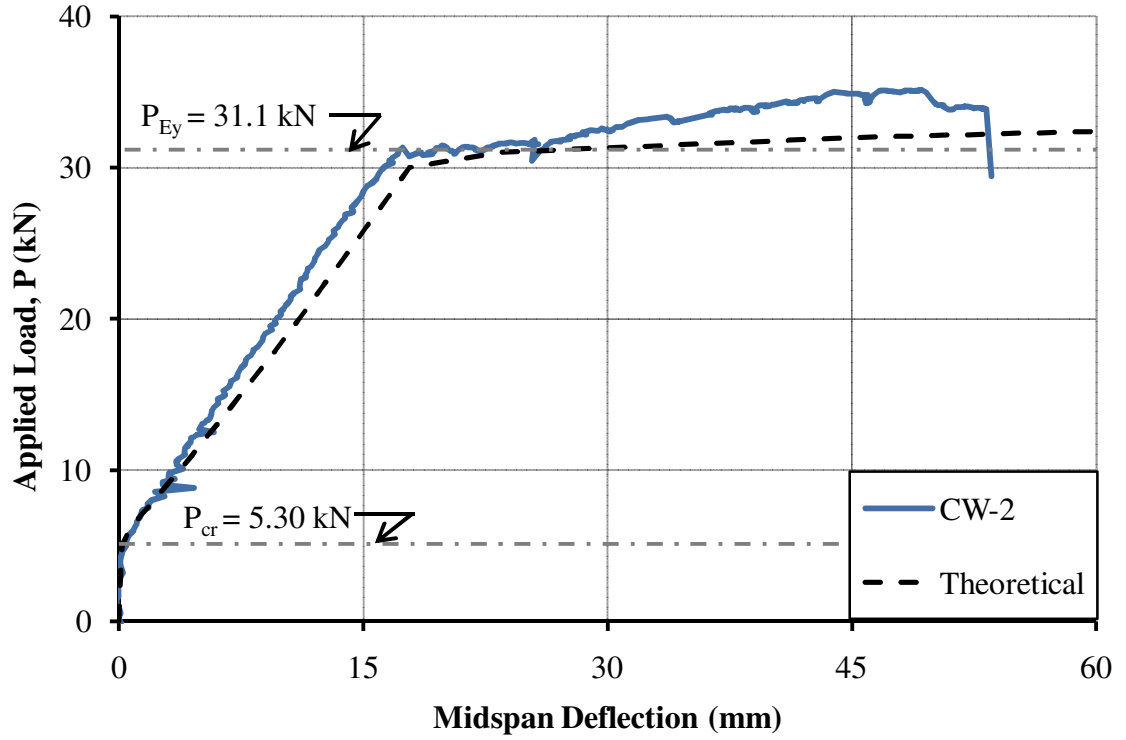
Figure 4B-2: Load versus midspan deflection - Specimen CW-2.
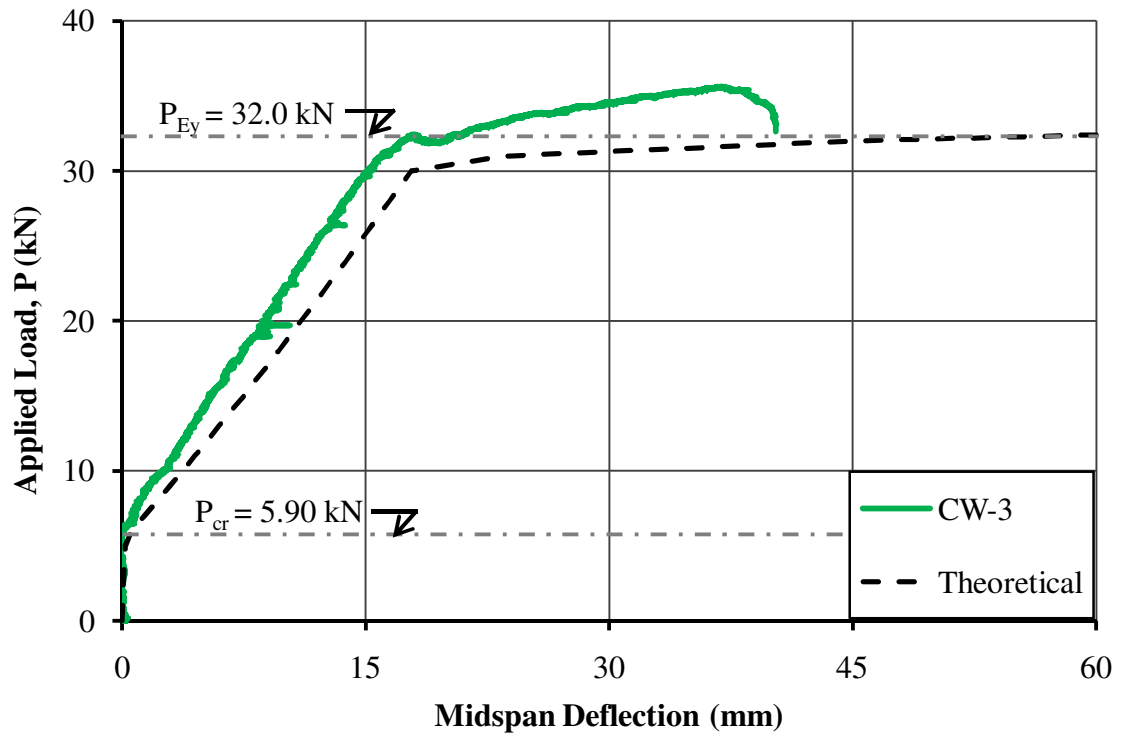


Figure 4B-3: Load versus midspan deflection - Specimen CW-3.
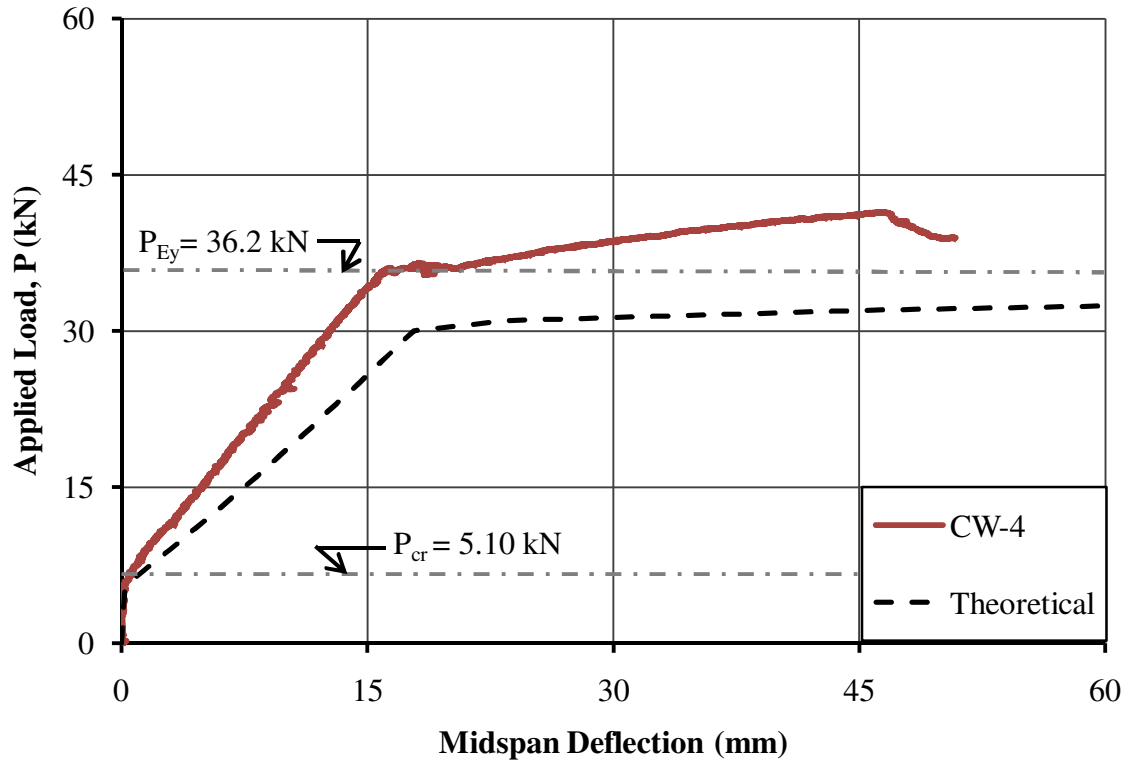
Figure 4B-4: Load versus midspan deflection - Specimen CW-4.
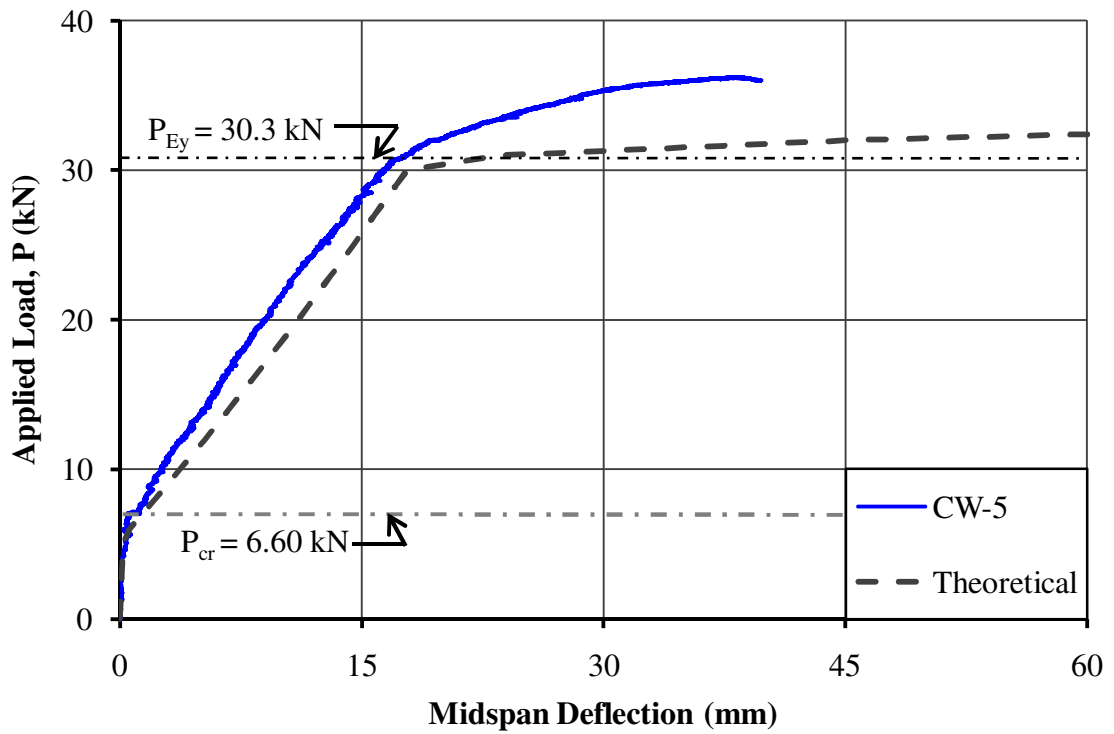


Figure 4B-5: Load versus midspan deflection - Specimen CW-5.
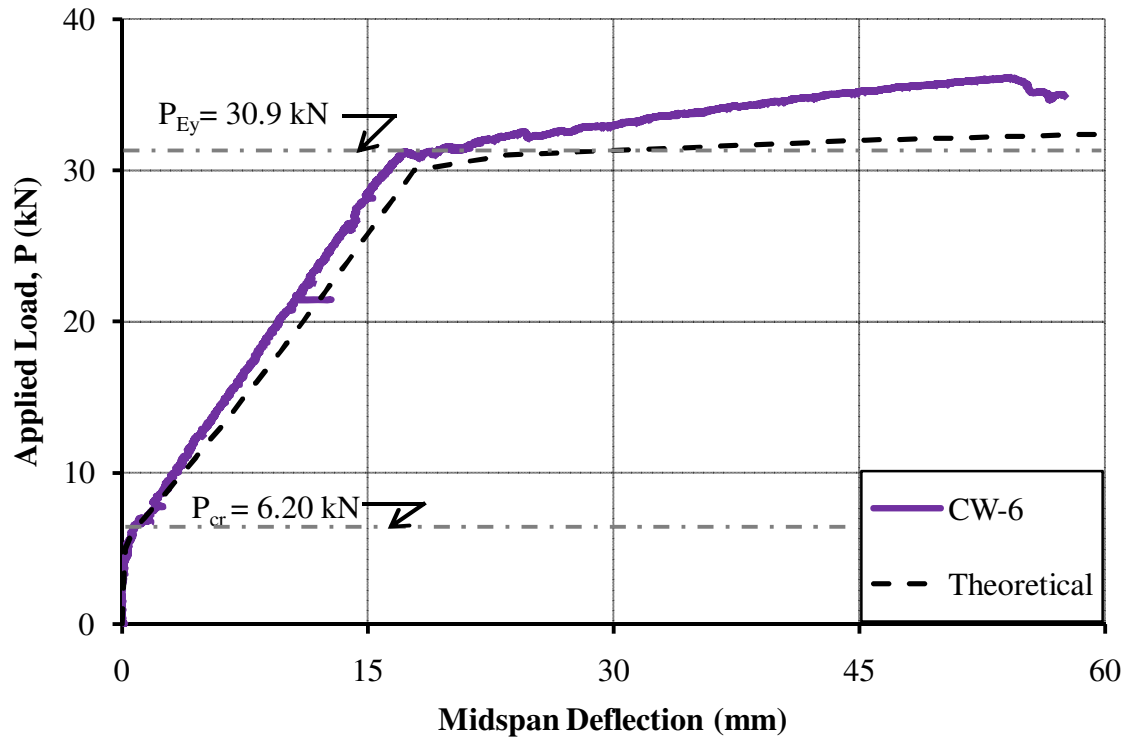
Figure 4B-6: Load versus midspan deflection - Specimen CW-6.
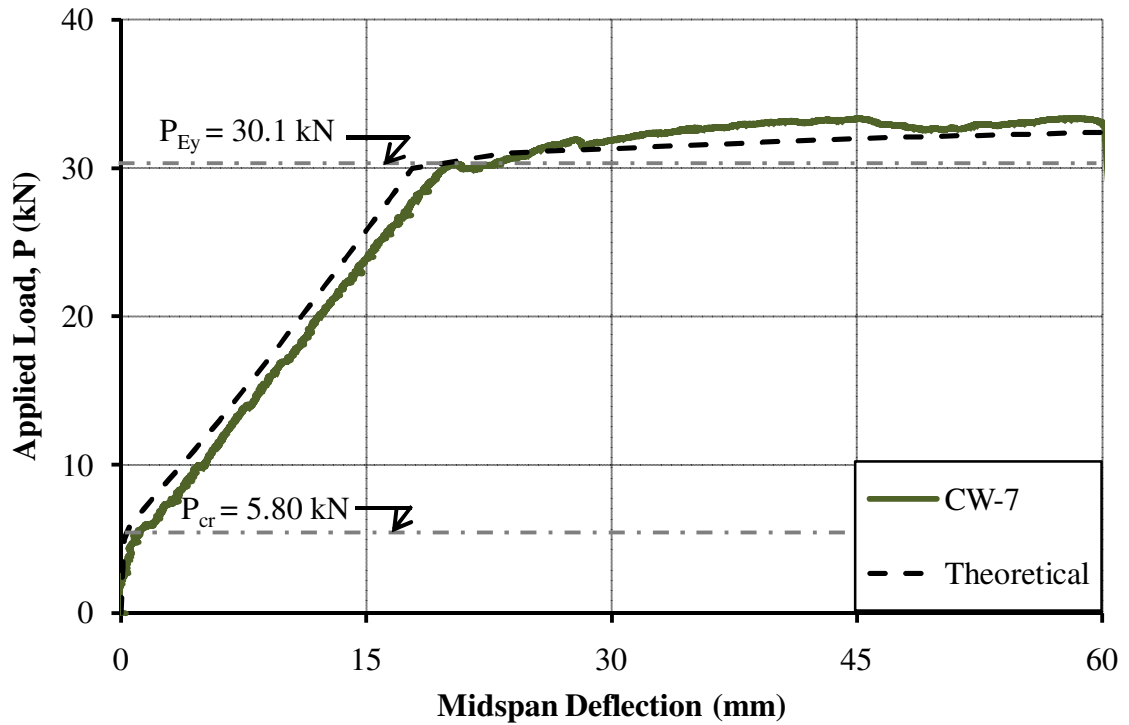


Figure 4B-7: Load versus midspan deflection - Specimen CW-7.

176
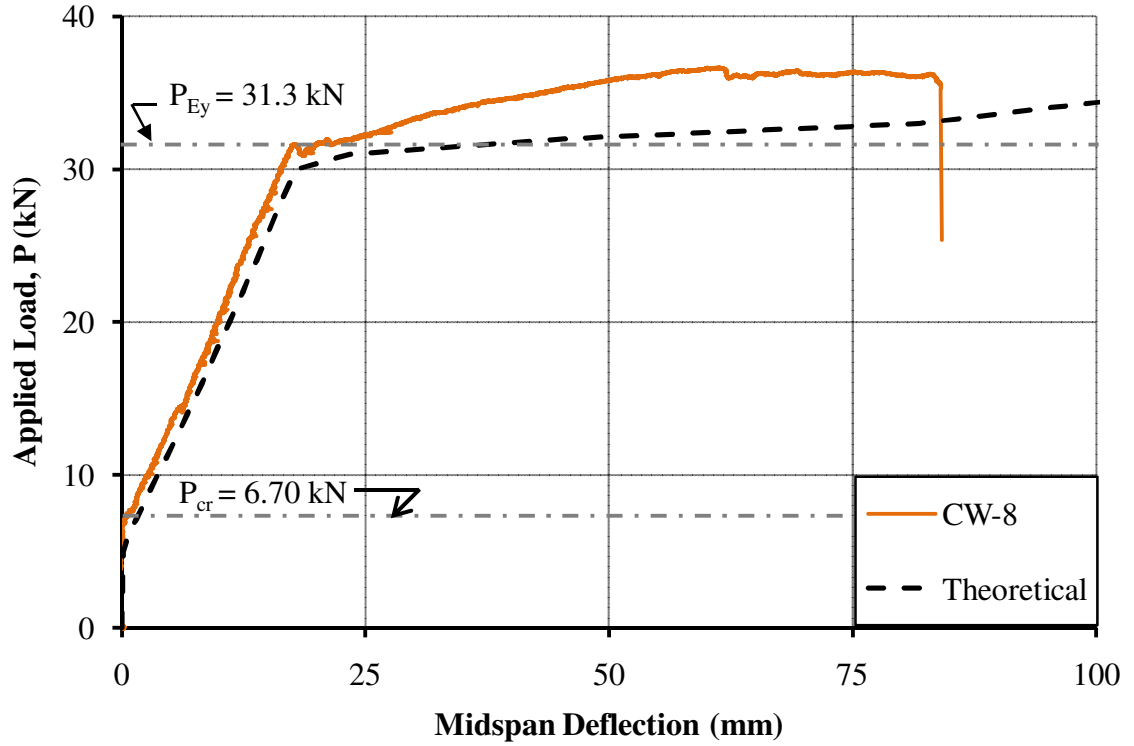
Figure 4B-8: Load versus midspan deflection - Specimen CW-8.
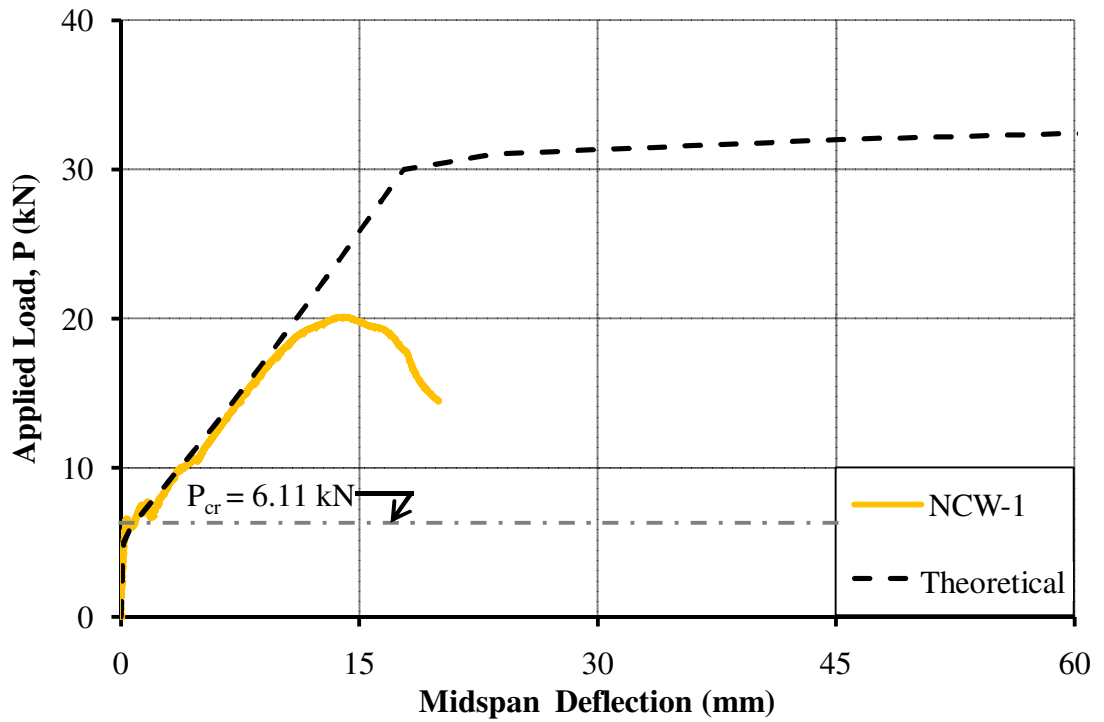


Figure 4B-9: Load versus midspan deflection - Specimen NCW-1.

177
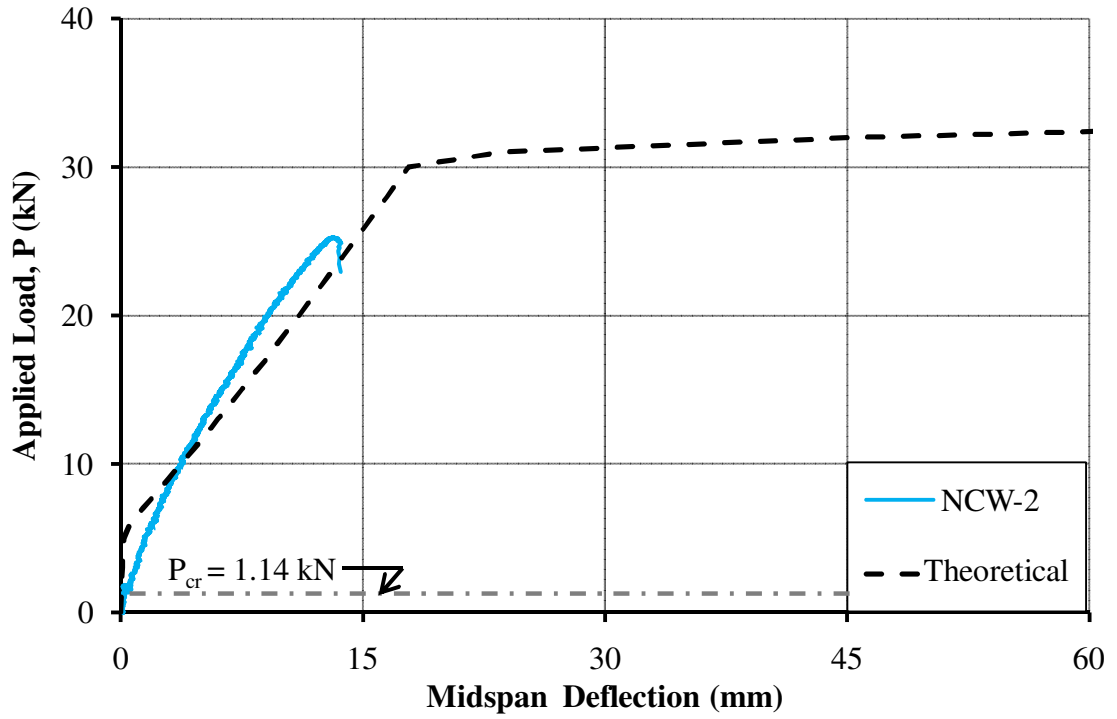
Figure 4B-10: Load versus midspan deflection - Specimen NCW-2.
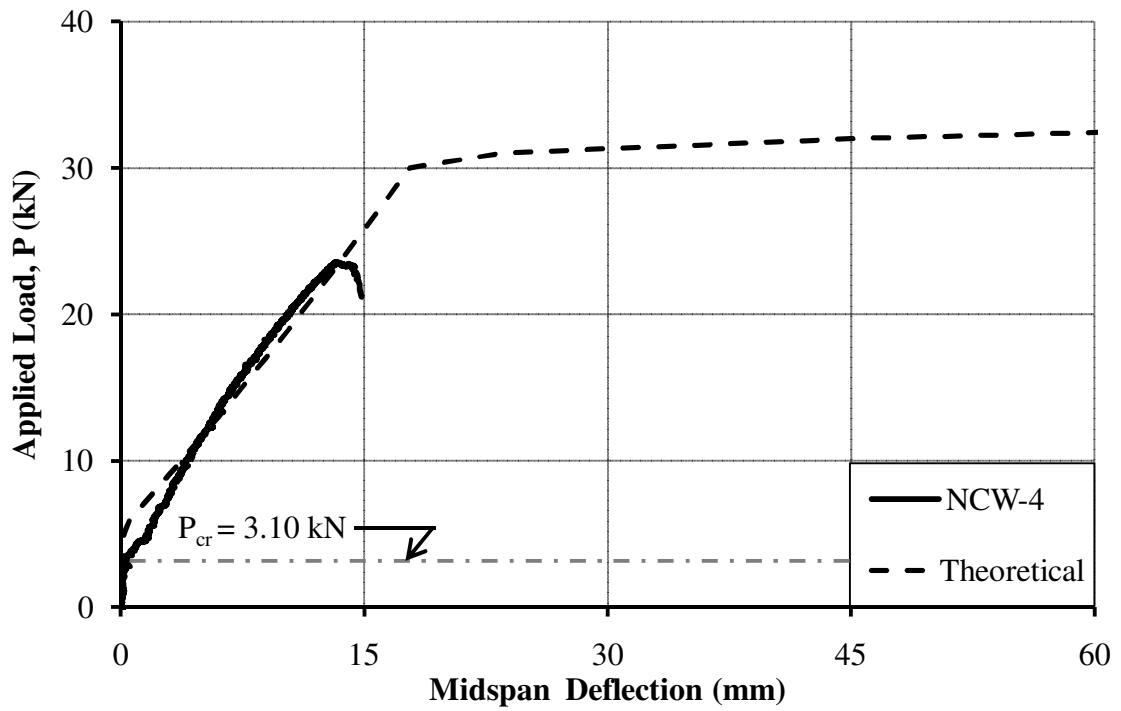


Figure 4B-11: Load versus midspan deflection - Specimen NCW-4.
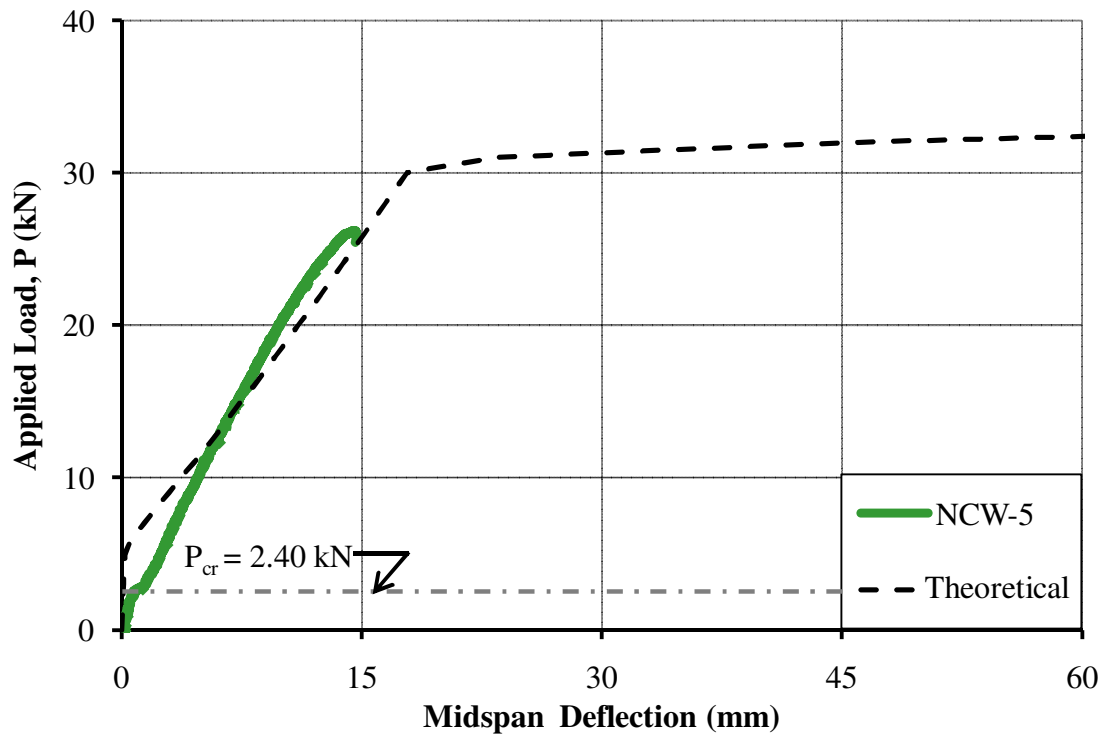
Figure 4B-12: Load versus midspan deflection - Specimen NCW-5.
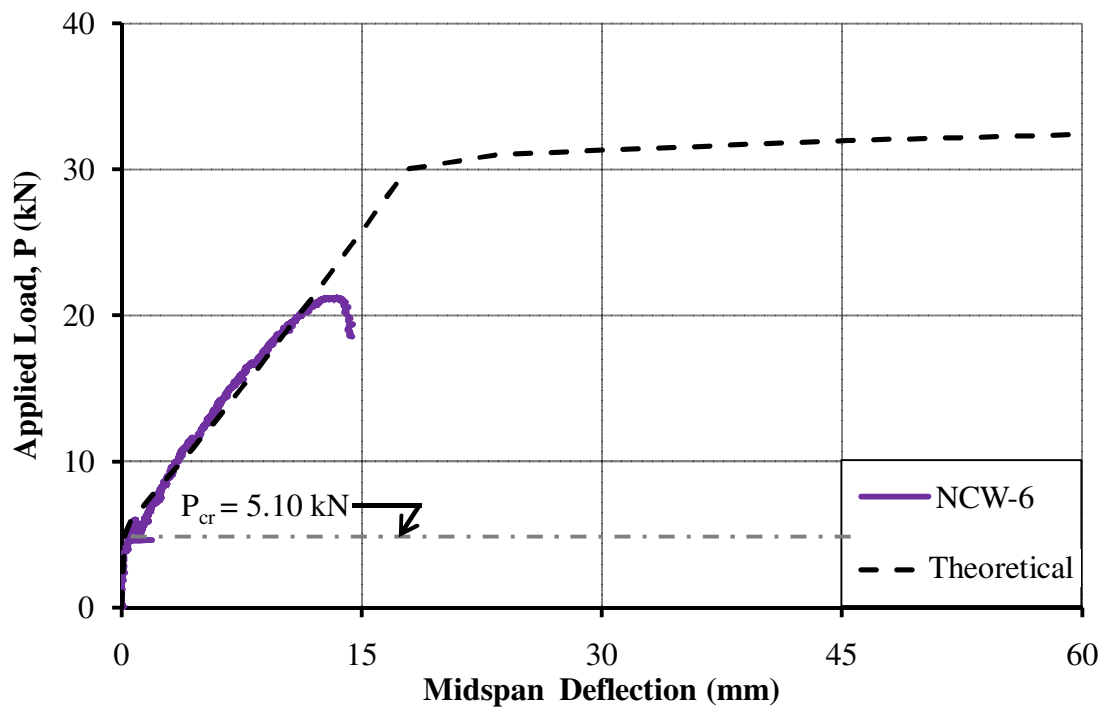


Figure 4B-13: Load versus midspan deflection - Specimen NCW-6.

179
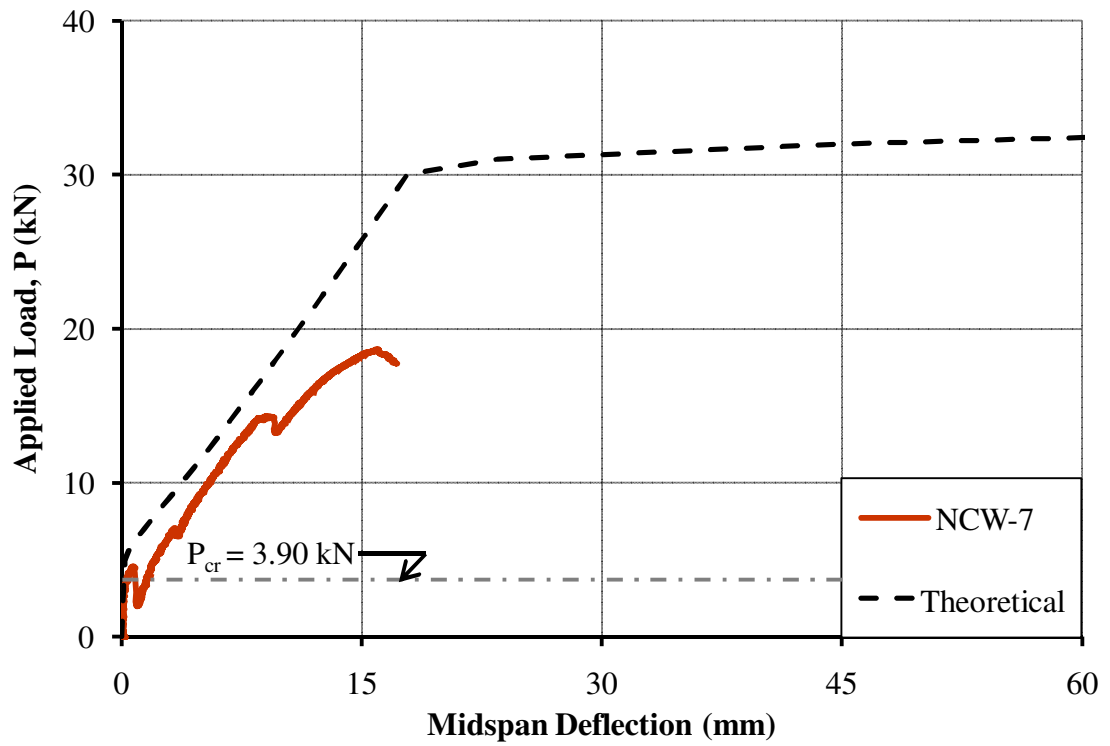
Figure 4B-14: Load versus midspan deflection - Specimen NCW-7.
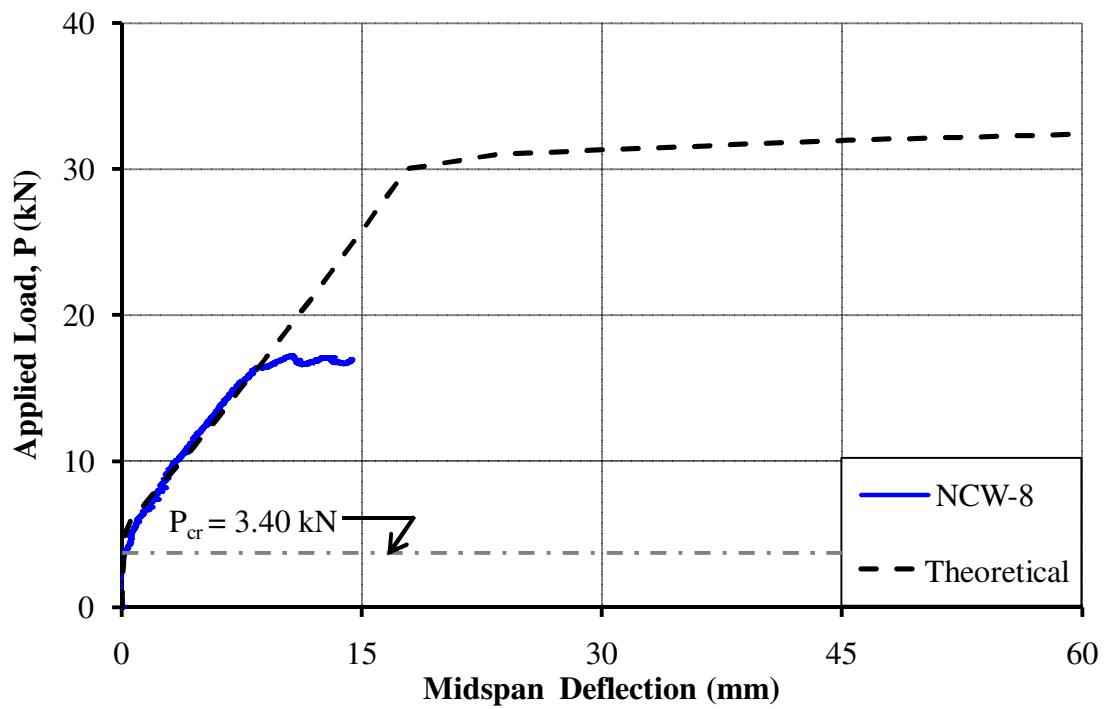


Figure 4B-15: Load versus midspan deflection - Specimen NCW-8.

APPENDIX 4C
THEORETICAL MOMENT-CURVATURE ANALYSIS

This section describes the mathematical expressions used to derive the theoretical moment curvature relationship for the wall splice specimens. The MathCAD code used to perform the finite difference method calculations and iterations that were required is also included. The theoretical stress versus strain profiles for the masonry in compression and the reinforcement in tension were used to calculate the moment corresponding to any curvature in the simply supported specimens. The moment curvature relationship, as generated, was then used to calculate the curvature corresponding to the ultimate moment. Using a similar numerical analysis, the tension in reinforcing steel was calculated from the curvature at the ultimate moment. Table 4C-1 presents a sample calculation for the experimental moment curvature calculation using the parabolic fitted curve in the deflection profiles.

**Development of the compression stress-strain response for the grouted masonry**

As discussed in Section 4.4.5, a modified Kent-Park curve (Park, Priestley and Gill, 1982) was adopted for the theoretical compressive stress-strain response for the grouted masonry. The modified Kent-Park curve has two segments: a parabolic rising curve, followed by a linear falling curve. The compressive stress, $f_m$, at any strain, $\varepsilon_c$, is given by:

Rising curve:

$$f_m(\varepsilon_c) = K f_m \left[ \left( \frac{2\,\varepsilon_c}{0.002K} \right) - \left( \frac{\varepsilon_c}{0.002K} \right)^2 \right] \dotfill (4C\text{-}1)$$

when, $\varepsilon_c \leq 0.002$

where, $f_m$ = the unconfined masonry prism strength (MPa)

        $K$ = strength enhancement factor, which is equal to 1.0 for unconfined masonry

        when no transverse reinforcement is provided.

With K = 1.0, Equation 4C-1 transforms into the original Kent-Park model (Kent and Park, 1971). The current study follows the modified Park-Kent model to obtain the empirical constants in metric units used in the falling curve:

Falling curve:

$$f_m(\varepsilon_c) = K f_m \left[ 1 - Z\,(\varepsilon_c - 0.002K) \right] \dotfill (4C\text{-}2)$$

when $0.002 \leq \varepsilon_c \leq 0.01$

Where $Z = \dfrac{0.5}{\left[ \dfrac{3 + 0.29\,f_m}{145\,f_m - 1000} \right] - 0.002\,K}$

**Development of the tensile stress-strain response for the reinforcing steel**

The tensile stress versus strain curve for the reinforcement has three segments: the linear elastic portion up to the yield strain, the yield plateau, and finally the assumed parabolic strain hardening curve. The stress, $f_s$, at any strain, $\varepsilon_s$, is:

Elastic curve:

$$f_s(\varepsilon_s) = E_s \varepsilon_s \quad \ldots\ldots\ldots\ldots\ldots\ldots\ldots\ldots\ldots\ldots\ldots\ldots\ldots\ldots\ldots\ldots\ldots\ldots\ldots\ldots\ldots\ldots\ldots(4C\text{-}3)$$

for $\varepsilon_s \leq \varepsilon_y$

where $\varepsilon_y$ = the yield strain of reinforcing bars,

$\quad\quad$ $f_y$ = the yield stress of reinforcing bars, and

$\quad\quad$ $E_s$ = the modulus of elasticity of the reinforcement = $f_y/\varepsilon_y$

Yield plateau:

$$f_s(\varepsilon_s) = f_y \quad \ldots\ldots\ldots\ldots\ldots\ldots\ldots\ldots\ldots\ldots\ldots\ldots\ldots\ldots\ldots\ldots\ldots\ldots\ldots\ldots\ldots(4C\text{-}4)$$

for $\varepsilon_y < \varepsilon_s \leq \varepsilon_{sh}$

where $\varepsilon_{sh}$ = the steel strain at the initiation of strain hardening

Strain hardening curve:

$$f_s(\varepsilon_s) = A + B\,\varepsilon_s + C\,\varepsilon_s^2 + D\,\varepsilon_s^3 \quad \ldots\ldots\ldots\ldots\ldots\ldots\ldots\ldots\ldots\ldots\ldots\ldots\ldots.(4C\text{-}5)$$

for $\varepsilon_{sh} < \varepsilon_s \leq \varepsilon_{ult}$

where $\varepsilon_{ult}$ = the strain corresponding to the ultimate stress.

Constants A, B, C and D were derived from the following boundary conditions:

$$f_s(\varepsilon_{sh}) = f_y$$

$$f_s(\varepsilon_{ult}) = f_{ult}$$

$$f_s'(\varepsilon_{sh}) = E_{sh}$$

$$f_s'(\varepsilon_{ult}) = 0$$

where $f_{ult}$ = the ultimate steel stress of the reinforcement, and

$E_{sh}$ = The slope at the beginning of strain hardening curve.

The reinforcing steel properties used to generate stress versus strain curve were obtained from averaging the values from the sample test data for the reinforcing bars presented in Table 4.2 and are as follows:

$E_s$ = 205000 MPa

$f_y$ = 441 MPa

$\varepsilon_{sh}$ = 0.014

$E_{sh}$ = 6000 MPa

$\varepsilon_{ult}$ = 0.1

$f_{ult}$ = 619 MPa

**Moment curvature analysis**

The curvature varies linearly prior to first cracking of the specimen. The curvature just before cracking is given by:

$$\phi_{uc} = \frac{M_{cr}}{E_m I_g} \dots\dots\dots\dots\dots\dots\dots\dots\dots\dots\dots\dots\dots\dots\dots\dots\dots\dots\dots (4C\text{-}6)$$

where $M_{cr}$= the cracking moment determined from the average experimental values reported in Tables 4.5 and 4.6.

$E_m$ = the modulus of elasticity for masonry = 850 $f'_m$ as calculated in accordance with Clause 6.5.2 in CSA S304.1, 2004.

$I_g$ = the gross moment of inertia of the wall splice specimen.

For any curvature greater than $\phi_{uc}$, the depth of the neutral axis c, is assumed. The strain at the extreme compressive fiber was then obtained using similar triangles from the linear strain diagram:

$$\varepsilon_x = \phi \, c \dots\dots\dots\dots\dots\dots\dots\dots\dots\dots\dots\dots\dots\dots\dots\dots\dots\dots\dots(4C\text{-}7)$$

The distance to the neutral axis, c, is then divided into n equal layers, each having a thickness c/n. The strain in the $i^{th}$ layer at a distance $d_i$ from the neutral axis was obtained from the linear strain profile as:

$$\varepsilon_i = \frac{\varepsilon_x}{c} \, d_i \dots\dots\dots\dots\dots\dots\dots\dots\dots\dots\dots\dots\dots\dots\dots\dots\dots\dots\dots\dots\dots\dots(4C\text{-}8)$$

where $d_i$ is the distance between the centroid of the overall section and the mid-height of the $i^{th}$ layer.

The compressive stress, $f_{mi}$, in the $i^{th}$ layer was obtained from Equations 4C-1 and 4C-2:

$$f_{mi} = f_m(\varepsilon_i) \dots\dots\dots\dots\dots\dots\dots\dots\dots\dots\dots\dots\dots\dots\dots\dots\dots\dots\dots\dots(4C\text{-}9)$$

The total compressive force developed in the compressive zone is obtained from summing the resulting forces in all layers:

$$C = \sum_{i=1}^{i=n} f_{mi} \frac{c}{n} b \dots\dots\dots\dots\dots\dots\dots\dots\dots\dots\dots\dots\dots\dots\dots\dots\dots\dots\dots(4C\text{-}10)$$

where b = the width of the wall splice specimen.

The steel strain, $\varepsilon_s$, at the effective depth of the reinforcement, $d_{eff}$, was obtained from similar triangles from the linear strain diagram:

$$\varepsilon_s = \frac{\varepsilon_x}{c}(d_{eff} - c) \ldots\ldots\ldots\ldots\ldots\ldots\ldots\ldots\ldots\ldots\ldots\ldots\ldots\ldots\ldots\ldots\ldots\ldots\ldots(4C\text{-}11)$$

The tension carried by the reinforcing steel was then computed using Equations 4C-3 to 4C-5 and the nominal cross-sectional area of the reinforcing steel, $A_s$:

$$T = A_s f_s(\varepsilon_s)\ldots\ldots\ldots\ldots\ldots\ldots\ldots\ldots\ldots\ldots\ldots\ldots\ldots\ldots\ldots\ldots\ldots\ldots(4C\text{-}12)$$

An iterative MathCAD program established the neutral axis depth, c, such that equilibrium was satisfied between the compressive and tensile forces (C = T) at a 0.5% tolerance level. Once the neutral axis depth was established, the resulting moment was obtained as:

$$M = \sum_{i=1}^{i=n} [f_{mi}\frac{c}{n}bd_i] + A_s f_s(\varepsilon_s)(d_{eff} - c)\ldots\ldots\ldots\ldots\ldots\ldots\ldots\ldots\ldots(4C\text{-}13)$$

**MathCAD Code:**

| | |
|---|---|
| $\varepsilon_O$ | Compressive strain at maximum stress |
| $\phi$ | Curvature |
| $A_s$ | Cross-section area of reinforcing bar |
| b | Width of the wall splice specimen |
| X | Neutral axis depth from the compression (i.e. top) face |
| C | Total compressive force in the masonry |
| Cur () | Curvature corresponding to moment in cracked section |
| Cur2 () | Curvature corresponding to moment in un-cracked section considering gross area |
| Cons, $A_c$, $B_c$, $C_c$, $D_c$ | Constants for parabolic strain hardening curve of reinforcing steel |
| $d_{eff}$ | Effective depth of the reinforcing bars |
| $d_i$ | Mid-segment depth of the $i^{th}$ segment with respect to the neutral axis |
| def() | Midspan deflection resulting from applied load in a four-point loading arrangement |
| $E_m$ | Modulus of elasticity for masonry |
| $f'_m$ | Compressive strength of masonry assemblage |
| $f_m$ | Compressive stress in masonry |
| $L_i$ | Distance of the $i^{th}$ segment from the left support. |
| $M_{cr}$ | Cracking moment |
| $M(\phi)$ | Moment corresponding to curvature in cracked section |
| M2 (x.P) | Moment at a distance x, from the left support resulted due to total applied load P in four-point loading system |
| P | Total applied load in a four point loading arrangement |
| t | Total depth |
| T | Applied tension |

Material properties:

Width of specimen,    $b := 990 \text{mm}$

Total depth ,    $t := 190 \text{mm}$

Moment of inertia for gross section,

$$I_g := \frac{b \cdot t^3}{12}$$

Effective depth,

$$d_{eff} := 95 \text{mm}$$

Area of steel

$$A_s := 400 \text{mm}^2$$

Compressive strength of masonry

$$f'_m := 13.6 \frac{N}{mm^2}$$

Modulus of elasticity for masonry,

$$E_m := 850 \ f'_m$$

Cracking moment

$$M_{cr} := 4.996 \text{kN} \cdot \text{m}$$

[average experimental cracking moment after correcting for self weight ]

## Stress strain curve for masonry:

Strain at maximum stress

$\varepsilon_o := 0.002$

$$Z := \dfrac{0.5}{\left( \dfrac{3 + 0.29 \cdot \dfrac{f_m'}{\dfrac{N}{mm^2}}}{145 \cdot \dfrac{f_m'}{\dfrac{N}{mm^2}} - 1000} - 0.002 \right)}$$

$Z = 97.2$

Stress :

$$f_m(x) := \left\|\begin{array}{l} \left[ f_m' \cdot \left[ \dfrac{2 \cdot x}{\varepsilon_o} - \left( \dfrac{x}{\varepsilon_o} \right)^2 \right] \right] \quad \text{if } x \le 0.002 \\[4mm] \left[ f_m' \cdot \left[ 1.0 - Z_n \cdot (x - 0.002) \right] \right] \quad \text{if } 0.002 < x \le 0.01 \\[4mm] 0 \quad \text{otherwise} \end{array}\right.$$
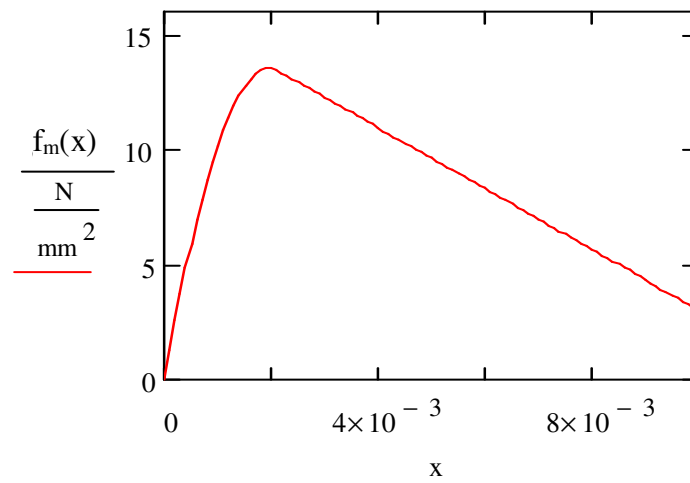
$x := 0, 0.0001 .. 0.015$

## Stress strain curve for steel:

$$\text{Cons} := \begin{pmatrix} 1 & 0.0143 & 0.000196 & 0.000002744 \\ 1 & 0.1 & 0.01 & 0.001 \\ 0 & 1 & 0.028 & 0.000588 \\ 0 & 1 & 0.2 & 0.03 \end{pmatrix}^{-1} \begin{pmatrix} 442 \\ 611 \\ 6000 \\ 0 \end{pmatrix}$$

$$\text{Cons} = \begin{pmatrix} 341.098 \\ 8.12 \times 10^3 \\ -8.143 \times 10^4 \\ 2.722 \times 10^5 \end{pmatrix}$$

$Ac := Cons_1$

$Bc := Cons_2$

$Cc := Cons_3$

$Dc := Cons_4$

$$f_s(\varepsilon) \quad := \quad \begin{vmatrix} \sigma 1_s \leftarrow \varepsilon \cdot 205000 \, \dfrac{N}{mm^2} & \text{if } 0 < \varepsilon < 0.0022 \\[2em] \sigma 1_s \leftarrow 442 \, \dfrac{N}{mm^2} & \text{if } 0.014 \geq \varepsilon \geq 0.0022 \\[2em] \sigma 1_s \leftarrow \left( Ac + Bc\varepsilon + Cc\,\varepsilon^2 + Dc \cdot \varepsilon^3 \right) \cdot \dfrac{N}{mm^2} & \text{if } 0.1 \geq \varepsilon > 0.014 \\[2em] \sigma 1_s \leftarrow 0 \quad \text{otherwise} \\[1em] \sigma 1_s \end{vmatrix}$$

**Moment corresponding to any curvature (cracked section):**

$$M(\phi) :=$$

$\quad$ for $k \in 60, 59.9 .. 10$

$\qquad X \leftarrow (k) \cdot 1\,\text{mm}$

$\qquad P \leftarrow 0\,\text{N}$

$\qquad \varepsilon_k \leftarrow X \cdot \phi$

$\qquad$ for $i \in 1 .. 100$

$\qquad\qquad d_i \leftarrow \dfrac{X}{100} \cdot (i - 0.5)$

$\qquad\qquad \varepsilon_i \leftarrow \dfrac{\varepsilon_k}{X} \cdot d_i$

$\qquad\qquad p_i \leftarrow f_c(\varepsilon_i)$

$\qquad \sigma_s \leftarrow f_s\left[\dfrac{\varepsilon_k}{X} \cdot (d_{eff} - X)\right]$

$\qquad C \leftarrow \left(\displaystyle\sum_{n=1}^{100} p_n\right) \cdot b \cdot \dfrac{X}{100}$

$\qquad T \leftarrow A_s \cdot \sigma_s$

$\qquad X_1 \leftarrow X \quad \text{if} \quad \dfrac{|C - T|}{T} \le 0.005$

$\quad \varepsilon ef \leftarrow X_1 \cdot \phi$

$\quad$ for $i \in 1 .. 100$

$\qquad\qquad d1_i \leftarrow \dfrac{X_1}{100} \cdot (i - 0.5)$

$\qquad\qquad \varepsilon1_i \leftarrow \dfrac{\varepsilon ef}{X_1} \cdot d1_i$

$\qquad\qquad p1_i \leftarrow f_s(\varepsilon1_i)$

$\quad \varepsilon s \leftarrow \dfrac{\varepsilon ef}{X_1} \cdot (d_{eff} - X_1)$

$\quad T \leftarrow A_s \cdot f_s(\varepsilon s)$

$\quad C \leftarrow \left(\displaystyle\sum_{n=1}^{100} p1_n\right) \cdot b \cdot \dfrac{X_1}{100}$

$\quad M_{tot} \leftarrow T \cdot \left[d_{eff} - X_1 + \dfrac{\left[\displaystyle\sum_{n=1}^{100} (n \cdot d1_n)\right] \cdot b \cdot \dfrac{X_1}{100}}{\left(\displaystyle\sum_{n=1}^{100} n\right) \cdot b \cdot \dfrac{X_1}{100}}\right]$

$\quad M_{tot}$

191

**Curvature and resulting moment database (Cracked section)**:

$$\text{Mom1} := \begin{array}{|l} \text{for } n \in 1..500 \\ \quad \begin{array}{|l} pi \leftarrow (n-1)\cdot 0.001 \\ p_n \leftarrow M\left(\dfrac{pi}{m}\right) \end{array} \\ p \end{array} \qquad \text{Cur1} := \begin{array}{|l} \text{for } n \in 1..500 \\ \quad p_n \leftarrow (n-1)\cdot 0.001 \\ p \end{array}$$

$$\text{Mom1} =$$

|    | 1     |
|----|-------|
| 1  | 0     |
| 2  | 0.466 |
| 3  | 0.93  |
| 4  | 1.395 |
| 5  | 1.857 |
| 6  | 2.321 |
| 7  | 2.78  |
| 8  | 3.237 |
| 9  | 3.7   |
| 10 | 4.154 |
| 11 | ...   |

$\text{kN}\cdot\text{m}$    $\text{Cur1} =$

|    | 1                    |
|----|----------------------|
| 1  | 0                    |
| 2  | $1\cdot 10^{-3}$     |
| 3  | $2\cdot 10^{-3}$     |
| 4  | $3\cdot 10^{-3}$     |
| 5  | $4\cdot 10^{-3}$     |
| 6  | $5\cdot 10^{-3}$     |
| 7  | $6\cdot 10^{-3}$     |
| 8  | $7\cdot 10^{-3}$     |
| 9  | $8\cdot 10^{-3}$     |
| 10 | $9\cdot 10^{-3}$     |
| 11 | ...                  |

$1/m$

**Curvature corresponding to any moment ( cracked section):**

$$\text{cur}(x) := \begin{array}{|l} p \leftarrow 0 \quad \text{if } x = 0\text{kN}\cdot\text{m} \\ \text{for } n \in 1..500 \qquad\qquad\qquad \text{if } x > 0\text{kN}\cdot\text{m} \\ \quad \text{if } x < \text{Mom1}_n \\ \qquad \begin{array}{|l} \text{cur1} \leftarrow (n-1)\cdot 0.001 \\ \text{cur2} \leftarrow (n-2)\cdot 0.001 \\ M1 \leftarrow \text{Mom1}_n \\ M2 \leftarrow \text{Mom1}_{n-1} \\ p \leftarrow \text{cur2} + \left(\dfrac{\text{cur1}-\text{cur2}}{M1-M2}\right)\cdot(x-M2) \\ \text{break} \end{array} \\ p\cdot\dfrac{1}{m} \end{array}$$

192

**<u>Total moment curvature relation for combined un-cracked and cracked section:</u>**

Curvature corresponding to any moment,

$$\text{cur2(M)} := \begin{vmatrix} k \leftarrow \dfrac{M}{E_m \cdot I_g} & \text{if } M \leq M_{cr} \\ \\ k \leftarrow \text{cur(M)} & \text{otherwise} \\ \\ k \end{vmatrix}$$



$\dfrac{M}{kN \cdot m}$

cur2 (M)
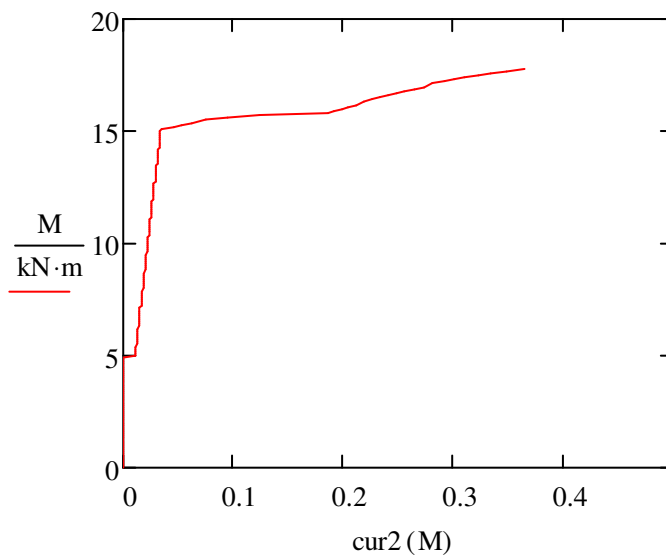
## Tension at reinforcement corresponding to any curvature:

$T_1(\phi) :=$ for $k \in 50, 49.9 .. 10$

$\quad\quad X \leftarrow (k) \cdot 1\text{mm}$

$\quad\quad P \leftarrow 0\text{N}$

$\quad\quad \varepsilon_k \leftarrow X \cdot \phi$

$\quad\quad$ for $i \in 1 .. 100$

$\quad\quad\quad\quad d_i \leftarrow \dfrac{X}{100} \cdot (i - 0.5)$

$\quad\quad\quad\quad \varepsilon_i \leftarrow \dfrac{\varepsilon_k}{100} \cdot i$

$\quad\quad\quad\quad p_i \leftarrow f_c(\varepsilon_i)$

$\quad\quad \sigma_s \leftarrow f_s\left[\dfrac{\varepsilon_k}{X} \cdot (d_{eff} - X)\right]$

$\quad\quad C \leftarrow \left(\displaystyle\sum_{n=1}^{100} p_n\right) \cdot b \cdot \dfrac{X}{100}$

$\quad\quad T \leftarrow A_s \cdot \sigma_s$

$\quad\quad X_1 \leftarrow X \quad \text{if} \quad \dfrac{|C - T|}{T} \leq 0.005$

$\quad \varepsilon ef \leftarrow X_1 \cdot \phi$

$\quad$ for $i \in 1 .. 100$

$\quad\quad\quad\quad d1_i \leftarrow \dfrac{X_1}{100} \cdot (i - 0.5)$

$\quad\quad\quad\quad \varepsilon 1_i \leftarrow \dfrac{\varepsilon ef}{100} \cdot i$

$\quad\quad\quad\quad p1_i \leftarrow f_s(\varepsilon 1_i)$

$\quad \varepsilon_s \leftarrow \dfrac{\varepsilon ef}{X_1} \cdot (d_{eff} - X_1)$

$\quad T \leftarrow A_s \cdot f_s(\varepsilon_s)$

$\quad P1 \leftarrow T$

$\quad P1$

$$T_1\left(\dfrac{0.275}{m}\right) = 191.589 \cdot \text{kN}$$

**Associated error with the selection of the number of segments, n**

Figure 4C-1 shows that the number of segments that the compression zone was divided into for the finite difference numerical analysis (n = 10, 50, and 100) yielded values of 11.237, 11.291, and 11.298 kN-m, respectively, for the moment corresponding to a fixed curvature $\phi$ = 0.025/m. The curvature value was selected such that it fell within the linear moment-curvature region and was lower than the curvature corresponding to yielding of the reinforcement. A regression analysis of this data provided the following relationship between the number of segments and the resulting moment:

$$M_\phi = \frac{11.305\,n}{n+0.06} \quad\text{.......................................................................................}(4C\text{-}14)$$
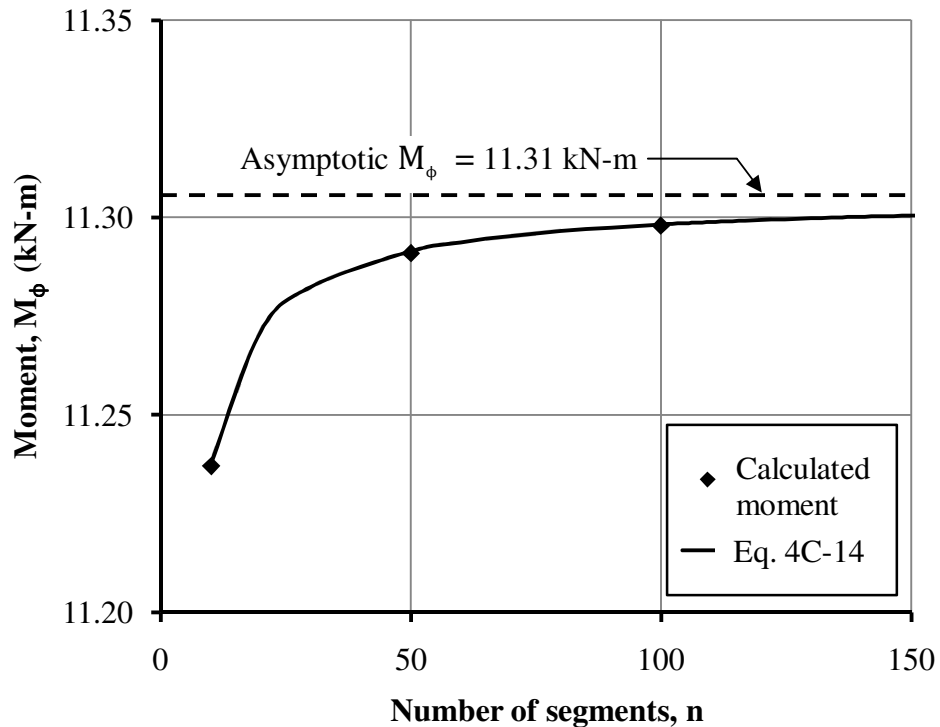


Figure 4C-1: Moment corresponding to a curvature, $\phi$ = 0.025/m versus the number of segments in the compression zone.

Figure 4C-1 shows that the curve corresponding to Equation 4C-14 approached an

asymptotic value of 11.305 kN-m. The error corresponding to the moment of 11.298

kN-m resulting from n=100 was therefore equal to 0.06%.

**Sample calculation for experimental moment-curvature relation:**

Table 4C-1 shows a sample calculation for the experimental curvature calculation

derived from the parabolic deflection profiles explained in Section 4.4.4. The constants

A and B were obtained from the parabolic equation of the best fit curve in the deflection

profile. The calculation method is described in Section 4.4.5.

Table 4C-1: Representative experimental curvature calculation for a wall splice
specimen with contact lap splices - Specimen CW-7.

| Load, P (kN) | Moment (kN-m) | $y(x) = Ax^2 + Bx$ | | Experimental curvature, $\phi = 2A$ (1/m) |
|---|---|---|---|---|
| | | A | B | |
| 5.00 | 2.00 | 0.001 | 0.001 | 0.001 |
| 10.0 | 4.00 | 0.003 | 0.007 | 0.006 |
| 15.0 | 6.00 | 0.006 | 0.013 | 0.011 |
| 20.0 | 8.00 | 0.008 | 0.020 | 0.016 |
| 25.0 | 10.0 | 0.011 | 0.026 | 0.022 |
| 30.0 | 12.0 | 0.014 | 0.032 | 0.027 |
| 31.0 | 12.4 | 0.014 | 0.033 | 0.028 |
| 32.0 | 12.8 | 0.018 | 0.043 | 0.036 |
| 33.0 | 13.2 | 0.024 | 0.058 | 0.048 |
| 34.0 | 13.6 | 0.029 | 0.069 | 0.058 |
| 35.0 | 14.0 | 0.034 | 0.081 | 0.069 |
| 36.1 | 14.4 | 0.043 | 0.102 | 0.085 |

THEORETICAL LOAD VERSUS MIDSPAN DEFLECTION ANALYSIS

The midspan deflection for the wall splice specimens was derived using the conjugate beam method as described in Section 4.4.4. The simply supported wall in its horizontal testing position was vertically loaded with the curvature corresponding to the moment along the length for any given value of the applied load such that the resulting midspan moment gives the theoretical midspan deflection. This section presents the mathematical expressions used to calculate the midspan deflection followed by the numerical program code (MathCAD).

To consider the effect of the gradual transition from the uncracked to cracked section properties, an expression for effective curvature was derived from Bischoff's (2005) proposed equation for the effective moment of inertia, $I_{eff}$ :

$$I_{eff} = \frac{I_{cr}}{1 - \left(1 - \frac{I_{cr}}{I_g}\right)\left(\frac{M_{cr}}{M_a}\right)^2} \quad \text{.............................................................................(4D-1)}$$

where $M_a$ = applied moment, and $M_{cr}$ = the cracking moment.

Let $\left(\frac{M_{cr}}{M_a}\right)^2 = A$

Substituting into Eq. 4D-1 gives:

$$I_{eff} = \frac{I_{cr}}{1-\left(1-\frac{I_{cr}}{I_g}\right)A} \dots\dots\dots\dots\dots\dots\dots\dots\dots\dots\dots\dots\dots\dots\dots\dots\dots\dots\dots\dots\dots\dots\dots\dots\dots\dots(4D\text{-}2)$$

Rearranging Eq. 4D-2 gives:

$$I_{eff} = \frac{I_{cr}I_g}{I_g(1\text{-}A)+I_{cr}A} \dots\dots\dots\dots\dots\dots\dots\dots\dots\dots\dots\dots\dots\dots\dots\dots\dots\dots\dots\dots\dots(4D\text{-}2A)$$

,or

$$\frac{1}{I_{eff}} = \frac{(1\text{-}A)}{I_{cr}} + \frac{A}{I_g} \dots\dots\dots\dots\dots\dots\dots\dots\dots\dots\dots\dots\dots\dots\dots\dots\dots\dots\dots\dots\dots\dots(4D\text{-}2B)$$

Multiplying both sides by $\dfrac{M_a}{E_m}$:

$$\frac{M_a}{E_m I_{eff}} = \frac{M_a}{E_m I_{cr}}(1\text{-}A) + \frac{M_a}{E_m I_g}A \dots\dots\dots\dots\dots\dots\dots\dots\dots\dots\dots\dots\dots\dots\dots(4D\text{-}2C)$$

noting that $\phi = M/EI$, Eq. 4D-2C becomes:

$$\phi_{eff} = \phi_{cr}(1\text{-}A) + \phi_g A \dots\dots\dots\dots\dots\dots\dots\dots\dots\dots\dots\dots\dots\dots\dots\dots\dots\dots(4D\text{-}2D)$$

$$\phi_{eff} = \phi_{cr}\left[1-\left(\frac{M_{cr}}{M_a}\right)^2\right] + \phi_g\left(\frac{M_{cr}}{M_a}\right)^2 \dots\dots\dots\dots\dots\dots\dots\dots\dots\dots\dots\dots\dots\dots\dots(4D\text{-}3)$$

The curvature of the cracked section in Eq. 4D-3 was obtained from the theoretical moment curvature relationship for the cracked section as described in Appendix 4C.

The length of the beam, L, is divided into n segments each having a width of L/n. The average moment, $M_i$, in the $i^{th}$ segment at $L_i$ away from the left support was established from elementary mechanics. The effective curvature, $\phi_i$, corresponding to $M_i$, was obtained using Equation 4E-7. The midspan deflection, $\Delta_{mid}$, was then calculated as:

$$\Delta_{mid} = \sum_{i=1}^{i=n} \frac{1}{4} \phi_i \frac{L^2}{n} - \sum_{i=1}^{i=\frac{n}{2}} \phi_i L_i \frac{L}{n} \quad \dots\dots\dots\dots\dots\dots\dots\dots\dots\dots\dots\dots\dots\dots\dots\dots\dots\dots\dots\dots\dots\dots\dots\dots\dots\text{(4D-4)}$$

**Associated error with the selection of the number of segments, n**

Figure 4D-1 shows that the number of segments along the beam length (n = 10, 120, and 240) when used in the finite difference numerical program described, resulted in midspan deflections of 12.484, 12.582, and 12.583 mm, respectively, for a constant applied load of 30 kN. A regression analysis yields:

$$\Delta_{30P} = \frac{12.590\,n}{n+0.10} \quad \dots\dots\dots\dots\dots\dots\dots\dots\dots\dots\dots\dots\dots\dots\dots\dots\dots\dots\dots\dots\dots\dots..\dots\dots\dots\dots...\dots\text{(4D-5)}$$
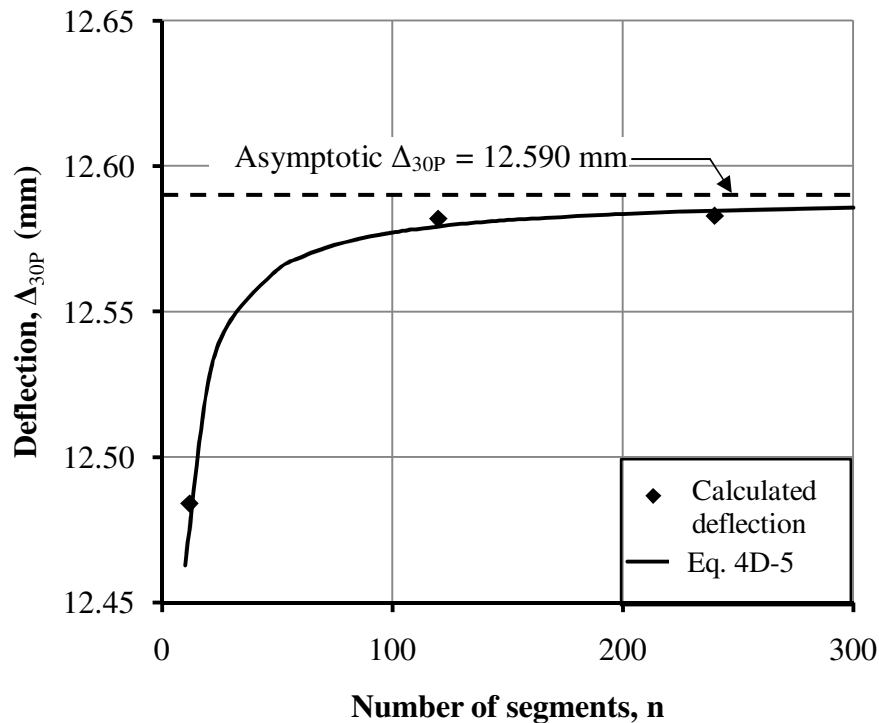


Figure 4D-1: Deflection corresponding to an applied load P=30 kN versus the number of segments along the wall splice specimen.

199

The function corresponding to Equation 4D-5 in Figure 4D-1 approached an asymptotic

value of 12.59 mm. The error associated with using 240 segments in the finite difference

was therefore 0.06%.

**MathCAD Code:**

**Moment corresponding to any applied load:**

$$M2(x, p) := \begin{vmatrix} m \leftarrow 0 \\ m \leftarrow \dfrac{p}{2} \cdot x \quad \text{if } x < 800\text{mm} \\ m \leftarrow \dfrac{p}{2} \cdot 800\text{mm} \quad \text{if } 800\text{mm} \leq x \leq 1600\text{mm} \\ m \leftarrow \dfrac{p}{2} \cdot 800\text{mm} - (x - 1600\text{mm}) \cdot \dfrac{p}{2} \quad \text{if } x > 1600\text{mm} \end{vmatrix}$$

**Un-cracked curvature from gross section:**

$$\text{cur2}(M) := \begin{vmatrix} k \leftarrow \dfrac{M}{E_m \cdot I_g} \quad \text{if } M \leq M_{cr} \\ k \leftarrow \text{cur}(M) \quad \text{otherwise} \\ k \end{vmatrix}$$

$$\text{cur2}(9.92\text{kN} \cdot \text{m}) = 0.022 \dfrac{1}{\text{m}}$$

**Deflection at midspan corresponding to any applied load, P :**

$$\text{def}(x) := \begin{array}{|l} P \leftarrow x \\[4pt] \text{for } i \in 1..240 \\[4pt] \quad \begin{array}{|l} L_i \leftarrow i \cdot 10\text{mm} - 5\text{mm} \\[4pt] \text{mom} \leftarrow M2(L_i, P) \\[4pt] \phi_i \leftarrow \dfrac{\text{mom}}{E_m \cdot I_g} \quad \text{if mom} \leq M_{cr} \\[10pt] \phi_i \leftarrow \text{cur(mom)} \cdot \left[ 1 - \left( \dfrac{M_{cr}}{\text{mom}} \right)^2 \right] + \dfrac{\text{mom}}{E_m \cdot I_g} \cdot \left( \dfrac{M_{cr}}{\text{mom}} \right)^2 \quad \text{otherwise} \end{array} \\[14pt] \text{middef} \leftarrow 10\text{mm} \cdot \displaystyle\sum_{n=1}^{120} \left( \phi_n \cdot L_n \right) \end{array}$$

$P := 0\text{kN}, 1\text{kN} .. 44\text{kN}$



$$\frac{\text{def (P)}}{\text{mm}}$$

201